UNIVERSITY OF CANTERBURY

DOCTORAL THESIS

Ultra-High Temperature Electrolysis of Molten Oxides: Titanium Extraction from Ironmaking Slag

---

Author:
Samuel Martín Treceño

Supervisory Team:
Dr. Aaron T. Marshall
Dr. Matthew J. Watson
Dr. Catherine M. Bishop

A thesis submitted in fulfillment of the requirements for the degree of Doctor of Philosophy

in the

Department of Chemical and Process Engineering
College of Engineering

November 23, 2020

UNIVERSITY OF CANTERBURY

Abstract

College of Engineering
Department of Chemical and Process Engineering

Doctor of Philosophy

**Ultra-High Temperature Electrolysis of Molten Oxides:
Titanium Extraction from Ironmaking Slag**

by Samuel Martín Treceño

This thesis is a comprehensive study of ironmaking slag produced from titanomagnetite concentrates and its use as a molten electrolyte for titanium metal extraction. The electrolysis of ironmaking slag, the largest by-product of the steelmaking industry, was investigated for its potential as a secondary source of metal whose use, unlike most common practices, would not lead to degradation of the environment and over-extraction of resources. Provided the electricity is generated from renewable resources, the implementation of such electrolytic route can contribute to decarbonization of the metallurgical sector.

The electrolysis of these metal oxide feedstocks is a promising alternative whose study has traditionally been hindered by the ultra-high temperature required for molten state operation. With liquidus temperatures above 1473 K, these complex oxide systems melt at temperatures higher than lava comes out of a volcano. In this work, a laboratory scale, electrolytic cell was designed inside a vertical tube furnace and was used to achieve the extreme temperatures required to melt the slags and perform electrochemical measurements. Additionally, synthetic $TiO_2 - SiO_2 - Al_2O_3 - MgO - CaO$ slags, with different TiO_2 concentrations, were used to study the effect of the continuous extraction of titanium from the slag. A new containerless approach was used to assess the thermochemical and electrical behaviour of these slags, which enabled precise measurement while avoiding containment contamination. A combination of electrochemical measurements, physicochemical techniques and computational thermodynamic calculations were employed to elucidate the potential use of ironmaking slag as a molten oxide electrolyte for the extraction of titanium metal.

The use of ironmaking slag as an electrolyte was first characterized in terms of the potential constraints arising from operating directly from the process. The results illustrated that the removal of any entrained iron in the slag is crucial for the development of an efficient electrolytic process, and for the production of pure titanium metal. A computational thermodynamic model was developed and validated by comparing experimental DSC and in situ high-temperature XRD measurements with the predicted phase relations for the slags. The predicted thermodynamic cell voltage for the possible decomposition reactions within the molten slags indicated a small potential window between the reduction of Si and Ti ions from the melt, suggesting poor selectivity.

Cyclic voltammetry, potentiostatic and galvanostatic electrolysis measurements were performed to investigate the reduction process of the electroactive species in the melt. The electrolytic decomposition to metal and oxygen gas was confirmed by post-mortem microscopy analysis and real-time visualisation during experimentation. Electrolysis experiments showed that titanium and silicon were deposited together, forming an alloy with the working electrode when iridium or

molybdenum was used. Changing the amount of TiO_2 in the slag composition was not able to yield titanium or silicon as pure metal products. Ti−Si alloys are the main products of the electrochemical reduction of molten TiO_2 - SiO_2 - Al_2O_3 - MgO - CaO slags, where pure Ti metal production is unlikely without the prior removal of SiO_2. To alter the electrochemical sequence, future work could explore modifying the chemistry of the system, e.g. using a supporting electrolyte.

While producing titanium metal would be the highest added-value product, the electrolytic extraction of Ti−Si alloys could still be a profitable endeavour as these alloys are well recognized as high-temperature structural materials. Electrochemical impedance spectroscopy and stepped-potential chronoamperometry experiments were performed to investigate the electrical behaviour of such a process. The results confirmed that TiO_2 - SiO_2 - Al_2O_3 - MgO - CaO slags are mixed conductors, where current is carried by both ionic and electronic carriers. Since electron hoping between oxidation states had a predominant effect on enhancing electronic conduction, in order to sustain a current efficiency that enables high production rates while minimizing energy consumption, the operating conditions of the cell should be chosen so the ratio of the different valences of the titanium ions present in the slag is minimized.

The electrolysis of molten oxides (MOE) is particularly attractive due to the possibility to electrochemically extract metals directly from their ores while producing only oxygen. For the first time, the use of ironmaking slag for such a purpose has been investigated with a containerless method and an oxygen-evolving counter electrode. The results of this work proved that the electrochemical recovery of metals from molten ironmaking slags is feasible and provides the foundations to develop an electrochemical process to extract valuable metals from ironmaking slag.

Acknowledgements

This work was carried out from June 2017 to November 2020 between the University of Canterbury's Department of Chemical and Process Engineering (CAPE) and the Massachusetts Institute of Technology's Department of Department of Materials Science and Engineering (DMSE). No acknowledgement section will ever do justice to how grateful I am to every individual with whom I have shared and work alongside during this journey. The successfully completion of this thesis would have not been possible without all of you.

To my supervisory team, Dr. Aaron T. Marshall, Dr. Matthew J. Watson and Dr. Catherine M. Bishop, thank you for supporting me in all the experiences I had for the past 3.5 years. Your constant encouragement and challenge has made me a better researcher. I would also like to express my gratitude to Dr. Antoine Allanore for hosting me at his lab. Thank you for showing an interest in my work and for the many very useful discussions.

To Glenn Wilson, Joanne Pollard, Rachel Rogers, Ranee Hearst, Leigh Richardson, Frank Weerts, Stephen Buezenburg, Graham Furniss, Graham Mitchell, Michael Sandridge, Kun Zhao and Shaun Mucalo who offered their technical expertise, produced the various parts of the experimental rig and helped me navigate the practical and administrative part of research, my most sincere thank you. I would also like to thank Dr. Ian Brown and Dr. Yaodong Yia for their assistance in the sample preparation.

To my peers, colleagues, friends and flatmates, thank you for giving me wings and making me feel at home wherever I was. I would list you all, but I am afraid I may go above the word limit.

To my family: no sé si alguna vez me subiré a un escenario a recoger un Oscar, así que voy a usar esta plataforma para expresarles mi absoluta adoración y apreciación. En especial a mis padres y hermano (Esther, Antonio y Alberto) que me dieron la vida y me la siguen dando cada día. Para acabar, quiero dedicar este trabajo a mis abuelos (Esmeralda, Araceli, César e Isidoro) los cuales son mi mayor orgullo y motivación.

Contents

Abstract **iv**

Acknowledgements **vii**

1 Introduction **1**
1.1 Thesis Framework . . . 1
1.2 Value Proposition . . . 1
1.3 Hypothesis . . . 3
1.4 Scientific Gap . . . 3
1.5 Thesis Outline . . . 4
1.5.1 Format and original contributions . . . 5
1.6 Pursuit of Culturally Responsible Research . . . 8

2 Background Information and Theory **11**
2.1 Introduction . . . 11
2.2 Iron and Steel . . . 12
2.2.1 Properties & applications . . . 12
2.2.2 Production . . . 12
2.3 Titanium . . . 15
2.3.1 Properties & applications . . . 15
2.3.2 Production . . . 16
2.4 Metallurgical Electrochemistry . . . 19
2.5 Principles of Molten Oxide Electrochemistry . . . 20
2.5.1 Thermodynamic and kinetic fundamentals . . . 21
2.6 Analytical Methods . . . 23
2.6.1 Electrochemical techniques . . . 23
2.6.2 Physicochemical techniques . . . 24
2.6.3 Computational thermodynamic calculations . . . 26

3 Literature Review **29**
3.1 Introduction . . . 29
3.2 Slag, an Opportunity . . . 30
3.3 Slag, a Resource . . . 30
3.4 Slag, a Source of Titanium . . . 33
3.4.1 R&D performance evaluation . . . 35
3.5 Electrolytic Production of Titanium . . . 39

3.5.1 Slag, a suitable electrolyte . . . 40
3.6 Summary . . . 42

4 Implications of the Direct Use of Slag from the Ironmaking Processes as a Molten Oxide Electrolyte 45
4.1 Introduction . . . 45
4.2 Experimental . . . 47
4.2.1 Sample - origin . . . 47
4.2.2 Analytical methods . . . 49
4.2.3 Thermodynamic predictions . . . 50
4.3 Results and Discussion . . . 51
4.3.1 Chemical considerations . . . 51
4.3.2 Electrical considerations . . . 54
4.3.3 Thermodynamic considerations . . . 57
Thermal stability . . . 57
Electrochemical stability . . . 57
4.4 Conclusions . . . 58

5 Electrochemical Behaviour of Titanium-Bearing Slag Relevant for Molten Oxide Electrolysis 59
5.1 Introduction . . . 59
5.2 Experimental . . . 61
5.2.1 Sample preparation . . . 61
5.2.2 Thermodynamic predictions . . . 61
5.2.3 Phase relations determination . . . 63
5.2.4 Furnace operation . . . 63
5.2.5 Electrochemical measurements and analysis . . . 64
5.3 Results and Discussion . . . 66
5.3.1 Validating thermodynamic predictions . . . 66
5.3.2 Cyclic voltammetry . . . 66
5.3.3 Potentiostatic electrolysis . . . 68
5.4 Conclusions . . . 71

6 Electrochemical Study on the Reduction of Si and Ti from Molten TiO_2 - SiO_2 - Al_2O_3 - MgO - CaO Slag 73
6.1 Introduction . . . 73
6.2 Experimental . . . 75
6.2.1 Sample preparation . . . 75
6.2.2 Experimental set-up . . . 75
Vertical tube furnace . . . 75
Electrochemical measurements . . . 77
6.2.3 Computational thermodynamic calculations . . . 77
6.3 Results and Discussion . . . 78

6.3.1 Materials compatibility . . . 78
6.3.2 Initial electrolysis experiments . . . 79
6.3.3 Effect of varying the slag composition on the electrochemical reduction sequence . . . 84
6.4 Conclusions . . . 88

7 Determination of the Partial Contributions to the Electrical Conductivity of TiO_2 – SiO_2 – Al_2O_3 – MgO – CaO Slags: Role of the Experimental Processing Conditions 89
7.1 Introduction . . . 90
7.2 Experimental . . . 91
7.2.1 Sample preparation . . . 91
7.2.2 Electrochemical measurements and operation . . . 91
7.2.3 Considerations and measurement principles for the determination of . . . 93
Phase relations . . . 93
Electrolyte resistance . . . 93
Ionic and electronic charge carrier contribution . . . 95
7.3 Results and Discussion . . . 97
7.3.1 Conductive mechanism . . . 97
7.3.2 Effect of TiO_2 content . . . 98
7.3.3 Effect of temperature . . . 99
7.3.4 Effect of oxygen potential . . . 99
7.3.5 Effect of melt structure . . . 101
7.4 Conclusions . . . 103

8 Main Findings and Outlook 105

A Co-Authorship Forms 109

Bibliography 113

Chapter 1

Introduction

1.1 Thesis Framework

There are not many universal truths. However, in a world with a limited amount of resources and a population that has and is expected to keep growing, the need to change current practices to sustain growth is one of them. This claim was brilliantly expressed in 2019's United Nations Sustainable Development Goals Report [1]:

> "Urgent action is needed to ensure that current material needs do not lead to over-extraction of resources and further degradation of the environment. Policies must be embraced to improve resource efficiency, reduce waste and mainstream sustainability practices across all sectors of the economy."

From the Earth Summit in Rio de Janeiro in 1992 to The Paris Agreement on climate change on 2015, policies that outline this issue have been gradually adopted. Furthermore, the urgency of implementing a multilateral plan of action led in 2015 to the creation of The 2030 Agenda for Sustainable Development, subscribed to by all United Nations Member States, including New Zealand [2]. The work presented in this thesis is set within the framework of the Agenda's 17 Sustainable Development Goals, in particular where it concerns Responsible Consumption and Production, and Industry, Innovation and Infrastructure.

1.2 Value Proposition

The recycling of industrial by-products, such as ironmaking slag, has been identified as essential to meet the current demand for materials in a sustainable manner, avoiding further degradation of the environment [1]. A slag is a mixture of oxides that contains all the gangue materials that are removed from their ores during the extraction and refining of a specific metal [3]. In this doctoral thesis, the direct extraction of titanium from local ironmaking slag is explored in light of the vast availability of the TiO_2 contained within (up to 33 wt.%). In New Zealand, the high content of titania in the slag is due to the use of titanomagnetite mineral deposits, commonly referred to as ironsand, as the main source of iron in the local

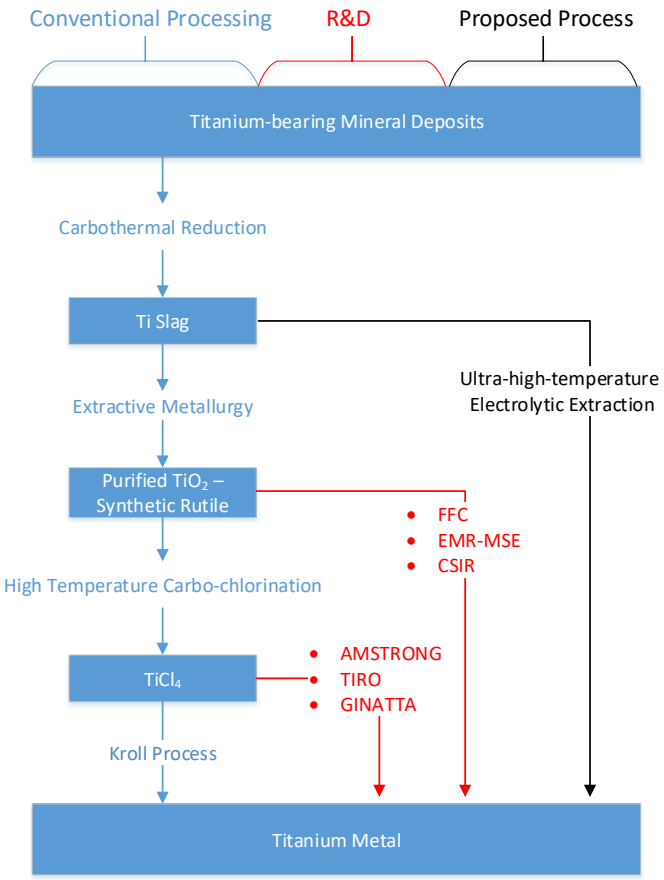

FIGURE 1.1: Comparison of processes illustrating the proposed process simplification, adapted from [5].

steelmaking process [4].

Ironmaking slag is currently sold as an aggregate for road construction or accumulated in polluting slag yards, without further metal extraction. Optimizing the use of the titanomagnetite mineral deposits by extracting not only iron but titanium has the potential to reduce environmental industrial impact. The conventional industrial manufacturing process for titanium, the Kroll Process, involves a series of initial steps before titanium can be extracted (see Figure 1.1). Hence, the development of a process to directly extract titanium from ironmaking slag aligns well with the values outlined in the 2019 United Nations Sustainable Development Goals Report of improving sustainability and resource efficiency of the mainstream practices.

Furthermore, recent research has been able to prove the detrimental effect of titanium in the mechanical properties of slag cements, with slags containing more than 1 wt.% TiO_2 showing compressive strength below European standards [6]. This is consistent with a report written by Opus International Consultants Ltd. [7] that studied the behaviour of slag as an aggregate in open-graded emulsion

mixes for road construction. The study implied that, even though it complied with New Zealand specifications, the crushing resistance was lower than the average for asphaltic mixes. Hence, the extraction of titanium from ironmaking slag can also have a beneficial effect on its current use, increasing its value and utilization in the global market.

Moreover, provided the electricity is generated from renewable resources, the implementation of an electrochemical route can also contribute to decarbonization of the metallurgical sector. New Zealand does not currently have the capability to produce titanium, but it has 850 MW of hydroelectric installed capacity. The development of a process to produce high-purity titanium metal through the electrolysis of molten ironmaking slag has the potential to create a new revenue stream for the country. A sustainable and environmentally friendly alternative to the conventional extractive metallurgical processes with the potential to create jobs and reduce dependence on imported titanium.

1.3 Hypothesis

Extracting more value from slags is not a new concept. Last century, Waseda and Toguri [8] already pointed to waste reduction techniques, such as the beneficial utilization of metallurgical slags, as key technological and social developments for the 21st century. However, only recently, molten oxides have been proven successful electrolytes for high-temperature, carbon-free metal electrolytic production [9, 10] opening a promising pathway towards sustainable metal production. In this doctoral work it is hypothesized that due to the mixed oxide nature of the slag, (a) no additional supporting electrolyte is needed for the implementation of an electrochemical route and (b) sufficient ionic conductivity should be present in the molten slag such that titanium could be extracted. Chapter 5 and Chapter 7, respectively, confirmed our hypothesis.

1.4 Scientific Gap

This work investigates the use of the slag directly from the industrial process. This is a major difference with traditional industrial electrochemical processes, such as the Hall-Heroult cell for the production of aluminium [11], where an additional supporting electrolyte was engineered to facilitate the process. Avoiding the use of an additional supporting electrolyte increases the sustainability of the process as it eliminates the initial purification step of conventional extraction processes and avoids the treatment of highly volatile, potentially hazardous metal halide mixtures [12]. This yields a simpler and more efficient process (see Figure 1.1).

While, recently, it has been proven possible to directly electrolyse a pure molten oxide (e.g. produce aluminium directly from molten alumina [13]), there are good reasons why the use of supporting electrolytes is predominant in the industry. Mainly, it allows you to optimize the physical-chemical properties (e.g. viscosity, thermodynamic activities, ionic conductivity) of the system under study. More critically perhaps, in the case of oxides, it allows operation of the electrochemical cell at temperatures below the melting point of your oxide of interest. Aluminium oxide has a melting point of 2355 K, however, the Hall-Heroult cell operates at temperatures below 1237 K as aluminium oxide is dissolved in cryolite, the supporting electrolyte. For the process proposed in this thesis, avoiding the use of an additional supporting electrolyte implies that the molten slag can be used straight from the industrial process, taking advantage of the available heat. But, on the other hand, it forces the cell to operate above 1750 K.

Unfortunately, such temperature imposes very demanding material constraints. This makes it extremely challenging to study high-melting oxide mixtures at a laboratory scale, where significant challenges remain for property prediction and measurement in high temperature melts (i.e. slag/crucible interaction [14]). Consequently, the thermodynamic understanding of ironmaking slag in its molten state is limited. Traditionally, these has led ironmaking slag to be treated as waste [15] or sold as inexpensive aggregate for road construction [16]. Since the success of using an electrochemical route to extract metals relies in having a profound understanding of the properties of the electrolyte at the conditions required for the proposed process, research efforts in this work are centred on closing the scientific gap around the characterization of slag in its molten state. In particular, determining the physical-chemical properties, the electrochemical behaviour and the electrical properties of the melt as temperature, composition and atmosphere changes.

1.5 Thesis Outline

This thesis is composed of eight individual chapters. In order to provide a detailed, insightful and structured answer to the proposed hypothesis, each chapter of this body of work aims to answer one question. This is summarized as follows:

- CHAPTER 1: *what is the problem this thesis works to solve and what are the motivations behind it?* This chapter sets the overall framework of the research and provides a quick summary of the structure and content of the document.
- CHAPTER 2: *what background information should I be familiarized with in order to follow this thesis?* This chapter breaks down the underlying theory and experimental techniques that are used throughout the thesis.

- CHAPTER 3: *what is the recycling method with biggest disruption potential for ironmaking slag?* This chapter provides an overview of the literature, highlighting the urgent need to recycle industrial large-scale by-product materials. It reviews the different slag recycling schemes and titanium metal extraction routes.
- CHAPTER 4: *what are the considerations one must have when attempting to use ironmaking slag in an electrochemical cell as the sole molten oxide electrolyte?* This chapter establishes the guidelines for the effective use of the ironmaking slag as electrolyte in molten oxide electrolysis.
- CHAPTER 5: *what is the electrochemical behaviour of the ironmaking slag at operating temperatures?* This chapter is centred on the development of a methodology to study high melting temperature, corrosive melts without containment issues, to finally discuss the initial results on the electrolysis of the molten ironmaking slag.
- CHAPTER 6: *can we obtain pure titanium metal from the electrolysis of molten ironmaking slag?* This chapter combines experiments and thermodynamic simulations to provide a critical assessment on the reduction process of molten ironmaking slag, focusing on characterizing the reduction of Ti and Si ions from the slag.
- CHAPTER 7: *what are the electrical properties of the ironmaking slag at operating temperatures?* This chapter quantifies the ionic and electronic charge carriers contributions to the total electrical conductivity, and expands the conductive mechanism theory to molten ironmaking slags.
- CHAPTER 8: *what are the main findings of this body of work and the next steps for future work in this field?* This chapter summarizes the overall conclusions and achievements and offers the author's personal recommendations and suggestions for future work in the field.

1.5.1 Format and original contributions

The literature review (chapter 3) and all the result chapters (chapter 4-7) have been written in an "article format" and have or will be published in peer-reviewed, international journals or conferences proceedings. Each result chapter is self-contained and, therefore, some introduction and experimental details were inevitably repeated.

CONFERENCE PROCEEDINGS:

- S. Martin-Treceno, C. Bishop, A. Marshall, M. Watson, Value extraction from waste in the steelmaking industry, in: Chemeca 2018, Institution of Chemical Engineers, Queenstown, NZ, 2018, pp. 28.1–28.9.

JOURNALS PUBLICATIONS:

- S. Martin-Treceno, N. Weaver, A. Allanore, C. M. Bishop, A. T. Marshall, M. J. Watson, Electrochemical behaviour of titanium-bearing slag relevant for molten oxide electrolysis, Electrochimica Acta 354 (2020) 136619.
- S. Martin-Treceno, A. Allanore, C. M. Bishop, A. T. Marshall, M. J. Watson, Implications of the direct use of slag from the ironmaking processes as a molten oxide electrolyte, JOM (In Preparation).
- S. Martin-Treceno, T. Hughes, N. Weaver, A. Allanore, C. M. Bishop, A. T. Marshall, M. J. Watson, Electrochemical study on the reduction of Si and Ti from molten TiO_2 – SiO_2 – Al_2O_3 – MgO – CaO slag, Journal of the Electrochemical Society (In Preparation).
- S. Martin-Treceno, A. Allanore, C. M. Bishop, A. T. Marshall, M. J. Watson, Determination of the partial contributions to the electrical conductivity of TiO_2 – SiO_2 – Al_2O_3 – MgO – CaO slags: role of the experimental processing conditions, Acta Materiala (In Preparation).

With the goal of disseminating the research outcomes to the scientific community and broader audience, promoting discussion and fostering collaboration. This research has been actively shared.

ORAL PRESENTATIONS:

- Martin-Treceno, S., Hughes, T., Bishop, C., Brown, I., Jia, Y., Marshall, A., Watson, M. (2018, March). Production of Titanium from Waste Slag. Oral presentation at the 147th TMS Annual Meeting, Phoenix, AZ, U.S.A.
- Martin-Treceno, S., Hughes, T., Bishop, C., Brown, I., Jia, Y., Marshall, A., Watson, M. (2018, March). Ultra-High-Temperature Electrolytic Titanium Extraction From Titanomagnetite Sands. Oral presentation at Boston Metals Headquarters, Woburn, MA, U.S.A.
- Martin-Treceno, S. (2018, September). Breaking the Wall of Titanium Production. Oral presentation at Falling Walls Lab New Zealand, Wellington, New Zealand.
- Martin-Treceno, S., Bishop, C., Marshall, A., Watson, M. (2018, September). Value Extraction from Waste in the Steelmaking Industry. Oral presentation at CHEMECA 2018, Queenstown, New Zealand.
- Martin-Treceno, S. (2019, May). Does NZ's ironmaking slag meet the conditions to be an electrolyte for the direct electrolysis of titanium? Oral presentation at Massachusetts Institute of Technology's Allanore Research Group Departmental Seminar, Cambridge, MA, U.S.A.

- Martin-Treceno, S., Weaver, N., Bishop, C., Marshall, A., Watson, M. (2019, August). Exploring the Electrochemical Extraction of Titanium from Complex Molten Oxides Systems. Oral presentation at the 70th Annual ISE Meeting, Durban, South Africa.
- Martin-Treceno, S., Bishop, C., Marshall, A., Watson, M. (2019, September). Characterization of Electrolytes at Ultra-High-Temperature Relevant for Molten Oxide Electrolysis. Oral presentation at CHEMECA 2019, Sydney, Australia.
- Martin-Treceno, S., Bishop, C., Marshall, A., Watson, M. (2019, November). Research above 1000°C: How to Avoid Burnout. Oral presentation at Materials@UC 2019, Christchurch, New Zealand.
- Martin-Treceno, S. (2020, January). How to Survive Presentations. Oral presentation at University of Canterbury's Chemical and Process Engineering Departmental Seminar, Christchurch, New Zealand.
- Martin-Treceno, S., Bishop, C., Marshall, A., Watson, M. (2020, August). High Temperature Electrolysis for Extraction of High Purity Metals from Slag. Oral presentation at the IChemE NZ meeting, Christchurch, New Zealand.
- Martin-Treceno, S. (2020, September). What a Waste! Oral presentation at 2020 University of Canterbury's 2020 3MT Competition Final, Christchurch, New Zealand.
- Martin-Treceno, S.(2020, October). 40 Thousand Elephants from Waste [Radio Broadcast]. In STeudaemonia International Students Living Well. Plains FM. Available from: https://accessmedia.nz/Player.aspx?eid=3d23bf3b-d4a5-43ac-86a7-7222348a8105
- Martin-Treceno, S.(2020, October). The waste of plenty is the resource of scarcity. Oral presentation at University of Canterbury College of Engineering's Postgraduate Dream Team Seminar, Christchurch, New Zealand.

POSTER PRESENTATIONS:

- Martin-Treceno, S., Hughes, T., Bishop, C., Brown, I., Jia, Y., Marshall, A., Watson, M. (2018, March). Ultra-High-Temperature Electrolytic Titanium Extraction From Waste Slag. Poster session presented at the 13th Workshop on Reactive Metal Processing, Cambridge, MA, U.S.A.
- Martin-Treceno, S., Hughes, T., Weaver, N., Bishop, C., Marshall, A., Watson, M. (2018, December). Methods and Tools to Electrolyze Complex Metal Oxide Systems at Ultra-High Temperatures. Poster session presented at the 2018 Materials Cluster Conference, Christchurch, New Zealand.

- Martin-Treceno, S., Bishop, C., Watson, M., Allanore, A., Marshall, A. (2019, October). Unlocking the Characterization of Oxide Electrolytes at their Molten State. Poster session presented at the University of Canterbury 2019 Summer Gradfest, Christchurch, New Zealand.
- Martin-Treceno, S., Bishop, C., Watson, M., Allanore, A., Marshall, A. (2019, October). Unlocking the Characterization of Oxide Electrolytes at their Molten State. Flash presentation + Poster session presented at the MacDiarmid Institute for Advanced Materials and Nanotechnology 2019 Future Leaders Programme, Wellington, New Zealand.
- Martin-Treceno, S. (2020, September). Too Hot to Handle! Flash presentation at 2020 University of Canterbury's 2020 Visualize Your Thesis Competition Final, Christchurch, New Zealand.
- Martin-Treceno, S., Allanore, A., Bishop, C., Marshall, A., Watson, M. (2020, September). Electrical Properties of molten $TiO_2 - SiO_2 - Al_2O_3 - MgO - CaO$ slag. Poster session presented at the 71th Annual ISE Meeting, ONLINE.

This body of work has been possible, in part, thanks to the following awards and funding received:

- This research was funded by NZ Ministry of Business, Innovation and Employment (MBIE) under the contract CONT-46287-CRFSI-UOC.
- Travel Award: 2018 Canterbury Chemeca Trust Fund.
- Travel Award: 2018 Doctoral Overseas Travel Grant.
- Travel Award: 2019 CHEMECA Fund scholarship.
- Best Poster at University of Canterbury 2019 Summer Gradfest.
- Best Talk with an engineering theme at Materials@UC conference 2019.
- 2nd place MacDiarmid Institute's 2020 Emerging Scientist Association 3MT finals.
- Top PhD student at University of Canterbury and Asia Pacific Semi-finalist on 2020's 3MT competition.

1.6 Pursuit of Culturally Responsible Research

The scientific investment by New Zealand's Ministry of Business, Innovation and Employment (MBIE) in this research represents a spring-board from which an entire industry can be revolutionised. It also comes with the responsibility of placing this research in New Zealand's bicultural context. New Zealand does not currently have

the capability to manufacture titanium, and a technology such as this has the potential to create jobs, reduce our dependence on imported titanium and to establish a healthy export revenue stream. This research provides a scientific foundation that can unlock the future development of a process that must include local hapū/iwi, specifically for the people of Ngāti Hikairo, Ngāti Mahuta and Tainui waka, all of whom have whakapapa links to the whenua (land) and associated natural resources.

Optimizing the use of the titanomagnetite mineral deposits by extracting not only iron but titanium will inevitably add value to ironsands developments by extracting greater value from a natural resource. According to Brendon Green, Chairman of Tainui Kāwhia Inc. (TKI), a development will provide employment and a sense of mana for the people of Ngāti Hikairo, Ngāti Mahuta and Tainui waka, and this in turn will enable regional growth. Furthermore, a new technology to strengthen ironsand development resonates with the local hapū /iwi who whakapapa to the whenua. If successful, this research has potential to enable further development of mana whenua providing economic growth. Therefore enhancing social and cultural well-being, and the benefits derived by potentially bringing whānau back to Kāwhia to connect with their hapū, and iwi.

Chapter 2

Background Information and Theory

2.1 Introduction

This chapter aims to provide the information needed to help the reader make their way through this body of work. The information provided consists of concepts, principles and definitions that should enable the reader to connect with the existing knowledge that the author intends to review and expand. This research focuses on evaluating the feasibility of using ironmaking slag as an electrolyte for the electrolytic extraction of titanium metal. Relevant to this work is the study of the feedstock's occurrence, i.e. ironmaking process, in particular the peculiarities of the local process in New Zealand is provided in Section 2.2. An overview of the industrial processes for titanium production, along with the characteristics that makes titanium such a valuable metal is provided in Section 2.3. For more general information, the reader is referred to previous work by this group [17, 18].

Electrochemistry was the reaction route chosen in this work (see Section 2.4). This work builds on the pioneer efforts of Chen *et al.* [9] which demonstrated that high purity titanium could be obtained from the electrolysis of an titanium-bearing oxide; and Sadoway's and Allanore's research groups at MIT which first developed the tools to investigate the use of oxides as molten electrolytes [3, 10]. Due to the novelty of the operating conditions employed, a big focus of this work is on the development of an understanding of slag's structure-property-composition relationships in the molten state. Hence, this work lies in the interface between material science, thermodynamics and electrochemistry. In order to navigate this thesis, Section 2.5 familiarizes the reader with terminology in those areas such as Gibbs Energy, thermodynamic activities and cell voltages.

The analytical techniques used to obtain experimental data are introduced in Section 2.6. Due to the technical difficulties accompanying the experimental conditions used, research efforts relied on computational thermodynamic calculations to

complete the understanding of the system at the operation conditions. These thermodynamic predictions were obtained using the thermodynamic software FactSage 7.2 [19], and were validated by experimental results as illustrated in Chapter 5. For more detailed information about the experimental and simulated investigative aspects of this body of work, the reader is referred to previous work by this group [17, 18].

2.2 Iron and Steel

2.2.1 Properties & applications

Iron is the fourth most abundant element in the Earth's crust and arguably an essential metal to life. It is vital to the conversion of solar energy into movement and, in the blood, it is involved in the transport of oxygen. It is because of the iron content in haemoglobin that blood has its red color. Out of all the metal refined in the world, 90% is iron [20]. Iron is present mainly in oxide ores. The most commonly found ore is haematite (Fe_2O_3), but it is widely found in other minerals such as taconite or magnetite (Fe_3O_4) deposits. Magnetite can be regarded as 1:1 combination of wustite (FeO) and haematite. In New Zealand, iron is found as part of titanomagnetite deposits [21], a mixture of magnetite and titanomagnetite (Fe_2TiO_4).

Today, most iron is used in steel manufacturing. Steel as a material needs little introduction. Steel is the most widely used alloy material in construction with a yearly production that keeps growing every year. Its lower price and broad range of applications make steel the main structural component with 1630 million tonnes produced in 2016 [22] and 1700 million tonnes in 2017 [23]. To give sense of the magnitude, the next most prolific material is aluminium with only 60 million tonnes [24] produced.

Steel refers to ferrous alloys with less than 2.1 wt.% of carbon. René Antoine Ferchault de Réaumur was the first person to show the effect of the different amounts of carbon in the final steel properties [25]. Since then, many chemical elements are added to the steel formulation in order to optimized desired physical-chemical properties. Chromium is used to improve its resistance to oxidation. This grade of alloys are commonly referred to as stainless steel. Other elements are also used: nickel improves its corrosion-resistance, cobalt enhances its magnetic properties, manganese increases its hardness, or molybdenum helps keeping mechanical properties at high temperatures.

2.2.2 Production

The conventional steelmaking processes are dominated by the reduction of haematite in blast furnaces. These furnaces are fuelled with high-grade coal and,

consequently, approximately 1.4 tonnes of CO_2 are emitted per each tonne of steel produced [26]. Modern blast furnaces today have the capacity to produce more than 11,000 tonnes of metal per day, with an inner volume of approximately 5000 m^3 and more than 100 m height [27].

The steelmaking plant in New Zealand presents a remarkable technological achievement due to its unique characteristics. The reduction of the ores does not take place in a conventional blast furnace, but it takes place in a rotary kiln followed by an electric melter. The reason is the different starting materials used. Titanomagnetite deposits, due to the presence of TiO_2 and other impurities, have a higher melting point than haematite and produce a slag that blocks blast furnaces [21].

New Zealand's Process

In New Zealand, mining of titanomagnetite deposits (commonly known as iron-sands) is the main source of iron but also titanium. Since 1970, the local facilities have reduced iron oxide from the titanomagnetite sands into metallic iron to produce steel [4]. New Zealand has the capacity to produce 650,000 tonnes per year of iron and steel products [28]. In this process, the iron-rich ore is processed to steel via two main stages. The first involves the production of pig (crude) iron and the second is that of actual steel manufacture.

The production of molten pig iron starts at the Waikato North Head mine where, before being pumped to the ironmaking process, the titanomagnetite deposits are concentrated by gravity and magnetic separation. The chemical composition of the product, called primary concentrate, was investigated using X-ray fluorescence (XRF) and is listed in Table 2.1.

TABLE 2.1: Chemical composition of primary concentrate (wt. %).

TiO_2	Al_2O_3	CaO	SiO_2	MgO	FeO	MnO	V_2O_5
7.9	3.7	0.5	2.3	2.9	81.4	0.6	0.5

Then, at the steel mill, the multi-hearth furnaces preheat and dry the feedstock. The combustion the volatiles generated in these furnaces is used to fuel electricity generation. The main reduction of the iron oxides occurs in the rotary kilns with temperature around 1173 K and excess carbon [21]. At that temperature, carbon monoxide is the main reducing agent (reactions 2.1 & 2.2):

$$Fe_2O_3(s) + 3\,CO(g) \longrightarrow 2\,Fe(s) + 3\,CO_2(g) \qquad \Delta H = -37\,kJmol^{-1} \qquad (2.1)$$

$$FeO(s) + CO(g) \longrightarrow Fe(s) + CO_2(g) \qquad \Delta H = -17\,kJmol^{-1} \qquad (2.2)$$

To produce the carbon monoxide, the oxides are reduced with carbon from coal in the rotary kilns. At 1173 K, carbon is oxidized in air producing carbon dioxide (reaction 2.3). The carbon dioxide then further reacts with more carbon to yield carbon monoxide in an endothermic reaction (reaction 2.4). Heat is produced from the partial reaction of CO with oxygen (reaction 2.5) and it is used in the process [21]. At those temperatures, the limestone ($CaCO_3$) that was added to the coal stockpile is decomposes into lime (CaO) as air is blown into the kiln shell, ensuring sufficient carbon monoxide participates in the reduction of iron oxide.

$$\mathrm{C(s) + O_2(g) \longrightarrow CO_2(g)} \qquad \Delta H = -395\,\mathrm{kJmol^{-1}} \tag{2.3}$$

$$\mathrm{C(s) + CO_2(g) \longrightarrow 2\,CO(g)} \qquad \Delta H = 169\,\mathrm{kJmol^{-1}} \tag{2.4}$$

$$\mathrm{2\,CO(g) + O_2(g) \longrightarrow 2\,CO_2(g)} \qquad \Delta H = -564\,\mathrm{kJmol^{-1}} \tag{2.5}$$

Nearly 70% of the material is metallic iron when leaving the rotary kilns. Electric melters are used to achieve the final reduction of the iron oxides present. In the melter, lime acts as a flux separating sulphur and other impurities from the metallic iron. Power is applied by pairs of carbon electrodes, increasing the temperature up to 1750 K and causing the mixture to melt. Two layers are then formed and separated due to their density. The slag or upper layer, contains most of the undesirable elements. The lower, more dense, layer is the molten pig iron. This is the final product of the ironmaking process. It consists of iron and some dissolved impurities [28]. The typical composition of both layers is listed in Table 2.2:

TABLE 2.2: Elemental composition (wt.%) of the products of the local ironmaking process in New Zealand. Pig iron composition as reported by manufacturer [28]. Ironmaking slag composition obtained from ICP-MS measurements, where the oxygen content can be obtained by mass balance.

	Ti	**Al**	**Ca**	**Si**	**Mg**	**Fe**	**Mn**	**V**	**S**	**P**	**C**
Ironmaking Slag	19.47	6.58	9.35	8.40	5.69	4.44	0.73	0.13	0.14	0.0034	-
Pig Iron	0.16	-	-	0.11	-	95.50	0.60	0.42	0.06	0.06	3.40

Molten pig iron and slag are drained periodically. Two holes are drilled in the refractory sidewalls of the melter to act as tapping points. The less dense slag layer is tapped from the higher hole, while a lower hole, down on the opposite side, is used for the molten pig iron. The molten pig iron proceeds to the steelmaking process. In that process, vanadium and the remaining impurities are recovered until composition is within specification. Finally, fine adjustments to the composition are made to obtain the desired grades of steel. The slag is the by-product of the ironmaking process, and currently, it is dumped to cool (see Figure 2.1) and later sold without further metal extraction. This ironmaking slag is the product of interest of this body work. Chapter 3 explores in detail the opportunities and benefits of recycling this material.

FIGURE 2.1: NZS Slag Tipping. Reprinted from [29].

2.3 Titanium

2.3.1 Properties & applications

Named after the sons of the Earth goddess of Greek mythology, the titans, titanium's unique properties makes the element ideal for a wide range of applications. From propeller shafts and power plant condensers to medical implants and aircrafts [30], it is astounding how reliant society is on the use of the 22nd element of the Periodic Table. Titanium was not discovered until 1791, as part of a black sand called menachanite [31], but the use of titanium and its compounds has played a major part in the development of the world up until today (see Table 2.3).

TABLE 2.3: Titanium based applications.

SPECIE	PROPERTIES	APPLICATIONS
Oxide	High absorbance UV light	Sunscreen, photocatalysts
Oxide	Good reflector of infrared radiation	Solar observatories
Metal	Resistance to corrosion	Propeller shafts, power plant condensers
Metal	Low density, high strength	Aerospace industry
Metal	Lack of reactivity with human body	Medical implant
Oxide	Excellent opacifying performance	Pigment in house paint
Oxide	Insoluble and not toxic	Medicines, toothpaste
Oxide	High inherant brightness & whiteness	Food industry

Titanium metal has a high strength-to-weight ratio, corrosion resistance, thermal stability and it is biocompatible with the human body [31]. It is also twice as strong as aluminium and as strong as steel, but 45% lighter [30]. These properties makes

it a valuable structural material, and potential substitute for steel. Today, however, less than 10 percent of all mined and synthetic titanium minerals are used to make titanium metal [32]. Its elevated cost has restricted its use to the development of high added value products, mainly in aerospace. Until a reduction in the production cost is achieved [33], most mined and synthetic titanium minerals will continue to be used to manufacture TiO_2 [32].

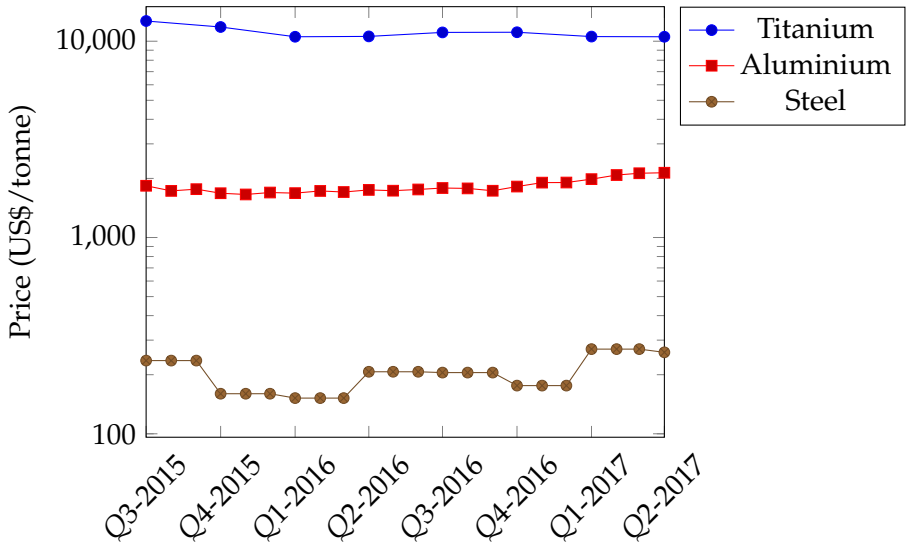

FIGURE 2.2: Metal price (US$/tonne) comparison [32, 34, 35].

Unlike its high price may suggest (see Figure 2.2), titanium is not a scarce resource. In fact, titanium is the ninth-most abundant metal in the Earth's crust [31]. Titanium is present in many igneous rocks and sediments, primarily found in the minerals: sphene ($CaTiSiO_5$), ilmenite ($FeTiO_3$) and rutile (TiO_2). China, Australia, India and South Africa are the main reserve holders [32]. The Holy Grail of titanium production would be to use these minerals directly [36]. However, due to titanium's affinity for oxygen, traditional practices are unsuitable for the separation of high-purity metal.

2.3.2 Production

The history of titanium production is marked by titanium's affinity for oxygen and its potential contamination with air's nitrogen [37]. So much so that up until the beginning of the 21th century, there was not an established route to extract pure titanium metal directly from titanium-bearing ores [38]. Today, almost all metallic titanium is industrially produced by the Kroll process [39].

However, the Kroll Process was not the first titanium production route that reached industrial scale [37]. In 1887, a report by Nilsen and Pettersen using sodium as a reductant for the metallothermic reaction was optimized into the commercial

Hunter process [40]. Then, in the beginning of the 20th century, Van Arkel studied the thermal decomposition of titanium tetraiodide to give highly pure titanium [41]. Years later, in 1940, William J. Kroll found that titanium tetrachloride, $TiCl_4$, was reduced with calcium at high temperatures to give hydrides that can be thermally processed to the pure metal [42]. The process was later refined using magnesium as a reductant [43]. Today, the Kroll process has displaced the Hunter process to high purity small-scale applications [43].

Kroll Process

In the Kroll process titanium metal is obtained in three stages. The first step is a high temperature chlorination of the titanium-bearing ore [44]. This pretreatment aims to change the chemistry of the titanium ore that contains TiO_2, as the high chemical stability of this compound complicates the reduction to titanium metal [45]. Titanium tetrachloride is more easily reduced. Therefore, the oxide is added to an active carbon bed and fed to a carbo-chlorination reactor where the reduction occurs:

$$TiO_2(s) + 2\,Cl_2(g) + C(s) \longrightarrow TiCl_4(s) + CO_2(g) \tag{2.6}$$

Still, $TiCl_4$ needs to be purified before it is used. The impurities are removed by distillation followed by a chemical treatment. This process implies a potential hazard since $TiCl_4$ is easily hydrolyzed, generating the corrosive hydrogen chloride [46]:

$$TiCl_4(l) + 2\,H_2O(l) \longrightarrow TiO_2(s) + 4\,HCl(g) \tag{2.7}$$

The second stage is where the main reaction takes place. Purified $TiCl_4$ vapour is reduced with molten magnesium in an argon-filled reactor at 1300 K:

$$TiCl_4(g) + 2\,Mg(l) \longrightarrow Ti(s) + 2\,MgCl_2(l) \tag{2.8}$$

The product of this exothermic reaction is a porous titanium structure commonly refereed to as titanium sponge. This is the raw form of the metal [47]. Before further processing, the unreacted $MgCl_2$ is removed and electrolysed, so chlorine and magnesium can be recycled in the process [39]. Reductant solubility plays a major role in the operation chosen to purify the sponge from the unreacted feed and salts [38]. The most common techniques are leaching and vacuum distillation [45]. Leaching is simple and continuous. However, acids are no longer used in the Kroll process for the removal of magnesium and $MgCl_2$ because they stop the unreacted magnesium from being recovered and recycled in the process [46]. Instead, high temperature vacuum distillation is used.

The development of this technology in 1948 led to large-scale commercialization, but it has changed very little since [48]. Hence, the process described so far

offers limited possibilities for improvements since it has a lot of fixed cost (e.g. $TiCl_4$ preparation or magnesium utilization) [38]. As a result, the main industrial extraction process to produce titanium metal is complex, potentially hazardous and very energy consuming [37]. This translates into the metal's high cost.

The nature of the magnesiothermic reduction [49] creates variable grades within the sponge. Consequently, after the sponge is removed from the reactors, it has to be manually inspected and shearing of the lower purity parts is required to obtain a homogeneous high purity grade [36]. The remaining sponge is crushed and melted to produce an ingot using the vacuum arc remelting technique. The sponge consolidation needed to fabricate an electrode and the reliance on the melting process required to obtain alloy homogeneity significantly contributes to increasing the cost of the process. However, this is still the most common industrial practice [44]. Furthermore, this batch-wise mode of operation can take more than a week to produce a single batch and to convert it into an semi-finished form such as sheet, bar or plate. [36].

Today, post-sponge operations contribute to approximately half of the final product price [43]. By far, the greatest opportunity to cut major cost is in this last stage, the processing of titanium metal from a porous granule to a semi-finished form. Cold hearth melting is receiving increasing acceptance as an alternative process for its capacity to directly cast titanium to rectangular slabs [50]. Other operations like powder metallurgy have the potential to make near-net shape parts directly by circumventing most of the fabrication steps. This would minimize the volumes of scrap generated and achieve higher production rates. Unfortunately, current high purity titanium powder cost is an impediment [43]. If the price of the powder was similar to that of sponge, ground breaking saving possibilities would be unlocked [39].

Hunter Process

The Hunter process was invented by Matthew A. Hunter, a chemist born in New Zealand, and it is very similar to the Kroll process [47]. It shares the same stages for producing $TiCl_4$, but sodium is used instead as a reductant [40]. In a one-step operation, the reduction proceeds as follows:

$$TiCl_4(g) + 4\,Na(l) \longrightarrow Ti(s) + 4\,NaCl(l) \tag{2.9}$$

In the process, sodium solubility in the molten sodium chloride increases the conductivity of the electrolyte facilitating the electrons to reach any available $TiCl_4$ [37]. The reduction occurs in the molten salt, forming fine titanium particles in the bulk electrolyte than later precipitate [51]. This way, titanium is produced in a

powder form (sponge fines) [52].

While the $MgCl_2$ is efficiently separated by distillation in the Kroll process, the lower vapor pressure of NaCl makes that option non viable [52]. Dilute hydrochloric acid is used to separate the final product from the salt in the Hunter process [47]. NaCl is leached away from the titanium metal product using hydrochloric acid because titanium subchlorides are soluble in sodium chloride. Recovering NaCl for that aqueous solution would require further processing. Since there is no recycling, new sodium must be introduced every run and the sponge price by the Hunter process is higher.

Today, the form and purity of the metal deposit produced in the Hunter process keeps it attractive despite Kroll process's predominance. However, there are some differences which made the latter the prevalent industrial practice. Mainly, the difficulty separating the final product and the lack of recycling process for the reducing agent, sodium metal [37]. Until those challenges are resolved, the production of titanium metal through the Hunter process, with the exception of the production of some electronic materials [52], will remain industrially irrelevant.

2.4 Metallurgical Electrochemistry

The primary extraction of metals can be accomplished in two ways: thermochemical and electrochemical [47]. The latter involves an electrolytic reduction in an ionic medium whereas the former requires a metallothermic reduction of the compound containing the desired metal. Today, 33 out of 70 of the most common metallic elements are electrolytically produced [53].

Electrochemistry dates back to the beginning of the 19th century after the discovery of a continuous source of electric current by Alessandro Volta [24]. In 1808, the decomposition of molten potash to potassium is credited to be the first demonstration of electricity's ability to isolate metals [54]. Since then, metallurgical electrochemistry has expanded to the point of being the only commercially viable means for the extraction of metals, e.g. aluminium, to compete with thermochemical processes, e.g. magnesium, and even to be considered for the future of extra-terrestrial metal extraction [55].

Metallurgical electrochemistry encompasses the use of electrochemical processing to extract metals from their ores (electrowinning), to purify and recycle (electrorefining) or for the formation of metal coating (electroplating) [56]. Electrorefining, in contrast to electrowinning's fierce competition, has an unrivalled capability to produce the most pure grade of metals. Copper, nickel and lead are

electrorefined metals, where the recovery of silver and gold from copper anode slimes is another application [57]. Electroplating work is concentrated on generating abrasion-resistant coatings, where molybdenum and titanium have received noticeable attention [56].

In this doctoral thesis, the focus is put on the electrochemical extraction of metals, specifically titanium. This process implies the use of an electrolyte where the metal is electrolytically reduced. Depending on the choice of electrolyte, different categories are defined. Aqueous electrochemistry employs aqueous solutions as electrolytes. This most traditional electrochemistry is quite restrictive for metal extraction as, broadly speaking (i.e without kinetic considerations), the desired electrochemical reaction must occur in the energy window between hydrogen and oxygen evolution [56].

A quick look to the electromotive force series in water shows that the most reactive metals, such as refractory metals and their compounds, require a non-aqueous electrolyte [54]. Molten salts and ionic liquids are liquids composed of merely ions. These media are excellent alternatives as one can selectively choose the constituent ions, engineering supporting electrolytes that allow for the electrochemical reaction of most chemical elements [58]. The use of molten salts unlocked the electrochemical deoxidation of TiO_2 [9], and even insulating materials such as SiO_2 has been electrochemically reduced [59].

Electrochemistry in molten salts has revolutionized the way we manufacture metals such as aluminium [53]. Still, they require the use of a supporting electrolyte which implies a fixed cost for the process and additional processing to separate the final product and recycle it. The Holy Grail of extractive metallurgy is to use the mineral deposit containing the metal of interest directly. As most metals in the Earth are bonded to either sulphur or oxygen, this reasoning gave birth to the two newest categories in electrochemical extraction of metals: molten oxide electrolysis [60] and molten sulfide electrolysis [61]. The electrolysis of molten ironmaking slag belongs to the former category as its composition is mainly a mix of oxides.

2.5 Principles of Molten Oxide Electrochemistry

The main objective behind any extractive metallurgical process that involves oxide ores is to accomplished the decomposition of the metal oxide (MO_2) into metal (M) and oxygen (reaction 2.10). This reaction is generally non-spontaneous and requires either work or heat [60]. This is the reason behind metals being present as ores and rocks in the Earth's surface. Traditionally, the combustion of fossil fuels (eg. reaction 2.3) has been coupled to reaction 2.10 as the source of the energy required to drive

the reaction, binding the metallurgical sector to the production of harmful emissions.

$$MO_2(s) \longrightarrow M(s \text{ or } l) + O_2(g) \tag{2.10}$$

Molten oxide electrolysis provides a shift in the status quo. It eliminates the direct process emissions as it does not require the coupling reaction. This process relies on the use of a molten metal oxide feedstock as the supporting medium (electrolyte) where the metal oxide of interest dissociates into its constitutive ions. Then, the charged species (cations and anions) are separated within the medium by applying a potential difference at the electrodes, where the electron transfer reactions occur.

The electrolytic cell is the device where this succession of physical events take place. The electrical charge (i.e. a potential difference) is transferred between two electrodes submersed in the ionically conducting liquid. The negatively charged electrode (working electrode or cathode) reduces the cations and deposits them as neutral metallic atoms. At the positively charged electrode (counter electrode or anode) oxidation produces gaseous evolution. The reaction depends upon the type of cell and electrode material used.

Using the decomposition of TiO_2, the metal oxide of interest in this work, as an example, if the counter electrode material used is inert under the reaction conditions, this process has the potential to emit only titanium metal and oxygen as products:

$$TiO_2 \longrightarrow Ti + O_2 \tag{2.11}$$

The cathodic reaction can be assumed to be:

$$Ti^{4+} + 4\,e^- \longrightarrow Ti + 2\,O^{2-} \tag{2.12}$$

And the anodic reaction:

$$2\,O^{2-} \longrightarrow O_2 + 4\,e^- \tag{2.13}$$

Electrons are collected from the anodic reaction and supplied to the working electrode via an external circuit. There the use of a potentiostat or power supply provides the driving force for the reaction to happen.

2.5.1 Thermodynamic and kinetic fundamentals

To assess the feasibility of using a molten oxide mixture, such as an ore or slag, as the chosen electrolyte for a MOE, the electrochemical window of operation needs to be defined. It is important that none of the components of the electrolyte are less stable that the metal oxide of interest [60]. Their stability can be compared by the minimum thermodynamic cell voltage (ΔE°) required for their decomposition and

it is given by:

$$E^{\circ}_{cell} = \frac{\Delta G^{\circ}}{-nF} \tag{2.14}$$

where ΔG° is the standard Gibbs energy of dissociation at the temperature and pressure of interest with products and reactants at unit activity, n is the number of electrons involved in the reaction, and F is the Faraday constant.

However, MOE systems do not operate at unit activity. Liquidus temperatures for oxide solutions tend to be above 1000 K. Moreover, these complex liquid solutions tend to present negative deviation from ideal behaviour, indicating short-range ordering [62]. The effect of the melt structure is particularly relevant for ironmaking slags where nuclear magnetic resonance and raman spectroscopy studies [63, 64] have consistently found a 3-dimensional interconnected network of tetrahedral silicate anionic units. The thermodynamic cell voltage (E_{cell}) is calculated from the Nernst equation and it varies as a function of the activities of the reactants and products:

$$E_{cell} = E^{\circ}_{cell} - \frac{RT}{nF} \cdot ln \frac{\prod a^{\nu}_{products}}{\prod a^{\nu}_{reactants}} \tag{2.15}$$

where R is the universal gas constant, T is the temperature of interest, ν are the stoichiometric coefficients and a_i are the thermodynamic activities of the species under cell conditions for the reaction.

Still, during electrolysis, the potential difference required to drive the process is going to be higher than the thermodynamic minimum calculated by the Nernst equation. The Hall-Heroult cell, for example, operates at voltages more than three times higher than the thermodynamic minimum [12]. Kinetics factors associated to ohmic drops and to the cathodic and anodic reactions require an increase in the energy consumption (overpotentials) that must be taken into account:

$$U_{cell} = E^{\circ}_{cell} + (\eta_a + \eta_c)_{cathode} + (\eta_a + \eta_c)_{anode} + \eta_{electrodes} + iR \tag{2.16}$$

where η_a and η_c are, respectively, the activation and concentration overpotentials at each electrode, which depend on temperature, current density and melt chemistry. $\eta_{electrodes}$ corresponds to the voltage drop associated to the electrode probes. The iR drop is the ohmic losses and is governed by the electrolyte's electrical resistance and distance between electrodes. Its value is optimized in MOE as certain ohmic drop is necessary to maintain thermal balance in the cell [65].

At the ultra-high temperatures required for MOE, reaction kinetics are expected to be very fast and, consequently, mass transfer is expected to determine the production rate. Therefore, detailed knowledge of the mass transport properties of the

chosen electrolyte is vital to optimize operation. Their characterization, for ironmaking slag, is the central part of this body of work.

2.6 Analytical Methods

2.6.1 Electrochemical techniques

Cyclic voltammetry (CV)

Cyclic voltammetry is arguably the most widely used technique to assess the thermodynamics and kinetics of electron transfer reactions. In this work it was used to identify the reduction and oxidation processes involving electroactive species in the electrolyte. It can also be used to obtain information regarding the electrode's active surface area and capacitance.

In this technique the potential of the working electrode is linearly scanned, forward and backwards (cyclic), between two potential limits at a constant scan rate (V/s). The resulting voltammogram is the measured current response vs the applied voltage. The shape of the voltammogram is commonly referred to as "duck-shaped" and it gives an idea of the chemical and electrochemical reversibility of the electron transfer reaction [66]. For a full discussion of cyclic votammetry one may refer to Brownson and Banks [67].

Electrolytic Polarization

This analytical method consists of measuring potentiometrically or galvanometrically the change to the potential-current relationship. Single step chronoamperometry is a technique where the potential applied at the working electrode is stepped to a final value and held for a period of time. If the potential was initially held at a value where no faradaic reactions occurred, the resulting current-time dependence recorded provides an estimation of change in concentration at the electrode surface [67].

Double step chronoamperometry is another useful technique where there is a second potential step that returns the final potential value to the initial condition. This current step technique is fully discussed in Chapter 7 where is used to estimate the individual contributions to the total electrical conductivity. Chronopotentiometry can also be an useful technique, as monitoring the potential as the current is held constant allows to compare, for example, the performance of different electrodes at a given current density.

2.6.2 Physicochemical techniques

X-Ray Diffraction (XRD)

X-ray diffraction is a technique used to characterize the structure of materials. This non-destructive technique is primarily used for phase identification of crystalline materials, but it can also provide structural information (unit cell dimensions, orientation of grains) [68], and mechanical properties such as strain in the crystalline lattice [69]. It is commonly used to characterize single crystals, but can also be used to investigate powders or polycrystalline solids.

It is important to remember, however, that this technique only provides information for the crystalline part of the sample, not amorphous. Also, it does not provide surface structure information as the incoming X-rays penetrate the material to probe its internal structure. An X-ray diffraction pattern is then a plot of the intensity of X-rays diffracted at different angles by the sample. X-ray scattering occurs when the angle of the incoming X-ray and that of a component of the crystal lattice share the same orientation. The resulting diffraction angle can be correlated to the particular crystal orientation using the Bragg relationship and, hence, XRD provides a method to identify crystalline phases. In this study, powder X-ray diffraction was used to qualitatively determine ironmaking slag's various mineral phases after cooling.

X-Ray Fluorescence (XRF)

The X-Ray Fluorescence spectrometry is a quantitative technique to determine a material's elemental composition. It requires minimal preparation and it can be used for powdered, liquid and solid samples [70]. During this non-destructive technique, the core-level electrons of a sample are excited by incident X-rays. The return of these electrons from the excited states results in the emission of fluorescent (secondary) X-rays. These X-ray signals are unique to the energy levels of each atomic species and, hence, when detected by the XRF detector they produce a characteristic spectrum for every element present in the material under study [71].

Since the intensity of the XRF signal correlates to the amount of atoms of a particular species that are present, depending on the XRF spectrometers' mode used, not only the elemental composition but also the thickness of the material can also be measured [70]. A limitation of the XRF is that it does not distinguish variations of isotopes or ions of an element, so valance states of elements such as titanium and iron cannot be determined [72]. XRF was used to investigate the chemical composition of the titanomagnetite ore and ironmaking slag. For both, the elemental composition is reported using an oxide basis.

Electron microscopy

Electron microscopy operates in a similar manner as conventional light microscopy but uses electrons instead of photons to probe the sample [73]. When the electron beam scans the sample's surface different techniques can be employed depending on which signal is read by the detector:

- In scanning electron microscopy (SEM), primary (backscattered) electrons and secondary electrons are emitted from the sample when the beam of electrons interacts its surface. The low energy level of the secondary electrons dictate that, in order to be detected, they must belong to the surface of the sample, and hence, they provide information about the surface morphology. The backscattered electrons are the beam's primary electrons that have been reflected back out of the sample after interaction with the atomic nuclei [74]. The resulting image can be used to study the element distribution in the sample as the reflection (backscattering effect) correlates with atomic number.
- Energy dispersive spectroscopy (EDS) provides a quantitative composition analysis by detecting the X-Rays emitted when electrons from higher-energy orbitals relax to fill the hole left by the secondary electrons ejected from the sample after the electron beam probed its surface. The emitted X-rays have a distinctive energy and wavelength, which, similar to XRF, allows to identify elemental composition of the sample.

In this work, SEM combined with EDS was used to investigate the materials used (e.g.. electrodes, slag and crucibles) before and after experimentation (e.g.. electrolysis, thermal treatment). The images produced were mainly used to investigate samples' morphology, topology, chemical composition and elemental distribution.

Simultaneous Thermal Analysis (STA)

Simultaneous thermal analysis is a powerful tool that allows the performance of different thermoanalytical methods at the same time, in one sample, and in a single instrument. Generally, it refers to the simultaneous application of a thermogravimetric analysis (TGA), and a differential thermal analysis (DTA) or differential scanning calorimetry (DSC). TGA measures the change in mass of a sample as a function of temperature or time. The changes in the sample under study are measured relative to a reference material and are associated with transitions in the material happening along the programmed thermal cycle.

During an STA measurement, the sample can be exposed to an inert atmosphere (i.e. nitrogen, argon), to an oxidizing environment (i.e. oxygen, air) or even to

reducing conditions (i.e. hydrogen) if specialized equipment is used. As TGA measures the gain or loss of mass, one can determine the thermal and chemical stability (e.g.. oxidation, dehydration, decomposition or phase transitions) of the sample under different experimental conditions [75].

DTA and DSC techniques share most of theory behind them. Basically, when the reference and the sample are identically heated, if the sample experiences a physical transformation heat will be absorbed or released (endothermic or exothermic processes) and, consequently, more (or less) heat needs to flow to the reference to keep it at the same temperature as the sample. The difference between both techniques is that DTA measures the temperature difference between the sample and reference, and DSC the heat flow difference. In both techniques, such difference can be associated with the sample's physical transformations [76].

The calibration of the reference material using inert standards is vital to obtain any accurate information. It is crucial that the reference material has a well-studied heat capacity over the range of temperatures of interest. These techniques are most commonly use to obtain information about a sample's liquidus and solidus temperature. However, a properly calibrated instrument can measured other phase transitions such as glass transition temperatures. It can also be used to measure polymerization, percent of crystallinity and heat capacity.

It is worth noting that the DSC technique that is used in a STA instrument is commonly refereed to as Heat-Flux DSC. Power Compensating DSC is another type of calorimeter technique that involves heating the sample and the reference in different furnaces. Different DSC methods for slag characterization have been successfully developed in the past [77, 78]. The application of these techniques helped to assess the phase relations of the ironmaking slag in this work.

2.6.3 Computational thermodynamic calculations

Due to the analytically complex nature of high temperature materials processing, the use of computational thermodynamic software is frequently required by material scientists and metallurgists. The methodology behind these thermodynamic software packages is the so-called CALPHAD [79] (CALculation of PHAse Diagram). This method feeds all the available thermodynamic information (i.e. experimental phase equilibria data, and thermochemical and thermophysical studies of a system) to mathematical models that perform the optimization of Gibbs energy functions to best match existing phase diagrams [80]. The thermodynamic models with optimized parameters are then used to predict unknown phase equilibria and thermochemical properties such as thermodynamic activities.

This is particularly useful when exploring complex multicomponent systems, like ironmaking slag, whose low-order subsystems are well studied. As the thermodynamic model that has been optimized for the binary and ternary subsystems will provide a good estimate of the higher-order system. It is clear then that the accuracy of the thermodynamic prediction will depend on the accuracy of the available thermodynamic data for the system under study, and on the accuracy of the Gibbs energy minimization routine used [62].

FactSage [19] is the most widely used thermodynamic software package in steelmaking. Per calculation, its Fortran routine to minimize Gibbs energy function can handle up to 40 elements and 1500 stoichiometric phases [62]. Since the early 2000s, their oxide database, FToxide, has been assessing and evaluating data for more than 23 elements. This database includes pure oxides, liquid solutions and oxide solid solutions. The solid solutions are modelled using the Compound Energy Formalism [81], which takes into account the crystallographic information of each solution.

Moreover, it uses the Modified Quasichemical Model for liquid solutions such as molten oxide (slag) systems or metallic liquid solution [19]. This model [82] was first introduced for molten slags and it takes into account the melt structure and uses the Ising model to describe the solution entropy of mixing. This is important for liquid solutions as quite often they exhibit negative deviations from ideal solution behaviour, indicating short-range ordering. This is especially relevant as most commercial software use the Brandon-Williams model that assumes ideal entropy of mixing [62]. Hence, FactSage meets all the prerequisites for accurate thermodynamic calculations involving molten ironmaking slag and it was chosen as the thermodynamic software package for this study.

Chapter 3

Literature Review

3.1 Introduction

During the 20th century alone, the world's population grew from 1.65 billion to 6 billion [83] and, consequently, the need for structural materials increased exponentially. To meet that demand, several metallurgical processes were developed and implemented to extract metals from their natural deposits. However, metallurgy is an energy, carbon, and waste-intensive sector. Today, the annual demand on resources exceed what Earth can regenerate in a year [84]. In an effort to meet the requirements for sustainable growth, pathways toward deep decarbonisation, waste minimization and reutilization are enforced by environmental regulation and encouraged by international agreements [85].

Optimizing the use of natural resources by recycling industrial waste is a potential solution to meet the current demand of materials in a sustainable manner. In steelmaking, where the production of solid waste is inevitable, extracting more value from metallurgical by-products appears vital to cope with the advances in the field of environmental regulation in the 21st century. In this work, we take a close look at the steelmaking process since with a yearly production of 1700 million tonnes in 2017 [23], steel is the most widely used alloy in the world. Accordingly, waste management in the steelmaking industry must be considered in order to meet the current needs without compromising the ability of future generations to meet their own needs.

The aim of this chapter is to demonstrate that the direct extraction of titanium from ironmaking slag by ultra-high-temperature electrolysis is the route to recycle this metallurgical by-product with the biggest disruptive potential from a New Zealand context. The following literature review:

- starts introducing the motivation of developing a new process for the production of titanium from ironmaking slag (Section 3.2).
- investigates the current uses for ironmaking slags and highlights the disadvantages of different methods that have been employed to treat them (Section 3.3).

- compares the available routes to produce titanium metal (Section 3.4).
- finishes by outlining the features and challenges of the chosen route, the electrolytic extraction of titanium from ironmaking (Section 3.5).

3.2 Slag, an Opportunity

Conventional steelmaking processing is dominated by the reduction of haematite in blast furnaces [85]. Nevertheless, titanium-bearing iron ores are an alternative source of iron. New Zealand has the capacity to produce 650,000 tonnes per year of iron and steel products, and holds more than 150 million tonnes of titanomagnetite mineral deposits [28]. China is also rich in titanomagnetite minerals, which are also used to produce steel. However, these mineral deposits are also an alternative source of titanium. So much so that China, which holds approximately 50% of the total titanium reserve in the world, has 98% in the form of vanadium-titanium magnetite ores [86].

Based on the yearly production of steel, between 320 to 384 million tonnes of ironmaking slag and 190 to 280 million tonnes of steelmaking slag are estimated to be produced [87]. In countries like China [15] and New Zealand, these slags are available as by-products of the local steelmaking processes, and can contain more than 30 wt.% TiO_2. Obtaining high-purity titanium metal from this inexpensive by-product, would be ground-breaking considering the current titanium price [23], and the high extraction and processing costs of the current commercial process [33]. This work explores the direct extraction of titanium metal from ironmaking slag. A process with the potential of minimizing environmental industrial impact by further utilization of titanomagnetite natural resources. Extracting not only iron but titanium would inevitably increase the value of ironmaking process's most abundant by-product.

3.3 Slag, a Resource

For every tonne of iron produced in the smelter, approximatively 300 kg of ironmaking slag is formed [88]. Without proper recycling, this large amount of slag can become a significant source of waste. Increasing global environmental awareness is forcing the metallurgical industry to meet their environmental responsibility. This may be achieved, in part, by minimizing and reutilizing the slags. Research attention has been drawn to the different types of industrial slags and their environmental consequences has been extensively characterized before [89]. However, it remains a great challenge today to, both, utilize the solidified slag while recovering the heat from the molten slag [90].

The disposal of ironmaking slag accounts for 10% of the waste energy in the steel industry since it is drained in its molten state at temperatures above 1500 K [91]. Based on China's 2012 steel production, Sun *et. al* [92] estimated that wasted heat corresponds to what would be produced by 16.5 million tons of standard coal. The opportunities for managing this waste have been studied before [93–95]. The existing heat recovery technologies are still in early stages of their development [90, 91]. Uncontrolled heat treatments, such as dumping and water quenching, are still the conventional method for disposal of slag. Since Roman times, uncontrolled heat treatments have limited slag recycling to civil engineering applications, such as road construction [93]. Fast cooling rates facilitates the vitreous solidification of these silicate glasses. Then, due to the similar chemical composition of slag to that of cement, fast-cooled slags meet the hydraulic properties required for cementing components [96]. That is the case in New Zealand, where the slag is used for road construction as an aggregate in open-graded emulsion mixes [7]. In Europe, where the reutilization ratio is high, still 35% of these slags are dumped [97].

The lack of land available for disposal, the shortage of water and the environmental concerns are preventing the continuity of these mainstream methods [98]. Interest has increased towards studying dry granulation as a substitutional technology [99]. This is a promising alternative which could be coupled to a heat recovery unit [100]. Despite that, its development has been hindered by cost-effective uncertainties [23]. Alternatively, controlling the heat profile when disposing the slag has the potential of expanding its potential uses, as the solidification step defines the applications for ironmaking slag [88]. Glass-ceramics materials can be produced this way. By controlling the heat treatment of the slag, the nucleation and growth of the crystalline phases dispersed in the glass's matrix can be tuned and, therefore, the physical and chemical properties of these materials can be tailored.

Research in this field focuses on optimizing compositions and thermal treatments to match the desired properties of the glass-ceramics. The possibility of engineering a material with high electrical resistivity, mechanical strength and low thermal expansion made missile nose cones one of their first applications [101]. Nonlinear optical properties and unusually high dielectric constants have been reported in glass-ceramics containing titanium [102]. Recently, glass-ceramic scaffolds have received noticeable attention in tissue engineering where they benefit from the bioactive properties of these materials, which can form chemical bonds with mineral components of bones [103, 104]. Manufacturing glass-ceramics materials from slag is a promising alternative that is currently understudied [88]. Today, the detrimental effect of the presence of iron and the required low basicity needed (CaO/SiO_2 ratio below 0.5 wt. %) limits the rate of utilization of ironmaking slag for this application [90].

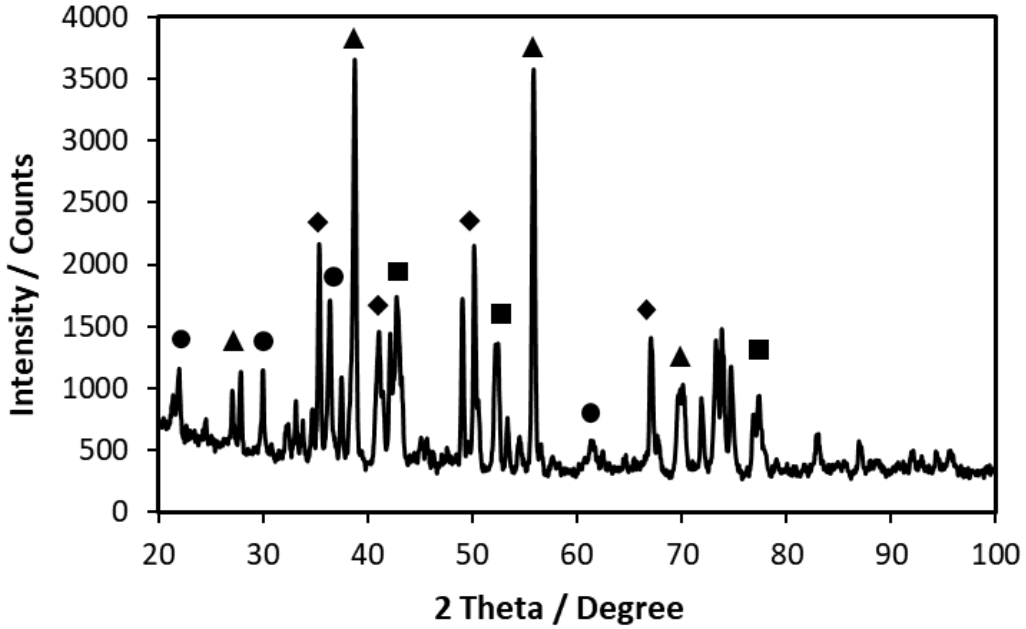

FIGURE 3.1: XRD analysis of ironmaking slag representative of the local process in New Zealand that shows perovskite (triangular shapes), armalcolite (circular shapes), magnesium iron aluminate (rectangular shapes) and calcium magnesium silicate (diamond shapes) as the main mineral phases.

Furthermore, to process the solidified slag remains a challenge. The recycling of slag back in the steelmaking process as a source of calcium or manganese can reduce material costs, but it can be harmful for the mechanical properties of the steel since phosphorus and sulphur are normally partitioned to the slag [105]. The selective crystallization and phase separation (SCPS) method [106] aims to increase the recyclibility of the slag. It uses controlled crystallization to enrich a phase with the undesired element that can then be separated. Although useful, this method does not address the poor volume stability caused by the expansion of CaO after hydration, which would still be a factor limiting slag reutilization [88].

Further metal extraction is the most disruptive route to improve the utilization of titanomagnetite ores. In particular, the extraction of titanium, as it is the highest value component of the slag. Research exploring its extraction has highlighted the difficulty of recovering metallic titanium through traditional separation processes [107]. She *et al.* attributes this difficulty to the scattered distribution of titanium components in various mineral phases with complex interfacial combinations [108]. X-ray diffraction was used in this work to confirm that complex phase distribution. Solidified ironmaking slag representative of the local process in New Zealand (see Figure 3.1) is an array of at least 4 primary mineral phases: perovskite ($CaTiO_3$), armalcolite ($Mg_{0.5}Fe_{0.5})Ti_2O_5$), magnesium iron aluminate ($Mg(Fe_{0.6}Al_{1.4})O_4$) and calcium magnesium silicate ($Ca_{0.8}Mg_{1.2}$ Si_2O_6).

It seems obvious that a different approach is needed to find a solution that unlocks further utilization. Recently, molten oxides have been proven as candidate electrolytes for high-temperature, carbon-free metal electrolytic production [109, 110]. Along those lines, the electrolytic separation of titanium metal from ironmaking slag directly from the industrial process, in its molten state, has the potential to be a game changing opportunity. Extracting valuable metals from molten slag is proposed as a solution in this work that would allow us to tap into all the titanium content while still utilizing the available heat. The next section justifies electrolysis as the chosen route by reviewing the established and R&D titanium manufacturing technologies.

3.4 Slag, a Source of Titanium

As discussed in the previous chapter, the inability to explore the full potential of titanium is due to its high manufacturing cost. According to a study by Norgate and Welwood [111], a 50% fall in the price of titanium could overcome its current restriction to high-added value applications, increasing its use by 200%. While such a price drop appears to be unrealistically large, their results show a great potential for market penetration influenced by the production cost. Consequently, research on cost effective alternatives to produce titanium metal has received noticeable attention [112].

It is worth noting that research into cost effective alternatives did not stop with the development of the Kroll Process and large scale commercialization plants. The intended users of a more affordable titanium metal drove it [47]. In the 1950s military space applications drove the entire market [31]. In the early 1990s, the end of the Cold War and the changes to missile-based defense meant a collapse in the demand of titanium metal. Domestic application in consumer goods then entered the market [43]. In recent years, the wide range of titanium's application such as structural engineering (potential substitute of steel) or medicine (implants) has led to an increase in the research intensity (see Figure 3.2).

In fact, the research interest on studying titanium extraction has multiplied by a factor of four in the past ten years (blue bars in Figure 3.2), based on the number of specific entries in the *Scopus* database. The amount of research focused on using an electrolytic route to produce titanium has also notably increased (red bars in Figure 3.2), in particular since the year 2000. In that year, pioneering research efforts by Chen *et al.* [9] demonstrated that high purity titanium could be also obtained from the electrolysis of a titanium-bearing oxide. The announcement of the direct electrochemical extraction of Ti metal from solid TiO_2 in molten $CaCl_2$ salt, the FFC process, probably triggered the current pace of extraction projects involving electrolysis [38].

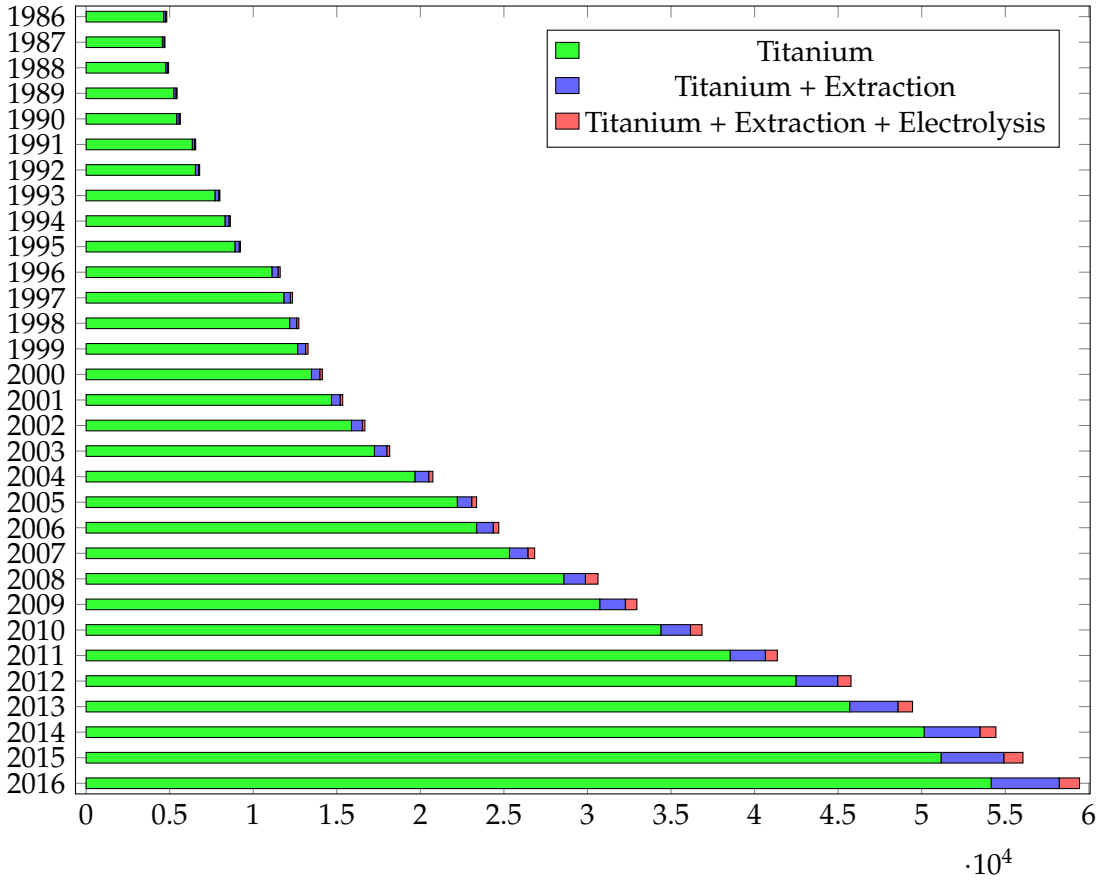

FIGURE 3.2: Number of titanium specific database entries per year using the keywords indicated in the legend. According to *Scopus* database.

3.4.1 R&D performance evaluation

New cost-affordable titanium routes have attracted noteworthy research attention with many extraction processes under development [113]. The consultant Roskill stated in 2007 that there were over 20 active R&D projects [114]. It is particularly hard to elucidate how advanced any particular project actually is since most of these developing processes have unpublished associated intellectual property (i.e. trade secrets). Yet, Table 3.1 provides an overview of the main work published.

It should be stated that the intention of this section is not to provide a detailed description of the available literature, which can be found elsewhere [33, 36, 38, 39, 43–45, 47, 50, 113, 114], but a performance summary that justifies the chosen process to develop in this thesis. These projects were classified (see Table 3.1) and assessed according to the type of precursor, reductant, and reaction route used:

Precursor

Historically, titanium tetrachloride has been used as the precursor for the production of titanium. It was thought that only by transforming the ore into a compound, which contains no oxygen or carbon, high purity grade metal could be yielded. Recent research has proven that wrong [9]. Furthermore, the use of different precursors could potentially halve the extraction cost since it is estimated that 52% of the titanium sponge's (i.e. raw form of the metal in the Kroll process [47]) production costs come from the preparation of $TiCl_4$ [38].

However, from the point of view of those precursor production, $TiCl_4$ is the cheapest option. TiO_2 is more expensive than $TiCl_4$, as the latter is a precursor used in TiO_2's most common production route [36]. Additionally, high purity grade TiO_2 is, itself, a product [45]. The use of fluorotitanates would not be cheaper than TiO_2 since their production requires a more complex process and it is not produced at large scale. Nevertheless, at an industrial level, the possibility of recycling fluorides could decrease the cost significantly [115]. The use of other titanium halides such as TiI_4 has been considered [41], but the high cost associated with iodine has shifted away large-scale commercialization approaches [45].

Direct extraction from ore or slag would be the ideal solution because it would eliminate the costly production of an intermediate precursor. Attempts have been made [109, 116], but the maturity of the Kroll process attracts the major part of the investment and academic coverage (see Table 3.1).

Reductant

TABLE 3.1: Classification of the different research projects for producing titanium metal reviewed, adapted from [117].

PROCESS NAME / ORGANISATION	DESCRIPTION		COUNTRY	PRODUCT	ROUTE	PRECURSOR	REDUCTANT
TIRO / CSIRO	Fluidized bed $TiCl_4$ reduction with Mg	[118]	Australia	Powder	Chemical	$TiCl_4$	Mg
Armstrong / ITP	$TiCl_4$ vapour reduction with Na	[119]	USA	Powder	Chemical	$TiCl_4$	Na
Idaho Titanium Tech.	Hydrogen plasma reduction of $TiCl_4$	[120]	USA	Powder	Chemical	$TiCl_4$	H_2
SRI International	Fluidized bed $TiCl_4$ reduction with H_2	[121]	USA	Powder	Chemical	$TiCl_4$	H_2
Tresis International	Argon plasma reduction of $TiCl_4$	[50]	USA	Liquid titanium	Chemical	$TiCl_4$	Mg/Na
Ginatta / GTT S.R.L.	$TiCl_4$ electrolysis in molten salt	[122]	Italy	Liquid titanium	Electrolysis	$TiCl_4$	e-
Polar Titanium / BHP Billiton	TiO_2 electrolysis in molten salt	[123]	Australia	Liquid titanium	Electrolysis	TiO_2	e-
CSIR	TiO_2 electrolysis in molten CaF_2	[124]	South Africa	Liquid titanium	Electrolysis	TiO_2	e-
DMR	TiO_2 aluminothermic reduction	[50]	USA	Liquid titanium	Chemical	TiO_2	Al
Preform Reduction / Tokyo University	TiO_2 reduction with Ca	[125]	Japan	Powder	Chemical	TiO_2	Ca
MIR-Chem	TiO_2 reduction with I_2	[126]	Germany	Powder	Chemical	TiO_2	I_2
EMR-MSE / Tokyo University	TiO_2 calciothermic EMR in molten salt	[127]	Japan	Powder	Electrolysis	TiO_2	e-
FFC / Metalysis	Sintered TiO_2 electrolysis in molten $CaCl_2$	[9]	UK	Powder	Electrolysis	TiO_2	e-
MER Corp.	TiO_2 carbothermic reduction followed by electrolysis	[128]	USA	Powder	Electrolysis	TiO_2	e-
OS / Kyoto University	TiO_2 calciothermic reduction in molten $CaCl_2$	[129]	Japan	Powder	Electrolysis	TiO_2	e-/Ca
QIT / Rio Tinto	Molten Ti slag electrolysis	[116]	Canada	Liquid titanium	Electrolysis	Slag	e-
MOE / MIT	TiO_2 electrolysis of molten Ti oxides	[109]	USA	Liquid titanium	Electrolysis	Slag	e-
Peruke (Pty) Ltd.	Fluorotitanate reduction with Al	[115]	South Africa	Powder	Chemical	M_2TiF_6	Al
SCPS / Peking University	Selective crystallization and phase separation	[86]	China	Liquid titanium	Other	Slag	
HDH	Ti hydride–dehydride process	[130]	USA	Powder	Other	$TiCl_4$	Mg

Changing the reducing agent of the process is another source of new routes. Magnesium, sodium, hydrogen, aluminium, calcium and electrons are the main reductants considered. Other metals, such as lithium or potassium, could be used but their high cost have limited their research [36]. The use of magnesium is the preferential industrial way. It requires less energy to be produced than sodium and calcium, but its low solubility makes the purification process complex [38]. Sodium facilitates the separation, but the high vapour pressure of NaCl makes the process potentially dangerous [45]. Calcium's high solubility and ability to remove oxygen provides a particular advantage when TiO_2 is reduced, but it is twice as expensive as magnesium [47].

Out of the metals, aluminium's low price could make it the most attractive alternative. However, titanium reacts with aluminium forming an alloy that makes separation or recycling of by-products difficult [43]. Hydrogen is used in the SRI International and Idaho Titanium Technologies processes to reduce $TiCl_4$. Although it has a relative low price when is produced from natural gas or oil, the low conversion of the reaction results in the need for large amounts of the reductant and recycle systems [45]. Iodine is used in the Mir-Chem process for the reduction of TiO_2. Reduction of the reaction's dwell time may be needed to achieve low cost titanium [44]. Scarce information is available from this collaboration between the company and Bremen University.

Electrons are the most promising option, as the use of electricity eliminates the need to separate the reducing agent from the product. Different processes are under study using the conventional halide precursor (Ginatta) or titanium dioxide (FFC, EMR-MSE, OS, MER, CSIR, BHP). The technology for the direct electrolysis of the titanium ore or slag (MIT, QIT) has been improved over decades, but suitable electrolytic cells for the electrowinning of titanium have not been scaled up yet [45]. Efforts have not ceased.

Route

Electrolytic or metallothermic reduction are the two main potential routes to reduce the precursors. However, the hydride-dehydride process (HDH) and the selective crystallization and phase separation (SCPS) are examples of two non-conventional extraction processes which are under study. The HDH process modifies the Kroll Process to continuously produce Ti powder by hydrogenating the Ti sponge, crushing it to the desired size and dehydrating it [39]. Optimisation work on this process has continued since 1961 [130]. It allows scrap Ti metal to be used as feedstock and reduces the cost notably if the reduction and hydrogenation steps are combined [47]. The demanding operational and safety requirements to yield specification are a drawback for industrial scalability [131]. The SCPS process corresponds to

the current effort in China to characterize vanadium-titanium magnetite ores, their biggest source of titanium [132]. Their goal, similar to this doctoral work, is to extract titanium from the slag. Their approach is different, selective crystallization for Ti-rich phase separation [86]. Their work is still at a laboratory scale.

In the quest for cost affordable titanium, modifying the conventional Kroll and Hunter processes has attracted noticeable attention. Processes based on the reduction of $TiCl_4$ by Mg (TIRO) or Na (Armstrong) have been developed. The search for process simplicity and time reduction are common in the new projects. Both processes reduce the operating and capital costs by changing the operation mode to continuous [38]. The commercialization of the Armstrong process is one of the most advanced, but the effectiveness of the complex purification process, when scaled, remains to be seen [133]. A common challenge for both processes is the difficulty in the control of the oxygen content in the titanium powder product [47].

Even though a large number of new processes have been investigated, there is no process to date that can replace Kroll at a commercial scale. Some concepts have been successful at a pilot plant scale and companies such as Metalysis are commercializing their developments [134]. However, no process will be able to compete with the conventional one until the economics of scale are achieved [47]. The lack of commercial success can be attributed as well to industry's immobility. There is an interest in the industry for more affordable titanium but there is also a need of amortizing the current plants and investment. Allanore argues, "if you don't pay for the environmental costs, and you have a steel plant that needs to be valuable for the next 30 years, there is no way you're going to change your technology" [135]. Nevertheless, the current push for sustainability growth and environmental awareness are reasons to be optimistic.

For the foreseeable future, any modern-day substitutes must address the availability and cost concerns derivative from the incumbent Kroll process. Then, in order to be realistic and scalable, the new process must present an improvement concerning its environmental hazards and process complexity issues [60]. Accordingly, an electrochemical process for the extraction of titanium is the route with the highest potential to displace the Kroll process [53]. This promising route has been proven by recent research published in the highest-ranking international journals [9, 10]. Furthermore, the direct electrolysis of an oxide ore to obtain metal and oxygen has attracted organizations like NASA or the U.S. NAVY who, intrigued by the possibilities that the new process could offer, have financed its study [55, 109]. Thus, this thesis is attracted to determine the feasibility of direct electrolytic extraction of titanium from ironmaking slag as a new route to high-purity titanium that aligns well with the values of a circular economy.

3.5 Electrolytic Production of Titanium

The electrolytic manufacturing of titanium is attractive because titanium is abundant, has many of the common refractory metal characteristics and a high near term market potential [54]. Furthermore, capital and operating cost of electric power are not new to the conventional titanium extraction processes as molten salt electrolysis is used in the Kroll and Hunter processes [47]. William J. Kroll, himself, predicted in 1953 that his metallothermic process would be displaced by an electrolytic route in 15 years [38]. It is legitimate to wonder then what is stopping the creation of an electrolytic route that can have the same positive effect that the Hall-Heroult process had in the aluminium industry. This process, invented independently in 1886 by Charles Martin Hall and Paul Heroult, changed aluminium from a precious metal to a commodity [53]. The answer is that the electrochemical processing of titanium has some major differences with well-established practices such as aluminium processing, which makes it more challenging.

The melting point of titanium is 1273 K higher than aluminium. The typical operating temperatures of electrolytic cells to electrowin lithium, sodium and magnesium are 723, 853 and 853 K respectively, while for titanium it would have to be above 1933 K to have liquid metal as a product [43]. If the product were solid, there would be another obstacle to overcome since solid-state deposition tends to result in nucleation and dendrite formation, which facilitates reoxidation [38]. Additionally, aluminium has only one stable valence while titanium has several, resulting in electronic conductivity and loss of current efficiency [133]. The possibility of contaminating the titanium product with carbon calls for more restrictive material constraints, and makes the mechanical design of the electrochemical cell a more complex task than for the commercially successful Hall-Heroult cell, which uses graphite electrodes [45].

The challenges discussed above have contributed to the failure of Kroll's prediction, but considerable research attention has been drawn since then [47]. Early on, an electrolytic route to reduce $TiCl_4$ was studied. The main drawbacks that stopped the development of that process were the low solubility of $TiCl_4$ in molten salts, the solid-state deposition difficulties, and the facility to reoxidize the product. However, work carried out by M. V. Ginatta [122] since the early 1980s has been successful at producing liquid titanium in such a fashion. The process uses a multilayer cathodic interphase to separate the molten titanium from the mixed fluoride-chloride electrolyte. The complexity of the reactor and the long process time at extreme conditions have limited its scalability to a pilot plant. Today it is clear that, if the objective of a new electrochemical process is to displace the incumbent Kroll process, $TiCl_4$ could not be used. The new process would have to present important economic benefit and that will not happen using $TiCl_4$, which represents half of the titanium

sponge production cost [38].

3.5.1 Slag, a suitable electrolyte

It was not until the year 2000 that the use of an alternative, non-chloride, route became a popular solution. The so-called FFC process [9] presented a simple electrochemical route for the direct cathodic reduction of solid TiO_2 in a molten salt. This discovery was important because, with the exception of molybdenum, all refractory metals (considering as such the chemical elements, including titanium, found in the Groups 4, 5 and 6 of the Periodic Table) are present in oxygen-bearing compounds [56]. This work increased the research attention in the reduction of titanium directly from an oxide ore.

Some significant examples are the OS process developed by Ono and Suzuki [129] and the EMR-MSE process [127], which is more complex but prevents the contamination of titanium utilizing an "electronically mediated reaction" (EMR) to avoid physical contact. Work by Okabe and Sadoway suggests that the metallothermic reduction is an electronically mediated reaction rather than strictly a chemical reaction [51], hence, contact between reactants is not necessary. The differences between both processes can be explained by the rate limitations of electron transport between the reactants [49]. Both of these technologies come from universities in Japan, where their study is still ongoing.

However, the direct use of TiO_2 is an obstacle limiting less expensive titanium production. The high purity required implies that TiO_2 must be previously manufactured to be worthwhile [43], turning it into a product itself. In the Hall-Heroult process, bauxite is refined to obtained pure alumina, a fraction of which is then dissolved in a supporting electrolyte (i.e. cryolite). It is obvious then that to create an electrolytic process, which is the real analogue to the Hall-Heroult process, first a suitable electrolyte from which dissolved titanium would be electrolytically reduced needs to be found [60]. The choice of a suitable electrolyte is the process enabler [53].

Metal reactivity delimits the choice of electrolyte [57]. Aqueous solutions are used for metals that can be electrochemically reduced more readily than H_2 is evolved from water or that rely on the kinetics of H_2 evolution being slow enough to have a negligible effect in the efficiency of the electrolysis. Zinc and copper are the main examples of metals extract from aqueous solutions, but manganese and cobalt are extracted that way as well [136]. An advantage of these processes is that the cell temperature is relatively low (308 K for zinc and cooper, and from 323 to 338 K for cobalt [136]). However, on the other hand, the ore has to undergo different stages before electrolysis (e.g. leaching, purification), which increases the production cost and diminishes the sustainability of the process.

TABLE 3.2: Standard reduction potentials in decreasing order.

Reduction half-reaction	Standard reduction potentials / V
$Cu^{2+}(aq) + 2e^- \longrightarrow Cu(s)$	+0.34
$2H^+(aq) + 2e^- \longrightarrow H_2(g)$	0.00
$Co^{2+}(aq) + 2e^- \longrightarrow Co(s)$	-0.28
$Zn^{2+}(aq) + 2e^- \longrightarrow Zn(s)$	-0.76
$Mn^{2+}(aq) + 2e^- \longrightarrow Mn(s)$	-1.18
$Ti^{2+}(aq) + 2e^- \longrightarrow Ti(s)$	-1.63
$Al^{3+}(aq) + 3e^- \longrightarrow Al(s)$	-1.66

The traditional aqueous electrolytes are not suitable for refractory metal extraction [56]. The standard reduction potentials[1] for these metals are so negative that the overpotential and thus rate constant for H_2 evolution will be high enough that the H_2 evolution will dominate over metal deposition. That is also the case for titanium (see Table 3.2), where the electrolysis in an aqueous media would result in the liberation of hydrogen and oxygen [38]. Consequently, non-aqueous solutions must be exploited.

The use of molten salts for electrolytic extraction has its hallmark in the Hall-Heroult process for aluminium [53]. Liquid metal is obtained by an electrolytic reduction of pure alumina in a molten cryolite bath (81 wt.% Na_3AlF_6, 11 wt.% AlF_3, 5 wt.% CaF_2) at approximately 1233 K. In aluminium smelting, 60% of the electrolytic extraction cost comes from electricity [24]. Electricity's low cost, simple process, and continuous mode of operation has allowed it to become the main route to aluminium metal. Magnesium is another metal that is reduced in a molten salt, mainly, for its use as reductant in the Kroll process, which drives the world's production of this metal [56]. Magnesium is also produced industrially via thermal reduction of magnesium oxide, mainly in China [137].

The fact that some electrochemical processing techniques are industrially mature practices does not prevent the presence of unresolved challenges. In aluminium smelting, the lack of suitable materials for the construction of the Hall-Heroult cell presents a limitation in the productivity of the process [54]. Furthermore, it is far from being a carbon-free extraction technology. The carbon consumption (0.45 kg of carbon per 1 kg of Al) is the main concern, and so the quest for a non-consumable anode has become the ultimate material challenge [138]. Following a conventional approach is an obstacle limiting the development of a technology that is environmentally respectful and produces cost-affordable titanium.

[1]The standard potentials are all measured at 298 K, 1 atm, and with 1 M solutions. They indicate the ease of reduction for a specie in an aqueous solution. The more positive the reduction potentials, the greater the likelihood of being reduced. If the value is negative, then hydrogen reduction from the aqueous solution will compete with the reduction of the desired specie.

Sadoway [60] realized that a change of paradigm was going to be needed to cope with these constraints and his group at MIT was one of the first to use a molten oxide feedstock as an electrolyte. The direct electrolysis of an oxide ore or a slag is a process capable of emitting only valuable products. The so-called molten oxide electrolysis (MOE) process enables the production of liquid metal at one electrode and the evolution of oxygen at the other electrode. This process is a simpler, one stage process that reduces energy consumption and CO_2 emissions [10]. All of these are advantages over the existing production methods.

With all this potential, it is reasonable to ask why the use of molten oxides as electrolytes has not gained more relevance as an alternative to traditional processing. The answer may be motivated by the cost, scarce information available and constraints in the choice of materials for cell construction [110]. Nonetheless, new opportunities are emerging with advances in the field of environmental regulation that aim to charge traditional practices a cost associated with the emission of CO_2 to the atmosphere [85]. Additionally, advances in material science are allowing researchers to overcome the electrolytic cell's construction difficulties by tailoring the composition and structure of construction materials [139] and taking on new experimental approaches [13].

It is the author's opinion that the current push for sustainable growth can portend the renaissance of this technology, facilitating clean electrochemical technology to replace the current one, which is incapable of meeting tighter environmental regulations. The industry has realized that and has started to patent their developments [116, 140–143]. Consequently, this literature review motivates experimental exploration to verify the feasibility of using ironmaking slag as an electrolyte.

3.6 Summary

The extraction of further value from ironmaking slag, an industrial by-product, has been investigated. Emphasis has been placed on understanding the unique features of titanium manufacturing. The recycling possibilities for ironmaking slag obtained from the processing of ironsand have been discussed. This literature review elucidates the timely need for a new process to extract titanium at a lower cost.

Several attempts have been made in the past with limited success, but the requirements for the new operation are now clear. The new process needs to be less time consuming than the conventional Kroll process. A simpler process, preferably continuous, could reduce capital and labor costs by 10% to 15% [48]. Additionally, it should present an improvement in sustainability. Severe environmental hazards such as the risks associated with the purification of $TiCl_4$ (i.e. possible formation

of HCl), the low efficiency (7257 kg of input metal are needed to yield 2743 kg of high grade Ti [44]) or the high energy consumption (98.68 kcal per kg are required to extract the metal in ingot form [144]) should be tackled.

The electrolytic extraction of titanium from ironmaking slag is a process that can potentially meet all those requirements. The possibilities that such a process could offer has attracted New Zealand's Ministry of Business Innovation and Employment to finance its study. This novel approach will be explored in the following chapters where extensive research was conducted to verify the feasibility of the proposed hypothesis in a purpose-built, lab-scale, ultra-high temperature electrolytic cell.

Chapter 4

Implications of the Direct Use of Slag from the Ironmaking Processes as a Molten Oxide Electrolyte

Abstract

The thermochemical and electrical behaviour of ironmaking slag produced from titanomagnetite concentrates was assessed in the vicinity of its liquidus temperature. A combination of electrochemical measurements in a modified thermal imaging furnace and computational thermodynamic calculations were employed to elucidate its potential use as a molten oxide electrolyte for the extraction of titanium metal. The results show that the presence of entrained iron species in the ironmaking slag decreases the faradaic efficiency of the electrolysis and would contaminate the final metallic product. Thermodynamic predictions reveal a small electrochemical window of operation between the decomposition of silica and titania, which might result in the co-reduction of titanium and silicon ions from the melt. Practical considerations based on the present work on the electrochemical production of titanium metal directly from the ironmaking process are discussed, and a further experimental investigation of the electrochemical behaviour of this material is justified.

4.1 Introduction

With the increase in environmental awareness and the world's population predicted to reach 10 billion by 2050 [145], society expects metal extraction industries to revisit their technologies for alternative solutions to meet current and future demand for materials in a sustainable manner. Aluminium's change from precious metal to commodity has demonstrated the potential of electrochemical processing to mass-produce high purity metals at lower cost than the more traditional pyrometallurgical processes [53]. The direct electrochemical decomposition of metal-bearing

compounds has been proven as an alternative carbon-free production route [9, 10], capable of minimizing the total use of carbon or fuel compared to the current metal extraction processes. The electrolysis of iron in a molten oxide electrolyte [146] and copper in a molten sulfide [147] are promising solutions, where O_2(g) and S_2(g) are the only by-products. While molten sulfides remain understudied [24], recent governmental efforts to cut down carbon dioxide emission have brought research attention to molten oxide electrolysis (MOE) as an alternative to decarbonize the metallurgical sector [85].

The direct electrolysis of molten ironmaking slag has been postulated [16] as a promising alternative to address the universal need to recycle large-scale waste materials. These slags can contain up to 30 wt.% TiO_2 [16] and are available at 1773 K as a by-product of the ironmaking process in countries such as China, South Africa and New Zealand. The use of this material as a molten oxide electrolyte has the potential to reduce emissions to the environment, stop land-fill disposal [148], and reduce energy inefficiency of the overall steelmaking process [91]. Processing the slag does not involved any mining costs compared with ilmenite, the most common feedstock for titanium production. In fact, based on the relative content of each material[1], ironmaking slag is more than 10 times cheaper than ilmenite as a source of titanium. Today, steelmaking companies typically contract outside processing companies to get rid of the slag. These companies tend to receive the slag for free, process it, and pay a small percentage of the sale revenue back to the steelmaker [150].

The extraction of titanium metal from slag has been studied in the past with limited success [107]. The scattered distribution of titanium in various mineral phases with complex interfacial combinations yields very low recovery rates with the use of traditional separation techniques in cooled slag [108]. The use of the slag directly from the process, in its molten state, to electrochemically extract high-purity metal is proposed in this work as a pathway towards clean metal production that enables tapping into all the available titanium and uses the embodied heat.

One of the major challenges towards this clean metal production route is the complexity of determining the properties of the electrolytes at the operating temperatures. The high temperatures required for operation and the highly corrosive nature of the oxide melts have traditionally imposed very demanding material constraints [14, 151], hindering the required characterization at temperature. Schiefelbein and Sadoway [152] pointed to silicate melts as promising candidate electrolytes for MOE, but highlighted the general lack of data to asses the properties of the melts. Experimental data is scare and only available for selected temperatures

[1]Calculations were made based on slags with 30 wt.% TiO_2 [16] and 54 wt.% TiO_2 for ilmenite [149]. Selling prices for air-cooled ironmaking slag average 8.53 USD per tonne [150] and 180 USD per tonne for ilmenite [149].

and composition ranges [153], so researchers mainly rely on empirical models [154] backed by computational thermodynamic calculations [62]. Nevertheless, motivated by recent technological advances [13], this work provides a comprehensive study of ironmaking slags, produced from titanomagnetite concentrates, with respect to its use as an electrolyte in prospective high-temperature electrochemical processes.

For the practical implementation of an electrochemical route to extract titanium the ironmaking slag should, at the operating conditions, (a) have high solubility for TiO_2, (b) be molten, (c) have sufficient ionic conduction, and (d) present metal oxide constituents that are thermodynamically more stable than TiO_2. When considering the industrial application of such a route, there are, of course, additional properties that an ideal electrolyte should possess to optimize the process for commodity metal extraction standards. The electrolyte should be inexpensive and, ideally, be benign to the environment. This material needs to be stable at the range of oxygen partial pressures experienced at the electrodes. Additionally, in order to efficiently harvest the metal produced, the electrolyte must be less dense than the product, and have low viscosity so it facilitates the movement and separation of charged species. Also, ideally, if a liquid metal pool is formed, the electrolyte should wet it.

In this work, a combination of electrochemical measurements in a modified thermal imaging furnace and computational thermodynamic calculations was used to characterize the use of ironmaking slag, directly from the ironmaking process, in an MOE cell. The aim of this paper is to assess the feasibility of extracting titanium metal from ironmaking slag. Consequently, the focus was set to investigate the potential constraints arising from operating directly from the process, i.e. presence of entrained iron in the slag; the electrical conduction of the slag, in particular, the fraction of the charge that goes to the reaction of interest; and the thermodynamic stability of the melt components, crucial for an efficient process and a pure metal product. This paper provides the knowledge required for an effective use of the ironmaking slag as electrolyte in an MOE process, and highlights the effect of iron, often overlooked in the literature where ironmaking slag is normally treated as $TiO_2 - SiO_2 - Al_2O_3 - MgO - CaO$.

4.2 Experimental

4.2.1 Sample - origin

In ferrous metallurgy, the raw materials used determine the amount of titania present in the slag phase formed during the ironmaking process. In New Zealand and China, the fraction of titania in the slag comes from the use of titanomagnetite deposits, commonly referred to as ironsands, as the source of iron in the ironmaking

TABLE 4.1: Titanomagnetite sand, primary concentrate and synthetic ironmaking slag compositions (wt.%) measured by XRF.

	TiO_2 wt.%	CaO wt.%	SiO_2 wt.%	Al_2O_3 wt.%	MgO wt.%	Fe_3O_4 wt.%	MnO wt.%	V_2O_5 wt.%
Titanomagnetite sand	1.8	12.6	46.2	9.0	8.6	12.9	0.4	0.1
Primary Concentrate	7.9	0.5	2.3	3.7	2.9	81.4	0.6	0.5
Slag#1	32.5	16.4	13.8	18.5	13.6	4.3	0.9	0.2

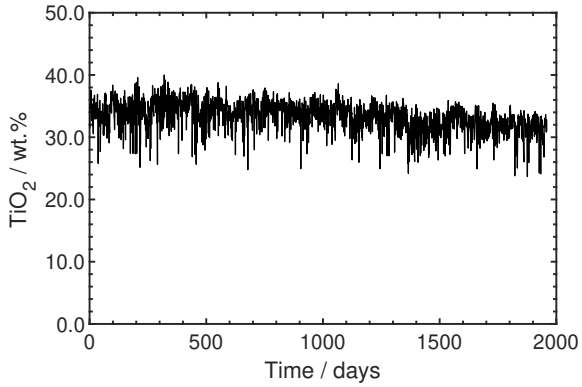

FIGURE 4.1: Daily measurements of the TiO_2 concentration for tapped ironmaking slag representative of the local process in New Zealand over a period of four years, 2013-2017. Data supplied by Blue Scope Steel.

proces [16]. These mineral deposits are first concentrated by magnetic and gravity separation processes [4]. Davis Tube tests [155] indicated that the strongly magnetic constituents separated are rich in iron and correspond to 20 wt.% $\pm$ 5 wt.% of the total sand weight. This concentrate, commonly referred to as primary concentrate, is the feedstock of the ironmaking process alongside coal and the fluxes.

Depending on the type of process, the last steps of the reduction occur in a blast furnace or in an electric melter. In both cases, the reduced, more dense, iron metal sinks to the bottom of the vessel, whence it is drained and collected. On top of the iron, an oxide layer is formed containing all the remaining elements. This less dense, left-over material is what is commonly referred to as slag, and it can contain a certain amount of trapped iron. The compositions of titanomagnetite sand, primary concentrate and ironmaking slag samples representative of the local, New Zealand ironmaking process were measured by x-ray fluorescence spectroscopy (XRF, Siemens/Bruker SRS3000), and are reported in Table 7.1. The multivalent species, iron and titanium, are reported as wt.% Fe_3O_4 and TiO_2, respectively, as the samples were heated to 1273 K to obtain the most stable oxides before the XRF measurement.

In 2019, between 320 and 384 million tonnes of ironmaking slag were produced worldwide [87]. With an average of more than 30 wt.% of TiO_2 dissolved within, ironmaking slags from titanomagnetite concentrates present concentrations of the

target metal cations higher than common industrial electrolytes such as cryolite [60]. From such a standpoint, the high solubility of the metal cations of interest in this molten oxide system makes it an ideal candidate for future industrial applications [24]. Furthermore, its stability over time is an important parameter that influences the quality of the final product (see Figure 4.1).

4.2.2 Analytical methods

A thermal imaging furnace (TX-12000-I-MIT-VPO-PC, Crystal Systems Corp.) that had been previously modified to carry out electrochemical measurements [13] was used to study the electronic conduction of the slag without container compatibility constraints. This containerless method uses the pendant droplet technique to configure the electrochemical cell, which has been described and illustrated elsewhere [156]. UHP Ar (99.999%, Airgas Inc.) was used inside the furnace during operation at a flow rate of 200 mL min^{-1} yielding a partial pressure of oxygen of 10^{-6} atm. The furnace lamp power-sample temperature relations were determined for the various samples by contacting the molten droplet with a type C (W–Re (5 wt.%) | W–Re (26 wt.%)) thermocouple.

Stepped-potential chronoamperometry was used to perform transference number measurements in the thermal imaging furnace. Fried *et al.* [157] proved this technique capable of differentiating between the ionic and electronic conduction in titanate melts. Chapter 7 reviews the use of this technique in molten oxides, acknowledging its limitations, and adapted the technique to obtain an estimation of the partial contributions to the total electrical conductivity. The electronic (t_e) and ionic (t_i) transference numbers obtained have been used before to quantify the current associated to the flow of electrons (I_e) or ions (I_i), respectively, in mixed conductor media [157–162], where both contributions sum to unity:

$$t_i + t_e = \frac{I_i}{I_t} + \frac{I_e}{I_t} = 1 \tag{4.1}$$

For each measurement, iridium wires (Ir > 99.9 %, diameter = 0.5 mm, Furuya Metals Co. Ltd.) were used in a three-electrode configuration inside an Al_2O_3 four-bore tube. Using a potentiostat (Gamry Reference 3000), the open circuit potential was recorded to confirm that the electrodes had contacted the molten slag droplet. For each transference number measurement, the working electrode was maintained at open circuit potential for 15 s before being stepped to 0.01 V vs Ir for 30 s. 100 measurements per second were recorded to accurately captured the potential step. The transference numbers can be calculated from the current response to the potential step as a function of time [158]. In particular, the electronic transference number is calculated by dividing the initial ($t \to 0$) from the long-time ($t \to \infty$) values of the

current (I) using:

$$t_e = \frac{I_{t\to\infty}}{I_{t\to 0}} \tag{4.2}$$

Additionally, Slag#1 was thermally treated to 1723 and 1823 K inside a a vertical tube furnace (GSL-1700x-100VT-UL, MTI Corp.). Graphite crucibles (Baofeng Graphite) were used to study the slag at similar conditions that the slag experiences in the industrial ironmaking processes. The system was purged with zero grade Ar (99.999 %, BOC) during the 1 K min^{-1} heating and cooling cycle. For the post-experiment analysis, the samples were cross-sectioned upon cooling using a high-speed diamond saw (Bühler), set in a conducting mounting compound (ProbeMet), and polished using progressively finer grades of silicon carbide paper (180, 320, 400, and 600 grit) and a diamond suspension with an average particle size of 9 μm. The composition and microstructure of the sample was examined using a scanning electron microscope (SEM, JEOL JSM-IT300LV) with LaB6 filament equipped with a X-Maxä 50 silicon drift energy dispersive spectroscopy (EDS) detector.

4.2.3 Thermodynamic predictions

The thermodynamic software FactSage 7.2 [19] was used to predict the equilibrium reduction potentials for the electrolytic extraction of metals from ironmaking slags (Section 4.3.3). The thermodynamic (minimum) cell voltage required for the reduction of metal ions from the slag (E_{cell}) was calculated using the Nernst equation:

$$E_{cell} = \frac{\Delta G^\circ}{-nF} - \frac{RT}{nF}\cdot\ln\frac{\prod a^{\nu}_{products}}{\prod a^{\nu}_{reactants}} \tag{4.3}$$

where F is the Faraday constant. R, T and ν are the universal gas constant, the temperature of interest and the stoichiometric coefficients from the overall cell reaction, respectively. In this study, all reactions were based on the formation of one mole of O_2 so the number of electrons involved in the reaction, n, is 4. ΔG° is the standard Gibbs energy of the dissociation reaction at unit activity in pure component state, and a_i is the activity of the ith species in the reaction at cell conditions. Model parameters were obtained from FactSage's FToxid and FactPS databases [19], where the molten slag phase is described using an optimized Modified Quasichemical Model [82]. The thermodynamic activities for the components of the molten slag system were obtained from this validated solution model [62], while unit activity was chosen for the metal and oxygen gas. Oxygen was assumed to be in equilibrium with pure O_2 bubbles evolved at the counter electrode.

4.3 Results and Discussion

4.3.1 Chemical considerations

In MOE, the choice of supporting electrolyte is the single most important process parameter. For the current study, the composition of the electrolyte is fixed as the study focuses on the direct use of ironmaking slag from the process, without the use of a supporting electrolyte. The elemental composition of Slag#1 given in Table 7.1 reports iron as Fe_3O_4 since the sample was oxidized before XRF measurements, but iron in melter slag at process conditions would be in the form of low valency iron ions, FeO, and metallic iron [163, 164]. This is mostly due to the operating conditions of the melter, where a liquid pool of pig iron metal forms at the bottom as the carbon content in the pig iron (around 3.40 wt.% [28]) reduces the melting point of the metal product about 300 K [165]. The slag floats on top of the reduced layer of pig iron metal at 1773 K [28].

At those operating conditions, most of the iron will be metallic and in equilibrium with wüstite in the slag phase. It is worth noting that prolonged exposure to high temperature oxidizing conditions favours the oxidation of metallic iron, but that gas-liquid reaction between oxygen and molten iron will be slower than the Fe^{2+} oxidation within the slag [163]. However, there is little Fe^{3+} expected, as hematite decomposes spontaneously at those temperatures [146, 164]. In this way, most iron in the slag is likely to be metallic iron trapped as it settles to the bottom of melter.

A significant number of small metallic droplets can be observed on the surface of the quenched Slag#1 after it was fired in a graphite crucible to 1723 K (Figure 4.2A). There were fewer metal beads suspended on top of the slag (Figure 4.2C), and most metal droplets were suspended near the bottom of the crucible (Figure 4.2D) for the experiment where Slag#1 was quenched from 1823 K. The large bubbles suspended in quenched slag in Figure 4.2B, and, to a lesser extent, in Figure 4.2D illustrate the viscous nature of the slag at temperature. An increase in temperature should decrease the viscosity of the slag, reducing the amount of entrained iron in the slag at temperature. While this may have allowed more droplets to sink under gravity, droplet coalescence was still hindered by metal carbide formation. The presence of these carbide precipitates has been reported to cause a rapid increase in the viscosity of the slag [163, 166, 167].

At the strongly reducing conditions of the melter due to the large carbon electrodes, metallic iron is trapped by solid carbide particles in the slag. At those operating conditions, V_2O_5 and TiO_2 in the molten slag can react with carbon to form mixed metal carbides precipitates at the liquid metal-slag interface [168]. The carbides heterogeneously nucleate at the liquid-liquid interphase interface [163],

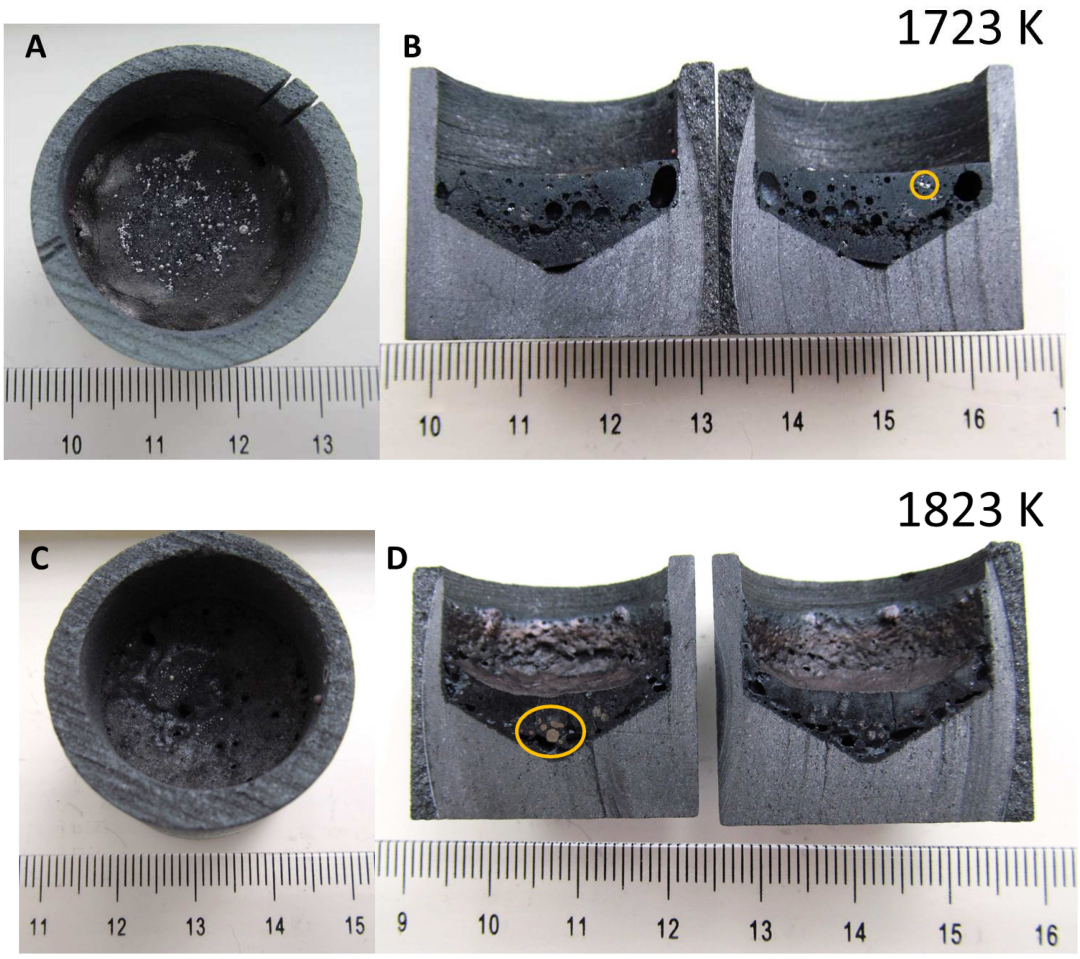

FIGURE 4.2: Slag#1 after being fired in a graphite crucible under an argon atmosphere. (A) and (C) are plan views of the crucible showing a number of small metal beads on top of the slag. (B) and (D) are complete cross-section of the crucible showing entrained gas bubbles and metallic droplets. The yellow circle in (B) indicates the region analysed in Figure 4.3, where the yellow ellipse in (D) shows a region of metal droplets near the bottom of the crucible.

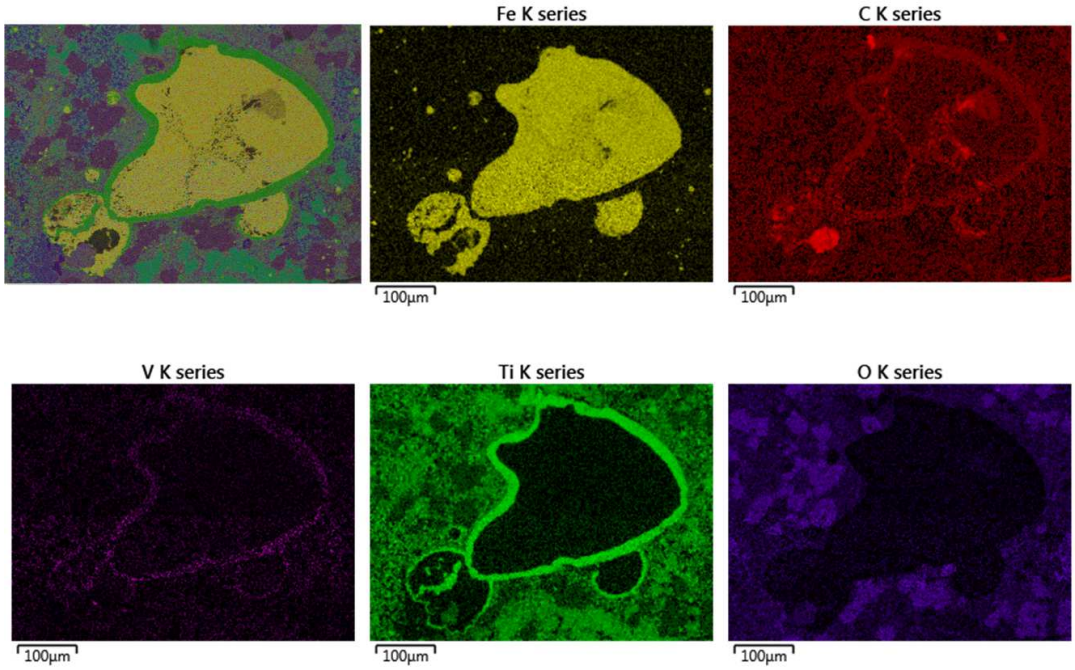

FIGURE 4.3: EDS elemental composition maps illustrating the distribution of the major elements around a metallic iron drop suspended in Slag#1 at the region indicated in Figure 4.2 after quenching from 1723 K.

which inhibits the growth and coalescence of metallic iron droplets [167]. The carbide shells of the several smaller solidified droplets that have coalesced are visible in the V and Ti x-ray maps in Figure 4.3.

Zhang *et al.* [167] found that TiC can be oxidised easily under dynamic oxidation conditions, causing a rapid decrease in the viscosity of the slag. Hence, increasing the oxygen chemical potential enables iron droplets to coalescence, facilitating the separation of iron from the slag [163]. This is consistent with the large metallic iron droplet found at the base of the quenched pendant droplet of molten slag formed during experimentation in the thermal imaging furnace at $P_{O_2} = 10^{-6}$ atm (see Figure 4.4A). The containerless method meant there was no carbon being used in the system, i.e. no carbothermal reduction was possible, and so it can be concluded that for the temperatures of interest the metal carbide precipitates contained in the slag had a larger effect on the viscosity than temperature.

The slag is considered to be fully molten as it is tapped from the process. That observation is consistent with the literature [169, 170]. Ratchev and Belton [170] also found that a decrease in the partial pressure of oxygen increased the liquidus temperature and reported a spinel phase precipitating above 1873 K for some compositions of a pseudo-quinary $TiO_2 - SiO_2 - Al_2O_3 - MgO - CaO$ slag system. It is important to know the state of the electrolyte because, unlike in aqueous or molten salt electrolysis where the analyte of interest can be a solid that dissolves in a molten

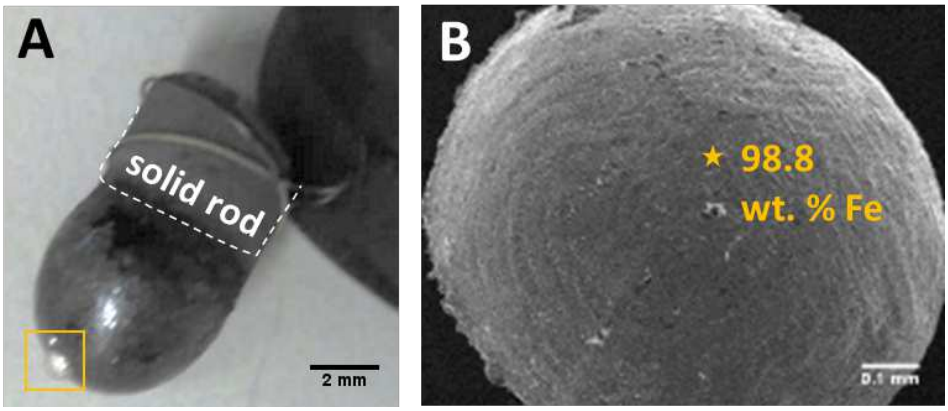

FIGURE 4.4: Assessment of the metallic iron content in Slag#1. (A) Pendant droplet sample of Slag#1 after being quenched from 1823 K in the thermal image furnace at $P_{O_2} = 10^{-6}$ atm. The yellow square shows a metallic droplet that coalesced after melting and settled in the bottom of the pendant droplet. (B) Back-scattered image of the metallic droplet. The yellow star indicates the location of the compositional analysis reported on the image.

supporting electrolyte, MOE depends on the molten state of the electrolyte (containing the dissolved metal cations of interest) in order for the charge to be transferred by the movement of ions. In the next section, the effect of the presence of iron and operating temperature on the slag's electrical conductivity will be explored.

4.3.2 Electrical considerations

All electrochemical reactions rely on the use of a solvent (i.e. supporting electrolyte) to enable the flow of current, providing the pathway for the charged species (i.e. dissolved ions and electrons) to flow between electrodes, balancing the flow of electrons in the external circuit [171]. The solute (compound of interest) dissolves in that medium. Oxide melts are known to be mixed conductors, where electrons and ions contribute to the charge transfer [158]. In molten slags, the current is known to be transported through the oxide melt mainly by ions [172]. Hence, in this work, it is postulated that, due to the mixed oxide nature of the slag, the fraction of the charge carried by ions (i.e. ionic conductivity) will be high enough to sustain a current efficiency that enables high production rates while minimizing energy consumption. Using the slag directly from the process, at temperatures above 1773 K, will facilitate the ionic mobility of the charged species, and it is hypothesized that this will enable a solvent-free process, i.e. no additional electrolyte would be needed.

In order to consider ironmaking slag a successful electrolyte, it is desirable that it possesses acceptable values of total electrical conductivity [152]. Following Ohm's law, a high total electrical conductivity, or low ohmic resistance, of the electrolyte is desired to maximize the production of the target metal as it will enable greater current densities for a given applied voltage. For comparison, the total electrical conductivity for pure cryolite is reported to be 2.8 S cm^{-1} [173] at 1273 K, a value

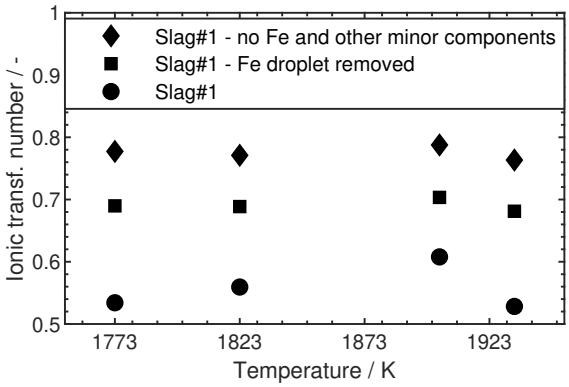

FIGURE 4.5: Ionic transference number variation as a function of temperature for Slag#1 with different amounts of iron in its base composition for a partial pressure of oxygen of 10^{-6} atm. Values correspond to the average of two measurements, where the maximum average deviation measured was $\pm$ 0.014.

which is close to Al smelting temperatures. For Ti-bearing blast furnace slag with 23 wt.% of TiO_2 and 4.8 wt.% of FeO, Wang *et al.* [174] reported a value of 1.2 S cm^{-1} at 1773 K. At that temperature, increasing the amount of TiO_2 in the slag to concentrations above 70 wt.% increased the total electrical conductivity up to 100 S cm^{-1} [175]. The reported range of values suggests that the total electrical conductivity of titanium-bearing slags can be tuned to what is required for a successful industrial electrolyte.

To maximize the production of metal in the proposed MOE system, the fraction of the charge carried by electrons (i.e. electronic conductivity) plays also an important role. On one side, electronic conduction constitutes a source of waste energy as the movement of electrons in the electrolyte is not linked to the production of metal [176]. This lowers the faradaic efficiency of the electrolysis and more energy is required to achieve a certain production rate. However, some electronic conduction is beneficial as that "wasted" energy can be used to self-heat the electrolytic cell (i.e. Joule heating), satisfying the thermal needs of the process [65]. Hence, in order to produce metal at an economically viable rate, the total electrical conductivity has to be maximized and the electronic conduction minimized [177]. The fraction of applied current that is used in the electrochemical reaction, i.e. the faradaic efficiency of the process, can be used to determine the feasibility of this approach.

The ionic conduction was investigated as a function of temperature (see Figure 7.3). Temperature between 1773 and 1933 K were chosen to study the slag in the vicinity of its tapping temperature. At those temperatures, the effect of temperature was minor and the ionic transference numbers obtained ranged from 0.53 to 0.61 for Slag#1. The ionic conduction in the slag depends on the concentration, charge and mobility of charge carriers [171]. As all the measurements were done at the same partial pressure of oxygen, the variation of the degree of polymerization of

the melt as a function of temperature is expected to be the main factor influencing ionic conduction. For the system under study, Liao *et al.* [178] illustrated that there is not a significant change in viscosity above 1773 K, with values less than 0.5 Pa s reported [153]. The negligible effect of temperature on the ionic conduction above 1773 K can be associated with the viscosity of the slag being stable at the operating temperatures and too low for mass transport to limit current efficiency.

As ironmaking slag may contain a small amount of iron, the effect of the iron on the transference numbers was also investigated. The concentration of Fe in the slag sample was reduced by separating the droplet of metallic iron, formed at the bottom of the quenched pendant droplet, from a sample of Slag#1 (Figure 4.4A). The amount of iron in the slag was not measured post operation, but Zhang *et al.* [167] reported a decrease from 2.50 wt.% to 0.07 wt.% after the metallic Fe in a Ti-bearing blast furnace the slag coalesced and settled to the bottom of their container. In this work, the ionic transference numbers for Slag#1 with Fe droplet removed (square shapes in Figure 7.3) were higher than for Slag#1. The decrease of the ionic transference numbers with increasing metallic iron content might be explained by the role of dissolved metallic iron at increasing the total electrical conductivity by increasing the electronic conductivity.

Rouaut *et al.* [177] compared the electronic conductivity of cryolitic melts with and without metals, and highlighted the role of dissolved aluminium metal as a source of mobile electrons. In metal-molten salts systems, the presence of dissolved metal not only increases the total electrical conductivity of the molten electrolyte, as it provides electrons that are highly mobile, but it decreases the faradaic efficiency of the electrolysis as the dissolved aluminium is reoxidized by the gas evolved at the counter electrode. The gain of efficiency resulting from the removal of multi-valency iron ions from the melt was further confirmed by measurements performed on a related synthetic slag sample with a similar base composition but with no iron and other minor components (diamond shapes in Figure 7.3). This synthetic TiO_2 - SiO_2 - Al_2O_3 - MgO - CaO slag, containing approximately the same composition ratios as Slag#1, resulted in even higher ionic transference numbers, ranging from 0.76 to 0.79.

To put the results for the compositions investigated herein into perspective, the use of cryolite as a supporting electrolyte yields ionic transference number values close to unity at industrial operation conditions [179]. *A priori*, this might suggest that an electrochemical route involving the direct use of ironmaking slag might be far from the creation of a commodity-cost extraction process, analogous to aluminium's Hall-Heroult process; however, the elevated cost associated with upstream processing to convert the ore to pure Al_2O_3 (i.e. Bayer Process) and the low concentration of Al_2O_3 in cryolite (between 2 and 5 wt.% [180]) are constraints that could be avoided with our proposed route. Furthermore, newly established routes such as the FFC

TABLE 4.2: Gibbs energy and minimum thermodynamic cell voltage for the decomposition reactions in the proposed electrolyte, Slag#1, at 1773 K predicted with FactSage.

	$\Delta G^{\circ}_{decomp}$ / kJ mol^{-1}	E_{cell} / V
$CaO\,(s) \rightleftharpoons Ca\,(l) + \frac{1}{2}O_2\,(g)$	445	-2.89
$Al_2O_3\,(s) \rightleftharpoons 2\,Al\,(l) + \frac{3}{2}O_2\,(g)$	1108	-2.00
$MgO\,(s) \rightleftharpoons Mg\,(g) + \frac{1}{2}O_2\,(g)$	367	-2.18
$Ti_2O_3\,(s) \rightleftharpoons 2\,Ti\,(s) + \frac{3}{2}O_2\,(g)$	1044	-2.10
$TiO_2\,(s) \rightleftharpoons Ti\,(s) + O_2\,(g)$	627	-1.70
$SiO_2\,(s) \rightleftharpoons Si\,(l) + O_2\,(g)$	596	-1.66
$FeO\,(l) \rightleftharpoons Fe\,(s) + \frac{1}{2}O_2\,(g)$	153	-0.98
$Fe_3O_4\,(s) \rightleftharpoons 3\,Fe\,(s) + 2\,O_2\,(g)$	560	-0.87

process report a faradaic efficiency of 50% [181] and the molten sulfide electrolytic route to produce copper is around 5% [61]. Hence, the further exploration of the electrochemical behaviour of the slag is encouraged.

4.3.3 Thermodynamic considerations

The stability of the metal oxide constituents of the molten slag at the operating conditions must be investigated as their decomposition will limit the operating temperature of the MOE cell [60] and define the purity of the final metallic product.

Thermal stability

The Gibbs energy for the disassociation reactions of the pure compounds in their standard state, $\Delta G^{\circ}_{decomp}$, is given in Table 4.2. At 1773 K, the thermal stability of all the pure major components found in the slag ($\Delta G^{\circ}_{decomp} > 0$) is guaranteed. No constituent of the electrolyte will decompose spontaneously and metal and oxygen gas can be produced by a faradaic reaction.

Electrochemical stability

In non-aqueous electrochemistry the selectivity of the process depends on the exclusive reduction of the metal ions of interest from the melt [182]. Hence, in order to produce high-purity titanium metal and oxygen gas from the electrolysis of molten slag, the melt must be free of elements more noble than titanium [152]. The relative stability of the metals at 1773 K ($\Delta G^{\circ}_{decomp}$) is: Fe < Si < Ti < Mg < Al < Ca. Hence, the first metal that will be formed is iron and it must be removed before operation. However, molten oxides are complex non-ideal solutions [62] and the relative stability of the components in the melt reported in Table 4.2 fails to take into account the electrolyte composition (i.e. thermodynamic activities). Using the Nernst equation, the minimum difference in electrode potential between the working and counter electrode required for any redox reaction to occur at the

operating conditions (E_{cell}) was calculated.

The small potential window between the reduction of Si and Ti ions indicates that they might co-reduce from the melt (see Table 4.2). However, the small potential window between both reduction reactions may imply that the deposition series could be altered by modifying the composition of the electrolyte or the concentration of the electronegative species (eg. through the use of a supporting electrolyte [182, 183]), which was out of scope of this study. Regardless, producing titanium silicides as a product is a promising high-added value alternative [184]. Either way, the results presented in this paper justify further study of the electrochemical behaviour of this material to investigate the kinetics of the reduction process, determining its potential as a secondary source of metals.

4.4 Conclusions

The implications of using TiO_2-rich ironmaking slag as a molten oxide electrolyte were investigated in this paper. To assess the feasibility of producing titanium metal directly from the ironmaking process, the following considerations must be taken into account:

- Operating in the vicinity of the liquidus temperature of the slag did not have a significant effect on the charge transfer
- The presence of iron in the melt, even in small quantities, increased considerably the electronic conduction in the melt, hindering the faradaic efficiency of the process.
- If pure titanium metal is the desired product, the melt should be free of any iron as it is easier to reduce than the target metal.
- The proximity of the thermodynamic cell voltage values for the reduction of Si and Ti ions from the melt calls for an electrochemical study to understand the overpotentials at the electrodes, which will ultimately control the composition of the metal produced.

The results presented in this paper, alongside the timely need to recycle large-scale waste materials, motivate further exploration of the electrochemical behaviour of titanium-bearing slags relevant for molten oxide electrolysis.

Chapter 5

Electrochemical Behaviour of Titanium-Bearing Slag Relevant for Molten Oxide Electrolysis

Abstract

A containerless approach was used to investigate the electrochemical behaviour of TiO_2 – SiO_2 – Al_2O_3 – MgO – CaO slags in their molten state. Iridium was used in a three-electrode configuration to perform a combination of electrochemical techniques inside a modified thermal imaging furnace. The real-time visualisation during experimentation and the post-mortem microscopy analysis confirmed the direct production of an Ir−Ti−Si alloy and the evolution of oxygen during electrolysis. Thermodynamic properties of the slag were predicted with FactSage and were consistent with experiment. The results justify the use of this method to better characterize the potential of these systems as a secondary source of materials.

5.1 Introduction

The electrolysis of molten metal oxide feedstocks has been proposed as a more sustainable and environmentally friendly alternative to the conventional extractive metallurgical processes [110]. This method is commonly referred to as molten oxide electrolysis (MOE). MOE uses electrons as the reducing agent to separate metals from molten oxide electrolytes. One key feature of this process is that oxygen can be the only by-product generated if the counter electrode (CE) material is inert at the operating conditions [185]. Provided the electricity is generated from renewable resources, the implementation of MOE can contribute to decarbonization of the metallurgical sector.

The success of using electricity to extract any metal from its ore relies upon finding an appropriate supporting electrolyte. A profound understanding of the physical-chemical properties of the electrolyte in its molten state is then crucial

to the development of this technique. However, the high melting points of most oxides have traditionally imposed very demanding material constraints making it extremely challenging to study them at a laboratory scale. Traditionally, crucibles have been used to place the oxide melts under study in the hot zone of a furnace. The containment compatibility issues (i.e. slag / crucible interaction [14]) derived from the use of this type of furnace have limited the thermodynamic data available. The larger the number of constituent elements in the melt, the scarcer the data. Characterizing the properties of the candidate molten oxide electrolytes remains a major challenge for MOE [60].

The push for green electrification and decarbonization of industrial processes brought attention to the application of MOE in steelmaking [85]. Steel is the most widely used alloy in the world with a yearly production of 1.8 billion tons [87]. For each ton of steel produced, 1.83 tons of CO_2 are produced [186], which makes steelmaking one of the largest industrial source of the greenhouse gas. Research in this field has been mainly focused on the extraction of iron from FeO_x containing melts [139, 146, 160, 186]. For the more complex, chemically-aggressive, Ti-bearing oxide melts, such as $TiO_2 - SiO_2 - Al_2O_3 - MgO - CaO$ slags, thermodynamic data is only available for narrow ranges of temperature and composition [153]. However, in countries like China and New Zealand, these slags are available as by-products of the local steelmaking processes, and can contain more than 30 wt.% TiO_2 [15]. The slag is tapped at temperatures above 1700 K, dumped to cool, crushed and sold as an aggregate for cement production or fill for roading. This practice is a waste of titanium resources and sensible heat, which constitutes around 10% of the waste energy of the steel industry [91]. With the universal need to improve resource efficiency and mainstream sustainability practices [1], research efforts have been drawn towards the extraction of further value from Ti-bearing slag [16].

Jiao *et al.* [15] performed two-electrode electrolysis in $TiO_2 - SiO_2 - Al_2O_3 - MgO - CaO$ slag. They used a graphite anode, a liquid iron cathode and a silicon nitride crucible to study the recovery of Ti. MOE is particularly attractive due to the molten state of the available slag and the possibility to electrochemically extract metals from the oxide melt while producing only oxygen [187]. The use of the slag for such a purpose would benefit from a containerless method and an oxygen-evolving anode. A more extensive study can help to bridge the knowledge gap around the physical-chemical properties of Ti-bearing slag in the molten state, determining crucial information to enable recycling of the slag. The study of the electrochemical behaviour of this complex oxide system is hence justified.

In this work, a containerless approach with in situ, real-time visualization was used to study the electrochemical properties of molten $TiO_2 - SiO_2 - Al_2O_3 - MgO - CaO$ slag. Following the pioneering efforts of

Nakanishi and Allanore [13], the pendant droplet technique was employed in a modified thermal imaging furnace. Cyclic voltammetry and potentiostatic electrolysis measurements were performed in a three-electrode configuration using iridium metal as working, pseudo-reference and counter electrodes. Thermodynamic predictions using FactSage were validated with measured phase relations, and the cell voltages required to deposit Si and Ti from the slag were determined. The results presented in this paper demonstrate a methodology to accelerate the pace of characterization of titanium-bearing slags.

5.2 Experimental

5.2.1 Sample preparation

The slag produced during the processing of titanium magnetite ores in China [15] and New Zealand [16] is composed mainly of TiO_2, SiO_2, Al_2O_3, MgO and CaO. The compositions studied in this paper represent New Zealand Ti-bearing slag where the TiO_2 concentration has been lowered to study the effect of the continuous extraction of titanium from the slag on its electrochemical behaviour. The relative amounts of the other oxides are kept approximately constant. The compositions of the samples were measured by x-ray fluorescence spectroscopy (XRF, Siemens/Bruker SRS3000), and are reported in Table 5.1.

Four compositions of a synthetic $TiO_2 - SiO_2 - Al_2O_3 - MgO - CaO$ slag were prepared using powders of Al_2O_3 (98%, CARLO ERBA Reagents), TiO_2 (99.9%, CERAC Inc.), $CaCO_3$ (99.95%, CERAC Inc.), SiO_2 (99.4%, CARLO ERBA Reagents) and $(MgCO_3)_4 \cdot Mg(OH)_2 \cdot 5\,H_2O$ (99%, SIGMA-ALDRICH) as starting materials. Approximately 100 g of the mixed powders were weighed into high-density polyethylene bottles and ball mill blended overnight in EtOH with ZrO_2 milling balls on a rotating roller mill. The powder was recovered using rotary evaporation, dried, then granulated through a coarse sieve. Granulated blended batch materials were fired in air at 1873 K in a platinum crucible and furnace cooled. The resulting solid was reheated in a platinum crucible to 1473 K and water quenched. The recovered material was micronized, placed into latex balloons (Pioneer Balloon Co.) and cold hydrostatically pressed at 300 MPa for 5 minutes.

5.2.2 Thermodynamic predictions

Thermodynamic properties were calculated for slags using the thermodynamic software FactSage 7.2. Model parameters are from FToxid and FactPS databases [19]. For each slag composition at a total pressure of 1 atm, the phase relations as a function of temperature were predicted. The maximum temperature for any solid phase to be stable, the liquidus temperature (T_{liq}), and the minimum temperature

TABLE 5.1: Thermodynamic properties predicted for the electrolyte compositions investigated in ascending order of their predicted T_{liq}. E_{cell,TiO_2} is the cell voltage for Reaction 5.3 at 1903 K.

	TiO_2 wt.%	CaO wt.%	SiO_2 wt.%	Al_2O_3 wt.%	MgO wt.%	T_{sol} K	T_{liq} K	E_{cell,SiO_2} V	E_{cell,TiO_2} V
Slag A	33	18	15	19	15	1486	1803	−1.61	−1.65
Slag B	15	24	25	18	18	1494	1823	−1.63	−1.72
Slag C	9	25	26	20	19	1494	1883	−1.66	−1.75
Slag D	21	21	11	26	21	1615	1960	−1.69	−1.73

for any liquid phase to be stable, the solidus temperature (T_{sol}), were determined. These values are given in Table 5.1.

The thermodynamic cell voltages required to deposit metals from the molten slag were calculated in the following manner. For brevity only the example for Ti deposition is given. The cathodic reaction was first assumed to be:

$$TiO_2 + 4\,e^- \longrightarrow Ti + 2\,O^{2-} \tag{5.1}$$

The anodic reaction was then assumed to be:

$$2\,O^{2-} \longrightarrow O_2 + 4\,e^- \tag{5.2}$$

Thus the full cell reaction was:

$$TiO_2 \longrightarrow Ti + O_2 \tag{5.3}$$

While the overall Gibbs energy change for Reaction 5.3 is independent of mechanism, the cell voltage for Reaction 5.3 will depend on pathway and thus should be treated as an indicative value only. At standard conditions and the temperature of interest, the cell voltage, E°_{cell}, was then determined by:

$$E^\circ_{cell} = \frac{\Delta G^\circ}{-nF} \tag{5.4}$$

where ΔG° is the standard Gibbs energy of dissociation for Reaction 5.3, n = 4 is the number of electrons involved in the reaction, and F is the Faraday constant. ΔG° for the full cell reaction was obtained at the temperature of interest from FactSage. At 1903 K, the standard cell voltage for Reaction 5.3, E°_{cell,TiO_2}, is -1.56 V. However, as the system under the examined conditions is not at standard conditions, the cell voltage (E_{cell}) is calculated from the Nernst equation:

$$E_{cell} = E^\circ_{cell} - \frac{RT}{nF} \cdot ln \frac{\prod a^{\nu}_{products}}{\prod a^{\nu}_{reactants}} \tag{5.5}$$

where R is the universal gas constant, T is the temperature of interest, ν are the

stoichiometric coefficients and a_i are the activities of the species present in the reaction. To account for the non-ideal properties of the molten slag system, the activity of TiO_2 in the melt, a_{TiO_2}, at T was calculated from FactSage. Unit activity was chosen for titanium metal as it was assumed that pure solid metal will be produced. All the ν of the reaction quotient are 1 (see Reaction 5.3). Since the pressure inside the furnace was low, and 1 atm pure O_2 gas was chosen as the standard state of the oxygen gas at the CE, the partial pressure of oxygen was assumed equal to the activity of oxygen. The P_{O_2} is 1 atm as dissolved O_2 is assumed in equilibrium with pure O_2 bubbles evolved at the counter electrode. The cell voltages for Si and Ti metal deposition were calculated according to Equation 5.6, and is reported in Table 5.1.

$$E_{cell,TiO_2} = E^{\circ}_{cell,TiO_2} - \frac{RT}{4F} \cdot ln \frac{1}{a_{TiO_2}} \tag{5.6}$$

5.2.3 Phase relations determination

Differential scanning calorimetry (DSC) and X-ray powder diffraction (XRD) techniques were utilized to validate thermodynamic predictions. Heat flow measurements were performed (NETZSCH STA 449 F3 Jupiter) under an argon atmosphere (120 mL min^{-1}, 99.999%). Platinum crucibles with a lid were used to contain about 10 mg of slag which was thermally cycled at 20 K min^{-1} up to 1873 K. An alumina spacer was used to protect the sensor from the crucible when operating at temperatures above 1673 K. In situ XRD analysis of slag was conducted at the Australian Synchrotron using the powder diffraction beamline. The samples were mounted in a 0.1 mm deep rebate in a platinum strip element in an Anton Paar Furnace. Diffractograms were measured every 60 seconds as the samples were heated from 1500 K to 1873 K at 5 K min^{-1}. The X-ray energy was set at 11 keV and the diffraction data acquired using a Mythen 1D detector between 10 and 85 degrees 2θ.

5.2.4 Furnace operation

The use of the pendant droplet technique in a modified thermal imaging furnace (TX-12000-I-MIT-VPO-PC, Crystal Systems Corp.) to carry out electrochemical measurements has been described before [13, 188, 189]. Briefly, at the beginning of each experiment, a cylindrical sample was suspended from the upper furnace shaft inside a quartz tube (Technical Glass Products Inc.). The sintered electrolyte samples were 5 to 7 mm in diameter and 60 to 80 mm in length, and sample position was controlled using a stepper motor with submillimeter precision. Vacuum was applied to certify that there were no leaks in the system. The quartz tube containing the electrochemical cell was then purged three times before turning on the furnace. UHP Ar (99.999%, Airgas Inc.) was used to refill the chamber and during operation with a flow rate of 200 mL min^{-1} (P_{O_2}= 10^{-6} atm). The operating temperature was determined by contacting the molten droplet with a thermocouple. W – Re (5 wt.%) | W – Re (26 wt.%) thermocouples (type C) were used, with a $\pm$ 1% maximum error

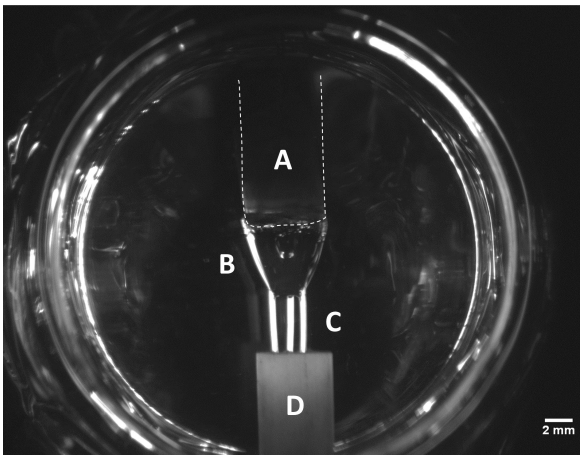

FIGURE 5.1: Optical image of the electrochemical cell: (A) solid sample rod, (B) molten pendant droplet, (C) electrodes, (D) electrode probe.

at the operating temperatures.

Once the operating temperature (i.e. furnace lamp power) was chosen, the sample was lowered until its bottom end was in the hot zone and it was rotated until a stable pendant droplet was formed. Then, the three iridium wire electrodes (Ir > 99.9 %, diameter = 0.5 mm, Furuya Metals Co., Ltd.), held inside an Al_2O_3 four-bore tube, were raised up while monitoring the open circuit potential (OCP). A sudden change in the OCP, and in situ visualization, confirmed that the electrodes had contacted the molten droplet. Once the electrodes had made contact with the molten droplet, the wires were raised further into the molten droplet to an immersion depth of approximately 2 mm. See reference [13] for details regarding the assembly of the iridium electrodes and electrical connections to the potentiostat. An image of the electrochemical cell configuration is shown in Figure 5.1. The image was captured through a flat window in the quartz tube by a camera (EOS Rebel T5i DSLR, Canon Inc.) with telescopic lens during operation at 1903 K.

5.2.5 Electrochemical measurements and analysis

Iridium wires were employed as the working (WE), counter and pseudo-reference electrodes. Iridium was chosen as the electrode material as it satisfied the technical requirements of being solid at the operating temperatures (melting point = 2179 K) and mechanically robust enough (elastic modulus = 528 GPa at room temperature) to insert a thin wire into the molten slag repeatedly. Tungsten and molybdenum also met the requirements and are cheaper, but, unlike iridium, they are susceptible to oxidation under the given experimental conditions. Initial experiments found that Mo and W wires were not stable during electrolysis as the oxygen gas that evolved at the counter electrode (which is very close to the other electrodes in the pendant droplet configuration, see Figure 5.1) quickly reacted with these metals

and formed volatile metal oxide phases leading to severe corrosion. The melting points of silicon, iron and platinum make them unsuitable for this application. The use of carbon is avoided due to the likelihood of a carbothermal reaction with Ti or Si to form carbides [190]. Other high melting point metals such as titanium and zirconium are not chemically stable in the slag as they can reduce metals from oxide species within the melt. Iridium has been intensively studied in MOE [13, 186, 188, 191], where it has been demonstrated to act as an oxygen-evolving anode [186]. While the price of iridium is too high for large-scale applications, iridium plays an important role in laboratory scale studies.

In this work, the pseudo-reference electrode consisted of an iridium wire immersed into the molten slag droplet. This type of reference electrode is commonly used in MOE when performing three-electrode measurements [13, 160, 186, 188, 191], where it provides a constant potential and has the advantage of having a low impedance [192]. However, its potential cannot be calculated thermodynamically as the species in equilibrium at the pseudo-reference electrode are unknown. All the potentials measured are referred to this pseudo-reference electrode, which was found to be stable throughout multiple measurements. While some have successfully used oxide / oxygen reference electrodes based on solid ZrO_2 electrolyte separators [139], in this system, the small size of the molten oxide droplet limits the ability to use this type of reference electrode. Furthermore, as ZrO_2 is soluble in this oxide melt [193], using this type of reference electrode would contaminate the system. An alternative approach is to use metal / metal oxide reference electrodes, which are essentially metal wires coated in a thin oxide layer [194]. While these have proved useful in some systems, the electrode material constraints stated above made these unsuitable for this study.

All the electrochemical measurements were conducted using a potentiostat (Gamry Reference 3000). The OCP was recorded to begin each measurement. The ohmic resistance between the working and pseudo-reference electrodes was calculated from electrochemical impedance spectroscopy measurements at OCP. The distance between both electrodes was approximately 2 mm. For each experiment, the value was obtained at high frequency when the phase angle was close to zero. A typical resistance value was 1.5 Ω. To account for the ohmic drop, 70% of this value was applied for positive feedback and the remaining 30% used for post-run IR correction. Cyclic voltammetry (CV) was used to determine the potential scan range and to identify the presence of redox couples within the electrolyte. Potentiostatic electrolysis experiments were performed to confirm the peak identified with the CV measurements.

Following the experiment, the quenched droplet was cross-sectioned from the remaining unmolten rod using a low speed diamond saw (Bühler). The sample

was polished down to 1 µm using a diamond suspension over abrasive pads. The microstructure and morphology of the product were observed using a scanning electron microscope (SEM, JEOL IT-300) equipped with an energy dispersive spectrometer (EDS).

5.3 Results and Discussion

5.3.1 Validating thermodynamic predictions

The thermodynamic predictions reported in Table 5.1 were validated by comparing the calculated T_{sol} with those determined by DSC, and the calculated T_{liq} with in situ XRD analysis. For Slag C, the T_{sol} was predicted to be 1494 K. The onset of the first endothermic peak detected in the heating path was used as a proxy for T_{sol} in the DSC measurements. The experimental solidus was 1488 K, which is consistent with the prediction. The T_{liq} was difficult to determine via DSC due to the decrease in sensitivity at very high temperatures, possibly aggravated by the use of a spacer [195]. In situ XRD, was used for further validation of thermodynamic predictions. FactSage predicted that the last stable solid phase would be magnesium aluminium spinel with nominal composition $MgAl_2O_4$. Indeed, on heating to the maximum experimentally achievable temperature (1873 K) the only crystalline phase present was the spinel. Complete melting at the maximum operating temperature of the in situ XRD heater (1873 K) was not observed for Slag C, which is consistent with the liquidus temperature prediction (1883 K) for this composition. Taken together, the DSC and XRD measurements validate the use of thermochemical data from FactSage for the complex, pseudo-quinary slag phase and support its use for reaction potentials in this composition space.

5.3.2 Cyclic voltammetry

The influence of the lower potential limit during CV was investigated (Figure 5.2). The scan rate was set to 1 V s^{-1} to mitigate the effect of the interaction between the metallic product and the WE. A slower scan rate would allow more time at reducing conditions, which could affect the dimensional stability of the WE. The potential was scanned from 0.5 V vs Ir towards negative potentials for three cycles. The upper potential limit was set at 0.5 V as, above this potential, the voltammograms became less reproducible, possibly because of the oxidation of the iridium or the oxygen evolution reaction (gas bubbles could be observed at 0.7 V vs Ir).

The negative potential scan limit was shifted to more negative values for each curve in Figure 5.2 in steps of -100 mV (from 0 V to -0.6 V). Decreasing the lower potential limit towards more negative potentials resulted in the cathodic current becoming more negative. Each curve corresponds to the third cycle of an individual

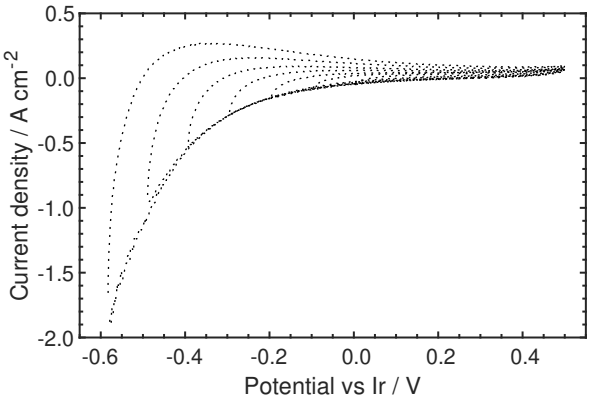

FIGURE 5.2: Cyclic voltammograms of Slag C at 1903 K. The upper potential limit was 0.5 V vs Ir for all measurements and the lower potential limit was varied across 0 V, -0.1 V, -0.2 V, -0.3 V, -0.4 V, -0.5 V and -0.6 V. Scan rate: 1 V s^{-1}.

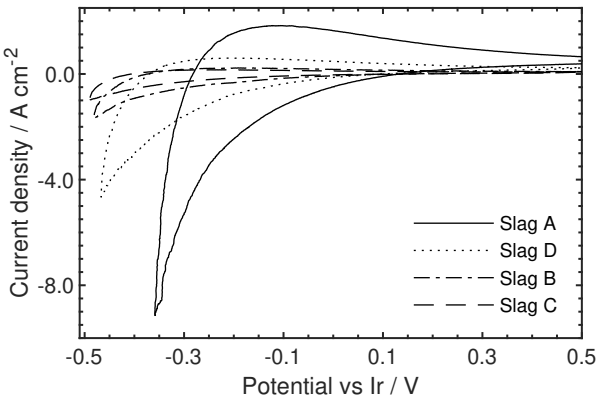

FIGURE 5.3: Cyclic voltammograms of the four slag compositions at 1903 K with a 1 V s^{-1} scan rate. The upper and lower potential limits were 0.5 V and -0.5 V vs Ir.

CV measurement for Slag C, where the features of the CV were reproducible from cycle to cycle. The CV is not reproducible when the lower potential limit is below -0.6 V. This may be due to changes in WE shape / area due to metal deposition and slag droplet disturbances caused by the gas bubbles generated at the CE. Based on the potential at which oxygen evolution reaction was observed (0.7 V vs Ir) and the potential for the cathodic metal deposition (-0.6 V vs Ir), the overall cell voltage was estimated to be -1.3 V. This is lower than the predicted cell voltages required for Si and Ti deposition from Slag C at 1903 K, which are -1.66 V and -1.75 V, respectively (see Table 5.1). This is possibly due to the underpotential deposition of Ti and Si on the Ir WE. It seems unlikely that two reduction events would be observed as there is less than 100 mV between the predicted cell voltages.

The effect of slag composition on the cyclic voltammograms was investigated (Figure 5.3). For all measurements, the potential was swept in the negative direction until -0.5 V vs Ir, and it was found that the current density increased with the concentration of TiO_2. This is consistent with thermodynamic predictions using FactSage

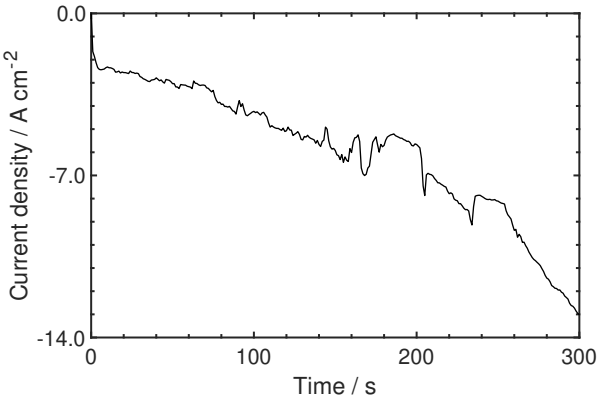

FIGURE 5.4: Current density vs time plot recorded from a potentiostatic electrolysis experiment for Slag D. Potential held at -0.6 V for 300 s. T: 1903 K. Electrode area: 0.035 cm^2.

(Table 5.1). Slag A has the most positive predicted E_{cell,TiO_2}, -1.65 V, compared with the least positive -1.75 V for Slag C. For a process involving the cathodic deposition of a metal, the cathodic current density increases as the potential becomes more negative. For all slags, the increase in the cathodic current density is consistent with the increase in the concentration of TiO_2. Interestingly, the concentration of SiO_2 seems to have little effect, where no clear trend was found. However, based on the thermodynamic predictions, the reduction of Si from SiO_2 is thermodynamically more favourable than Ti from TiO_2.

5.3.3 Potentiostatic electrolysis

Potentiostatic electrolysis experiments were performed to confirm the electrochemical deposition of metals and to investigate whether the shape of the CVs could be attributed to phenomena occurring after the electron transfer reaction. The current density during electrolysis of Slag D (21 wt.% TiO_2) was quite noisy (Figure 5.4). Kim *et al.* [196] associated the spikes in the signal recorded during electrolysis to an increase in the electrical resistivity caused by large bubble formation in the electrolyte. Similarly, in this system, the number of gas bubbles formed was such that they interfered in the electrical connection between the electrodes and the molten sample. Bubbling began as soon as potential was applied to the cell. The bubbles evolved at the CE were observed to disturb the shape of the molten droplet which would have altered the length of WE wire inserted into the droplet, and thus altered the current. The current density value in Figure 5.4 assumes a constant WE area.

After 300 seconds the lamps of the thermal imaging furnace were shut off, quenching the electrodes inside the droplet prior to terminating the experiment. SEM observations of the polished cross-section after electrolysis are presented in Figure 5.5. The Ir WE surface was noticeably modified (Figure 5.5A). The area of the pure iridum WE decreased slightly. As a result of the electrolysis, the remaining Ir

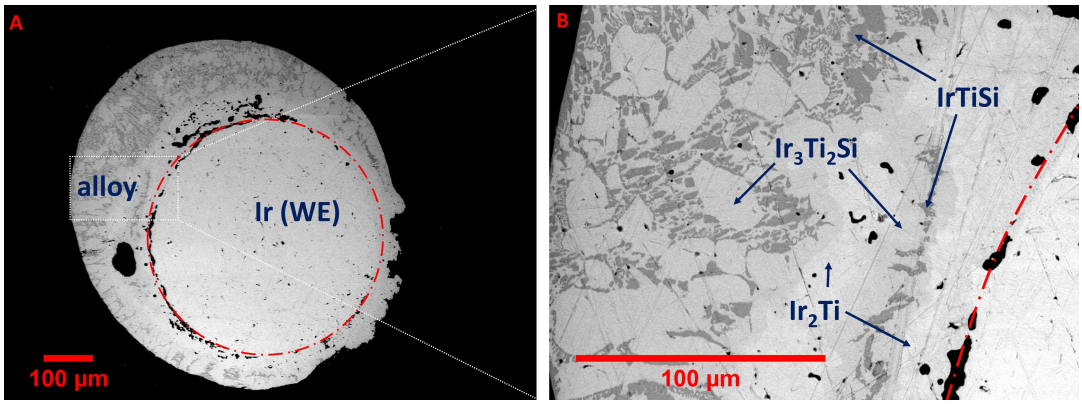

FIGURE 5.5: Back-scatter electron (BSE) images of the quenched iridium working electrode after the potentiostatic electrolysis experiment reported in Figure 5.4. (A) is a complete cross section with the pure iridium electrode area delimited by a red circumference. (B) is the higher magnification of left portion of product with Ir-Si-Ti phases labelled.

is part of an alloy that had formed around the surface of the WE. EDS compositional analysis indicated that it was an oxide-free Ir−Ti−Si region. This shows unequivocally that Ti and Si were reduced from the slag during the experiment. Along that deposited layer, three regions with different Z-contrast were identified (Figure 5.5B). The composition of each phase was determined from five EDS spot measurements from different regions of each phase. The ranges of normalised atomic compositions are given by $Ir_{0.29-0.40}Ti_{0.32-0.42}Si_{0.26-0.30}$ (dark grey), $Ir_{0.48-0.50}Ti_{0.32-0.34}Si_{0.17-0.18}$ (medium grey) and $Ir_{0.65-0.69}Ti_{0.31-0.35}$ (light grey). The light grey Ir−Ti phase has a composition between the reported TiIr and $TiIr_3$ intermetallics [197].

Thermodynamically, Si reduction from the melt was predicted to be the most favourable, which could suggest that Si would be preferentially deposited. However, based on the EDS compositional analysis, the Ti content in the different alloy phases is always larger than that of Si. This suggest that Si may not be reduced from SiO_2, but it may be reduced from a more stable complex or ion, which explains the lack of a clear trend with SiO_2 concentration in Figure 5.3. Nakanishi and Allanore [188] reported that a non-ideal mixing behaviour in the molten state for the $La_2O_3-Y_2O_3$ mixture led to selective extraction of La, contradicting simple thermodynamic predictions. Further research needs to address the non-ideal behaviour of the metallic product. The thermodynamic cell voltage of the reactions should be calculated with the chemical potential of the reduced metals in the intermetallic or solid solutions rather than in the pure metallic phase. However, no experimental ternary Ir−Si−Ti phases have been reported and no predicted phase relations are available. The lack of thermodynamic data makes detailed analysis of metal deposition challenging.

The faradaic efficiency, η, of the reaction was determined from:

$$\eta = \frac{V \cdot \rho \cdot F \cdot n}{M \cdot I \cdot t} \tag{5.7}$$

where V, ρ, and M are the volume, density and molar mass of the product, respectively, n = 4 is the number of electrons in the reaction, F is the Faraday constant, I is the current passed during t, time of the potentiostatic electrolysis. The area of product and the length of electrode inside of the melt were estimated from image analysis of Figure 5.5. A capped, cylindrical shell geometry was assumed for the deposition volume calculations. The product was assumed homogeneous with representative composition IrTiSi, and Vegard's rule was used to obtain the molar mass and density of the product at room temperature. From this, the faradaic efficiency for the electrochemical deposition of Ti and Si from the molten oxide was estimated to be approximately 29% $\pm$ 6%. The uncertainty in this value was calculated from the uncertainties in the measured composition and volume of the deposit.

We speculate that the main contributor to the low faradaic efficiency found in this electrolysis experiment was the oxygen reduction reaction occurring in parallel with metal deposition. During electrolysis, oxygen bubbles could be observed rapidly streaming off the counter electrode and mixing through the molten electrolyte droplet. This oxygen could then be reduced at the working electrode, and thus lower the current efficiency. While we could observe oxygen in the inert gas purge stream using an inline oxygen sensor, the measurements were not accurate enough to confirm that some of the oxygen evolved at the counter electrode was subsequently reduced at the working electrode.

The proposed electrochemical reaction mechanism consists of an initial electron transfer reaction followed by surface alloy reaction and diffusion, including any consequent new phase formation. The initial electron transfer reaction can be controlled by the imposed potential (see Figure 5.2), while the following phenomena are successive non-electrochemical steps. The reduced metal dissolves in the surface of the iridium WE creating a chemical potential gradient that drives solid state diffusion, lowering the activity of the deposited metal towards the thermodynamically stable state of the alloy. A similar mechanism was proposed by Gao *et al.* [139] in the recovery of iron from a silicate melt using an Ir WE. Alloying of the metal produced on a platinum-group metal electrode has been observed before with oxide melts [13, 139, 198].

5.4 Conclusions

A three-electrode cell configuration using the pendant droplet technique was used to investigate the electrochemical behaviour of $TiO_2 - SiO_2 - Al_2O_3 - MgO - CaO$ slag. Thermodynamic predictions from FactSage were in agreement with phase relations from DSC and high temperature XRD measurements. This validated the use of thermochemical data for the slag in FactSage in the composition and temperature range of interest. Cyclic voltammetry and potentiostatic electrolysis experiments were performed to investigate the reduction process of the electroactive species in the melt. Oxygen gas evolution was observed during the electrochemical measurements, and the post-experiment microscopy analysis confirmed the reduction of metal ions from the melt. An initial electron transfer reaction followed by surface alloy reaction and diffusion is the mechanism proposed to describe the formation of the ternary Ir−Ti−Si phases that formed during electrolysis. The results presented confirm that the electrochemical recovery of metals from molten Ti-bearing slags is feasible. The temperature requirements on electrodes for these experiments introduce additional challenges when characterizing the reduction products and highlight the lack of thermochemical data for Pt-group alloys. Overall, this work shows the importance of containerless methods to enable the study of the physical-chemical properties of molten oxides at ultra-high temperatures.

Chapter 6

Electrochemical Study on the Reduction of Si and Ti from Molten TiO_2 - SiO_2 - Al_2O_3 - MgO - CaO Slag

Abstract

The reduction process during the electrochemical production of titanium via the electrolysis of molten $TiO_2 - SiO_2 - Al_2O_3 - MgO - CaO$ slags has been investigated. A laboratory scale, electrolytic cell was designed to study the effect of TiO_2 concentration at ultra-high temperatures. Galvanostatic and potentiostatic experiments were performed using a molybdenum working electrode. The reduction of Si and Ti ions from the melt on a molybdenum electrode is a complex process that combines electron transfer and chemical phenomena. For the concentrations studied, the extraction of pure metallic Ti directly from ironmaking slag is unlikely without the prior removal of SiO_2 or other chemical modifications to the system.

6.1 Introduction

The focus on circular economy is pushing research to find beneficiation techniques for the abundant industrial by-products [1]. Ironmaking slag is the biggest by-product of the steel industry, and hence researchers have been attracted to study ways to extract further value [199]. Extracting high purity metals is a high added-value solution, which would allow traditional recycling practices to still be used for the remaining slag material [7], potentially increasing its value [6]. Furthermore, the direct electrolysis of molten slag has the potential to cut the direct emissions of green house gases associated to traditional metallurgical practices [146].

The study of the ionic nature of slags has been gaining relevance since the beginning of the 20th century [200]. These metal oxide mixtures have proven to be

good high temperature solvents of 3d transition metal oxides, achieving metal ion concentration higher than industrial electrolytes [60]. Moreover, the present of silica in the oxide network provides the thermal stability needed to operate at the high temperatures required to cast a liquid metallic product. Due to the timely need to find more sustainable alternatives to the current steelmaking practices [201], the use of ironmaking slag as a secondary source of metal has been mostly linked to the production of iron [10, 146]. The production of iron from the electrolysis of molten slag benefits from the fast kinetics of high temperature operation and potential high selectivity as iron oxide has the lowest thermodynamic stability compared to the other slag constituents.

At standard conditions, the Gibbs energy required for the reaction of a pure molten oxide into the most stable metallic phase can be obtained from the Ellingham Diagram. At temperatures in the vicinity of its liquidus temperature [156], TiO_2 – SiO_2 – Al_2O_3 – MgO – CaO slags are chemically stable and no reduction reactions are predicted to occur spontaneously for any constitutive oxide. Upon the application of a potential, any iron oxide dissolved will be reduced first as it requires the minimum thermodynamic cell voltage. Silica is the component of the slag that will be next to reduce, closely followed by titania. Thermodynamics seems to indicate that an electrolytic route for the production of more reactive 3d metals, such as titanium, might need silica-free electrolytes [60].

However, in this study the electrolyte is not a pure molten oxide but a solution of five different oxides. The non-ideal properties of the molten slag system are likely to shift the decomposition voltage predicted [202]. The small electrochemical window of operation between the decomposition of silica and titania [156], along with the high concentration (> 20 wt. %) of titania commonly present in ironmaking slags [16] have attracted research attention [15]. Recently, we electrochemically produced Ti-Si alloys from molten TiO_2 – SiO_2 – Al_2O_3 – MgO – CaO slag [156]. Our proof of concept study showed that reduction of Ti and Si was possible, but it did not elucidate the thermodynamic conditions for the reduction.

In this work, galvanostatic and potentiostatic electrolysis were performed to study the electrochemical reduction process of titanium and silicon ions from molten TiO_2 – SiO_2 – Al_2O_3 – MgO – CaO slags. Thermodynamic predictions using FactSage [19] were used to investigate the effect of composition changes on the cell voltages required to deposit silicon and titanium from the slag. Characterisation of the products of the molten oxide electrolysis (MOE) experiments give insight into the kinetic processes and are timely as Ti-Si alloys are gaining traction in the market for their high temperature structural properties [203, 204].

6.2 Experimental

6.2.1 Sample preparation

Two TiO_2 – SiO_2 – Al_2O_3 – MgO – CaO samples, Slag A and Slag C, were prepared by calcining reagent grade powder starting materials. The final compositions of the samples were measured by x-ray fluorescence spectroscopy (XRF, Siemens/Bruker SRS3000), and are reported in Table 7.1. Sample production has been described previously for these mixtures [156].

TABLE 6.1: Electrolyte compositions (wt.%) measured by XRF.

	TiO_2 wt.%	CaO wt.%	SiO_2 wt.%	Al_2O_3 wt.%	MgO wt.%
Slag A	33	18	15	19	15
Slag C	9	25	26	20	19

6.2.2 Experimental set-up

For this study, a vertical tube furnace (GSL-1700x-100VT-UL, MTI Corp.) was used to achieve the temperatures required to melt the slags and perform electrochemical measurements.

Vertical tube furnace

An alumina tube (Al_2O_3 > 99.5 %, 90.2 mm ID x 101.7 mm OD x 1000 mm H, MTI Corp.) was used to contain the entire system inside the vertical tube furnace, and a graphite crucible (45 mm OD x 35 mm ID x 80 mm H, Baofeng Graphite) was used to contain the sample. A secondary graphite crucible (80 mm OD x 60 mm ID x 60 mm H, Graphite Store) was used prevent any damage by leakage. The samples were placed in the centre of the hot zone using an internal support structure made of molybdenum (Figure 6.1A).

The design allowed electrodes to be raised/lowered into the molten material while maintaining an inert environment inside the tube. In order to reach the ultra-high temperature required for operation, insulating alumina blocks (Al_2O_3 foam, 80 mm D x 65 mm H, MTI Corp.) were placed on either side of the furnace hot zone. The two flanges (304 SS, MTI Corp.) sealing the alumina tube were water-cooled during operation to prevent them from overheating due to radiative heat transfer. A type B thermocouple (National Basic Sensor) was used to map the temperature of the hot zone. The temperature at the base of the secondary crucible was approximately 100 K lower than the controlled set-value for the furnace. During operation, the temperature was monitored by a thermocouple in the secondary

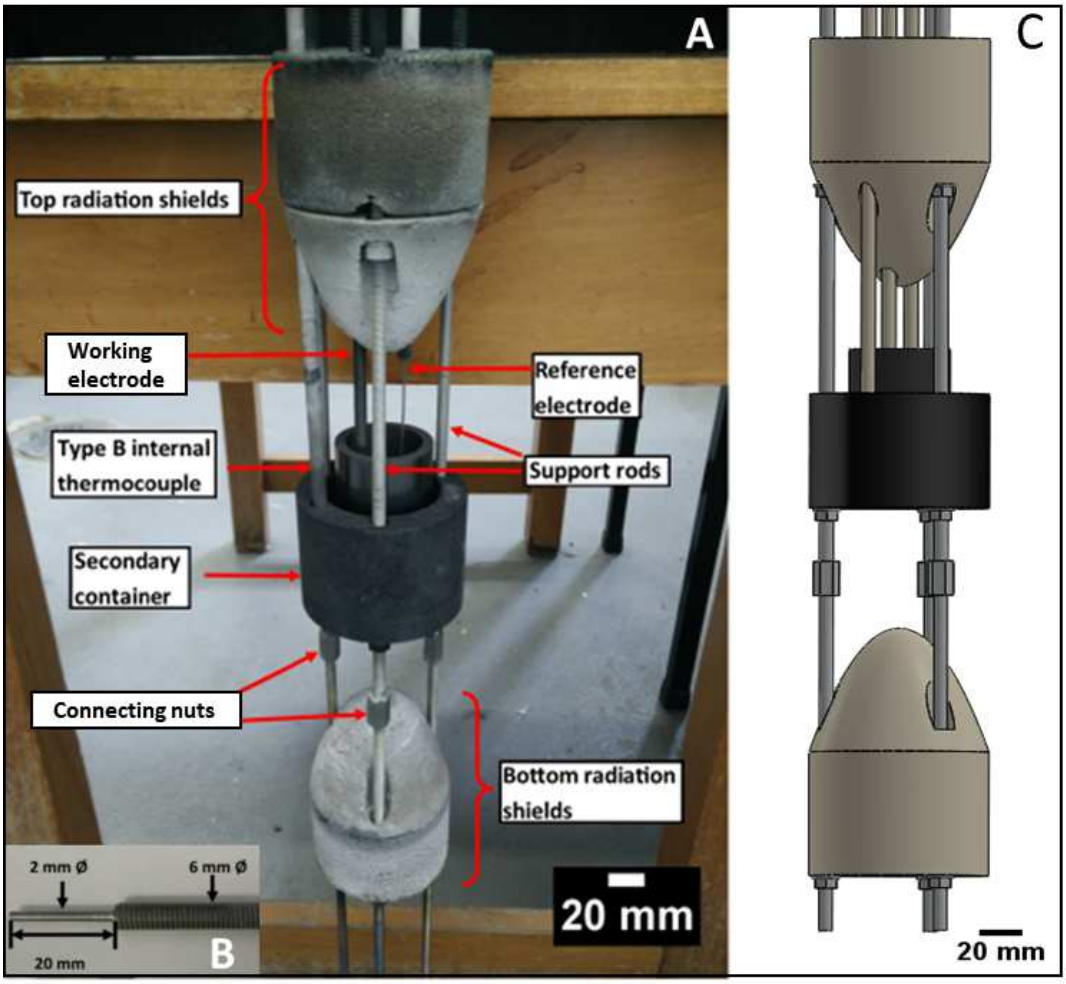

FIGURE 6.1: Electrochemical cell used in the vertical tube furnace adapted from [17], showing (A) the various individual components of the internal support structure system and (B) the modified area of the molybdenum working electrode in contact with the slag. (C) is the computer-aided design drawing of the set-up.

crucible.

To begin the experiments, while the furnace was at room temperature, the system was purged with zero grade Ar (99.999 %, BOC) for 90 minutes at a flow rate of 500 cm^3 min^{-1}. Once the oxygen content, detected by an oxygen analyser (Thermox CG-1000), was confirmed to be below 100 ppm, the flow rate was lowered to 150 cm^3 min^{-1} for the remainder of the experiment. After the purge sequence, the sample was heated at a rate of 1 K min^{-1} to a furnace temperature of 1923 K, which corresponded to an internal temperature of 1823 K. Once the system had been at temperature for an hour, the electrodes were lowered into the slag. During that process, the resistance between the working and counter electrode was measured with a voltmeter (Fluke 117 Handheld Digital Multimeter). A drop in the resistance value indicated when the electrodes had contacted the slag. The electrodes were

then lowered to their desired depth. The experiment finished by cooling the system at 1 K min^{-1} down to room temperature.

Upon cooling, the working electrode (WE) was cross-sectioned perpendicular to the electrode's longitudinal axis, using a high-speed diamond saw (Bühler). The sample was set in a conducting mounting compound (ProbeMet), and polished using progressively finer grades of silicon carbide paper (180, 320, 400, and 600 grit) and 9 μm diamond suspension. The composition and microstructure of the electrolysis product was examined using a scanning electron microscope (SEM, JEOL JSM-IT300LV) with LaB6 filament equipped with a X-Maxä 50 silicon drift energy dispersive spectroscopy (EDS) detector. For the post-mortem XRD analysis, fine crushed powders samples were scanned using a Bruker D8 instrument with CoK radiation. 2 Theta range 30-110 degrees.

Electrochemical measurements

A three-electrode configuration was used with the graphite crucible as counter electrode, and two molybdenum wires (Mo > 99.95 %, 600 mm L, Extreme Bolt & Fasteners) serving as the working and pseudo-reference electrodes. Molybdenum was used as the working and pseudo-reference electrode material as its physical properties make it robust enough for a wire to be inserted repeatedly into the molten slag. Molybdenum is an affordable, easily machinable and high melting temperature (2896 K) metal. However, molybdenum is not a suitable counter electrode material since it reacts easily with oxygen at the temperatures of interest, forming volatile oxides [205].

Galvanostatic and potentiostatic electrolysis experiments were performed using power supplies (Keithley 2260B-30-72 and Powertech MP3090, respectively). The voltages between the electrodes were recorded with a data logger (Measurement Computing 1808). The pseudo-reference electrode (1 mm D) was sheathed in an alumina (Al_2O_3 > 99.8 %, 6.35 mm OD, 1.3 mm ID, McDanel Advanced Ceramics) single bore tube. The top of the tube bore was sealed to prevent oxygen from entering the system. A thicker molybdenum rod (6 mm D, 600 mm L) was used as the working electrode in order to minimize the voltage drop along its length. However, to avoid large currents that the equipment could not support, the electrode's active area in contact with the slag was minimized by decreasing down to 2 mm the diameter of a 20 mm section at the end of the rod (Figure 6.1B).

6.2.3 Computational thermodynamic calculations

Thermodynamic cell voltages for the electrolytic extraction of metals from TiO_2 - SiO_2 - Al_2O_3 - MgO - CaO slags were predicted with the thermodynamic software FactSage 7.2 [19], using model parameters from its FToxid and FactPS databases.

Thus, thermodynamic activities, based on validated solution models and free energies of intermetallic products, rather than unit activities, as in Ellingham diagrams, or first-order ideal solution approximations, were used. The cell voltages were calculated from the Nernst equation:

$$E_{cell} = E^{\circ}_{cell} - \frac{RT}{nF} \cdot \ln \frac{\prod a^{\nu}_{products}}{\prod a^{\nu}_{reactants}} \tag{6.1}$$

where E°_{cell} is the thermodynamic (minimum) cell voltage at standard conditions, R is the universal gas constant, T is the temperature of interest, ν are the stoichiometric coefficients and a_i are the activities of the species present in the reaction. All reactions were based on the formation of one mole of O_2 as the anodic reaction:

$$2\,O^{2-} \longrightarrow O_2 + 4\,e^{-} \tag{6.2}$$

while the cathodic reaction was the reduction of one or two of the metal oxides from the slag. This allows direct comparison of the minimum energy required to drive the various reduction reactions.

The conditions inside the vertical tube furnace were simulated to model the gas phase. As a graphite crucible and an Ar purge gas were used in the experiments, the gas phase was modelled using 15 g of Ar, approximate amount contained in the vertical tube furnace at standard pressure and temperature, and the oxygen activity in the gas was determined from the equilibrium with graphite. Consequently, O_2 activities were around 10^{-17} at 1973 K. The activity of unary metallic products was assumed to be one. Cell voltages where the metallic reduction product was an intermetallic formed by co-reduction of two metals or by reaction of a reduced metal from the slag with the electrode material were also predicted. In those cases, the activity of the compound was assumed to be one and the standard chemical potential was the molar free energy of formation extracted from FactSage.

6.3 Results and Discussion

6.3.1 Materials compatibility

In order to guarantee that they are going to be able to perform as originally designed, ideally, all components should be inert at the conditions they are going to be exposed to. Graphite (crucible and counter electrode) and molybdenum (electrode and cell's support structure) are the main materials used on the electrochemical cell. An accurate knowledge on their behaviour in the presence of oxygen is of vital importance. Most metals upon contact with oxygen form an adherent protective oxide film on its surfaces which prevents further oxidation until certain temperature [206]. Gulbrasnsen *et al.* [205] established that for molybdenum this temperature

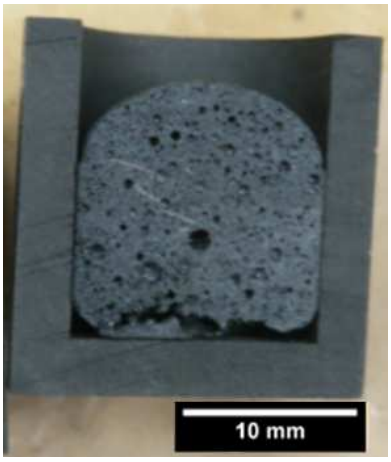

FIGURE 6.2: Slag A after being fired to operating temperatures in a graphite crucible. The convex meniscus indicates a lack of reactive wetting.

is 873 K. Additionally, they observed that between 873 and 1073 K both oxide film formation and oxide volatility occur, while above that molybdenum trioxide is spontaneously formed. The amount of oxygen inside the vertical tube furnace was not measured for these experiments, but the negligible weight change of the molybdenum support rods after each experiment confirmed the air-tightness of the designed system. The oxidation of metallic Mo will be faster than for graphite, whose activation energy (82.4 kJ/mol [205] and 163.2 kJ/mol [207], respectively) is nearly twofold.

For the system under study, thermodynamic calculations predicted no spontaneous metallothermic reaction of molybdenum with any of the components of the molten slag. The stability of the molybdenum as an electrode materials at the operating conditions was experimentally verified as it is known that molybdenum is susceptible to oxidation by iron oxide in molten slags [139]. Post-mortem electron microscopy of control experiments, i.e. experiments in which the system underwent the same thermal treatment but without electrolysis, validated this prediction. Additionally, no evidence of carbide formation was detected from post-mortem EDS analyses in the slag when fired using a graphite crucible, and no sign of any graphite was detected in any XRD trace. This is consistent with the non-reactive wetting behaviour observed in the present experiments (Figure 6.2), and with observations by Van der Colf and Howat [208], who studied ironmaking slags in graphite crucibles.

6.3.2 Initial electrolysis experiments

In electrolytic cells, a cell voltage threshold, E°_{cell}, has to be exceeded for ionic charge transfer to occur during an electrochemical reaction at the electrodes. The corresponding thermodynamic cell voltages for the reduction of metallic cations in the slag were predicted as a function of temperature for Slag A chemistry (Figure 6.3). Titanium was the only transition metal in the slag. As such, it could

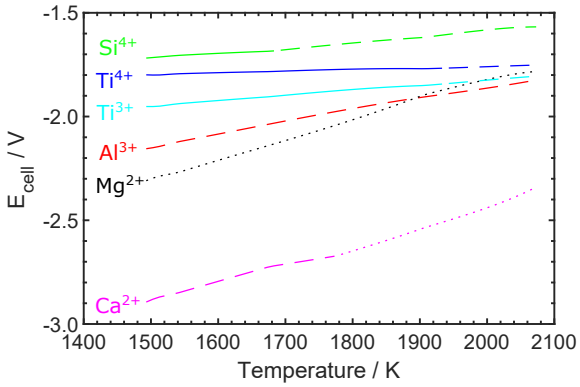

FIGURE 6.3: Thermodynamic cell voltages sequence for Slag A. Cell reactions are from the molten metal oxide to a pure metallic phase. Each line type represents a state of the stable metallic phase formed at the specified temperature: solid (solid line), liquid (dashed line) and gas (dotted line).

exist in multiple oxidation states (Ti^{4+}, Ti^{3+}, Ti^{2+} or Ti^{0}). Under the operating conditions of the experiments, Ti^{4+} is expected to be the main oxidation state in the melt [209]. Ti^{3+} is included in the thermodynamic calculations as it was the other main titanium species at equilibrium in the slag phase [170]. The predicted thermodynamic threshold for the conceivable decomposition reactions within the electrolyte indicated that silicon first, and then titanium ions will be reduced from the melt, with a potential window between both smaller than 200 mV.

This prediction was checked against experimental potentiostatic experiments performed on Slag A. For 150 minutes, a constant cell voltage of -2.0 V was applied at an internal temperature of 1823 K inside the vertical tube furnace. During this the average current was 4 A. 130 g of slag were electrolyzed until the system started its cooling sequence. At this point the applied voltage was halted and the working electrode was raised from the melt to allow easier sample manipulation for post-mortem microscopy analysis. The backscattered-electron images of the polished material indicated that phase segregation occurred on cooling (Figure 6.4). Large blocky spinel crystals and dendritic perovskite crystals were the main crystalline phases that precipitated from the slag below its liquidus temperature. In our previous study [156], in-situ XRD analysis identified this spinel phase as the last stable solid phase in the slag below the liquidus. The phase identification on cooling is consistent with reported by Ratchev and Belton [170] in similar titanomagnetite smelting type slags. Similarly, they also observed crystals on the slag segregating to the bottom of the container.

An ring of electrolytically reduced material surrounding the molybdenum working electrode is noticeable in Figure 6.4C. The composition of this cathodic deposit was investigated by EDS, where five different regions were identified (Figure 6.5). The first region represents the core of the molybdenum working electrode. Region II is bounded to the surface of the working electrode where a

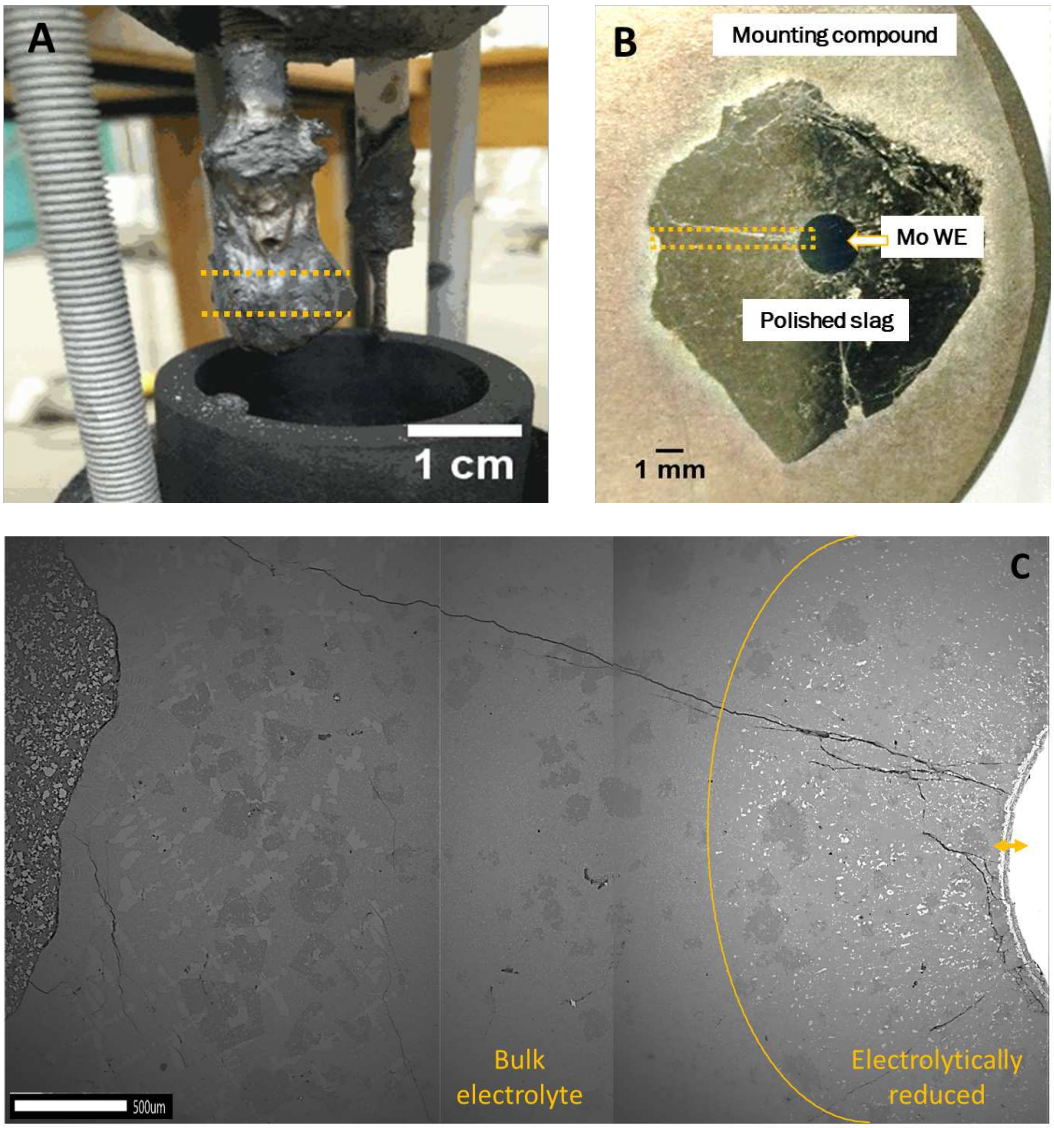

FIGURE 6.4: Procedure for the microscopy analysis after potentiostatic electrolysis on Slag A. (A) portion of the WE pulled out of the molten slag after electrolysis. (B) polished cross-section of the electrode, indicated by orange line in previous image, embedded in mounting compound. (C) superposition of three back-scatter electron images of the area surrounding the Mo WE, orange rectangle in previous image, containing the bulk slag and the region containing electrolytically reduced products.

TABLE 6.2: Gibbs energy for binary intermetallic formation in descending order. Predicted for the stable phases at 1823 K [212, 213] using FactSage's FTlite database.

	$\Delta G^{\circ}_{formation}$ / **kJ mol**$^{-1}$
Si (l) + 3 Mo (s) $\rightleftharpoons$ Mo_3Si (s)	-118
Si (l) + Ti (s) $\rightleftharpoons$ TiSi (s)	-131
2 Si (l) + Mo (s) $\rightleftharpoons$ $MoSi_2$ (s)	-147
3 Si (l) + 5 Mo (s) $\rightleftharpoons$ Mo_5Si_3 (s)	-339
3 Si (l) + 5 Ti (s) $\rightleftharpoons$ Ti_5Si_3 (s)	-564
4 Si (l) + 5 Ti (s) $\rightleftharpoons$ Ti_5Si_4 (s)	-634

combination of phases containing Si, Mo and Ti were formed. Since the cell voltage during the potentiostatic experiment was held above the thermodynamic threshold at which titanium and silicon ions can be reduced from the slag (see Figure 6.3), it is speculated that the product formed is a consequence of a surface alloy reaction that followed the electrochemical reduction of silicon and titanium ions from the melt. According to thermodynamic predictions, the formation of Mo_3Si, $MoSi_2$ and Mo_5Si_3, TiSi, Ti_5Si_3 and Ti_5Si_4 intermetallic phases will be thermodynamic spontaneous at 1823 K (see Table 6.2). A limitation of the computational model used is that it does not account for the possibility of reduced metals forming metallic solid solutions, as it would be the case of Ti-Mo [210], or ternary alloys. Regardless, the formation of any alloy would decrease the activity of the metallic species formed compared to the pure metals. Hence, it is speculated that the gradient of metallic alloy compositions formed in the surface of the working electrode is the result of different rates of diffusion of the reduced, Si and Ti, metal and the molybdenum working electrode. On the electrode surface, the nucleation kinetics would have defined the final size distribution, in particular the interfacial free energy barrier and the strain effects [211].

Region IV shares the same features of Region II, including the gradual decrease on the concentration of Mo with distance from the working electrode. We speculate that Region II and IV formed part of a compact reduced layer that grew radially surrounding the working electrode with time along the electrolysis. It is speculated that the layer broke on cooling, as the electrode was pulled out of the melt. Region III is part of the bulk electrolyte. This is in accordance with the composition of Region III mapped being with that of the spinel cubic crystals previously identified in the slag, where Ti has partially substituted Al. This also agrees with the formation of solid solution spinel of magnesium meta-aluminate, $MgAl_2O_4$, and magnesium meta-titanate, $MgTi_2O_4$, observed by Ratchev and Belton [170] for a titanomagnetite smelting type slags with a similar TiO_2 concentration. Region V is also part of the bulk electrolyte. The location mapped corresponds to that of amorphous slag phase, whose composition is depleted of TiO_2. Due to the presence of TiO_2 in the spinel and perovskite phases, the reduced amount of TiO_2 in the

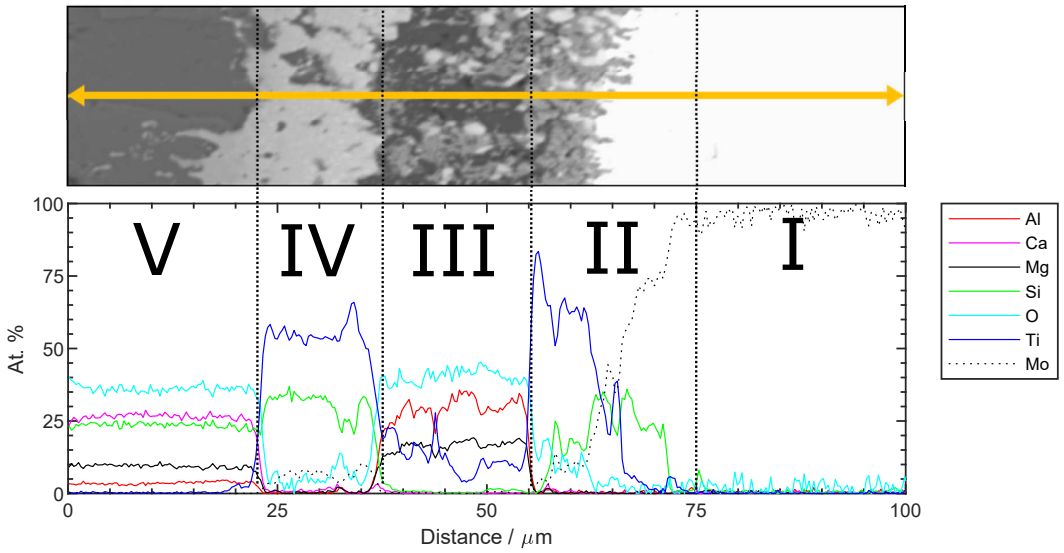

FIGURE 6.5: EDS linescan of the various product regions formed in the reduced layer around the molybdenum working electrode shown in in Figure 6.4C. Region I represents the core of the Mo We, Region II and IV are part of the products of the electrolysis, and Region III and V are phases representative of the bulk electrolyte.

slag can not be exclusively correlated to the electrolytically produced titanium metal.

In addition to this cathodic ring deposit, a bright speckled phase was also found dispersed in the area adjacent to the working electrode (Figure 6.4C). The composition of the speckled phase was determined by EDS analysis to be around $Ti_{1.7}Si$, which is close to the stoichiometric phase Ti_5Si_3 [212]. The difference might be associated to the use of standard-less EDS. The lack of molybdenum in its composition suggests that, as the $Mo_xSi_yTi_z$ intermetallic phases (Region II) grow, no Mo will be available for reaction. At that point Ti_xSi_y intermetallic phases would start forming onto the cathodic surface. The presence of pockets of this phase dispersed in the bulk electrolyte, instead of being attached to the working electrode, was not expected.

This phenomenon could be explained by the separation of precipitated crystals from the melt during solidification by convention currents. Alternatively, Lei *et al.* [214] reported that, contradicting the Ellingham diagram, TiO_2 in a Ti-bearing blast furnace slag could be reduced by Si. In this study, the electrochemically reduced Si would be liquid at the operating temperature. Liquid Si could drift away from the working electrode due to the density difference with the slag and react in the bulk, reducing TiO_2 from the melt. In the Hunter process, dissolved sodium metal in molten sodium chloride enhances that electrolyte's conductivity and allows the reaction to take place in the bulk, where titanium particles nucleate [37]. As another option, Si could have reacted in the bulk with electrochemically reduced Ti dissolved in the slag forming the observed precipitates. Otherwise, the

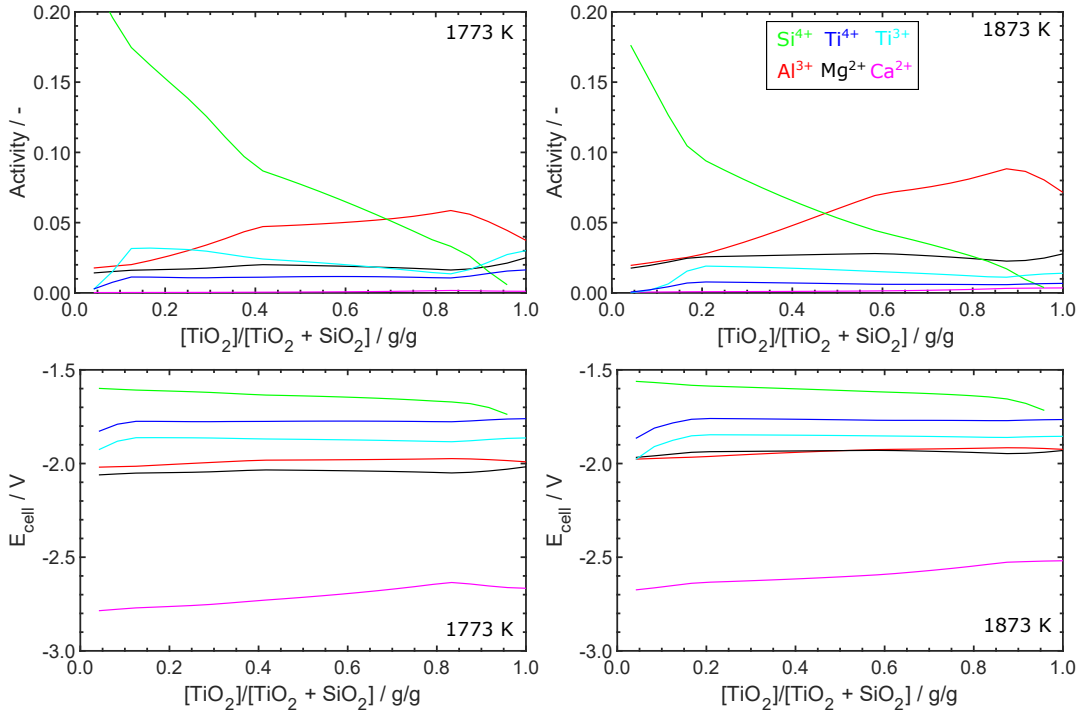

FIGURE 6.6: Effect of changing the amount of SiO_2 and TiO_2 in the slag composition on the predicted thermodynamic activities and cell voltages for the molten slag phase components at 1773 K, and 1873 K. At x = 0, there is no TiO_2 in the molten slag phase, while x = 1 equates to no SiO_2.

Ti_xSi_y pockets could be part of a sponge structure that can not be appreciated in the one dimensional cross-sectioned material. Dendrites could have grown radially outward from the working electrode, which would have connected the pockets to the charged working electrode. Regardless of its location, this phase is further evidence of the product of an electrochemical reaction as it was not present in control experiments (same thermal treatment, no electrolysis).

6.3.3 Effect of varying the slag composition on the electrochemical reduction sequence

The initial electrolysis experiment showed that titanium and silicon were deposited together, with titanium seemingly kinetically favoured. This is relevant since with the small potential window between silicon and titanium reduction, kinetics might be able to alter the reduction sequence, and enable selective reduction of titanium. The effect of varying the slag composition and temperature on the electrochemical reduction sequence were predicted using FactSage (see Figure 6.6).

The thermodynamic activities and cell voltages for the constituents of the slag phase were investigated at 1773 and 1873 K, the range of operating temperatures of ironmaking melters. By varying the ratio of SiO_2 and TiO_2 while keeping the total concentration of the two components in the melt constant, the effect of extracting

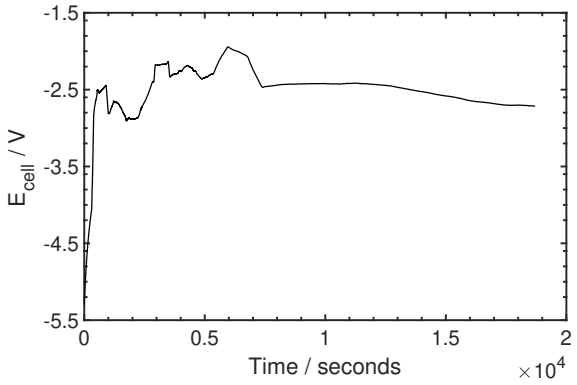

FIGURE 6.7: Cell voltage vs time plot recorded from a galvanostatic electrolysis experiment for Slag C. Current held at 5 A for 317 min at 1823 K. Black line represents a 10 min moving average of the recorded data.

concurrently silicon along with titanium from the slag on the thermodynamic cell voltages was investigated. For the range of temperatures and compositions studied, the results from the computational model illustrate that the reduction of silicon ions from the melt will still be the most favourable. According to the thermodynamic predictions, the change in temperature has a minor effect. The activity of SiO_2 was always greater than TiO_2, which results in lower cell voltages for the reduction of silicon independent of the amount of TiO_2 in the slag. Titanium reduction is preferred only when there is no silica in the system.

However, the model used is purely thermodynamic and had no consideration for the kinetics of the process. Hence, further electrochemical experiments need to be performed in order to elucidate the effect of the overpotentials at the electrodes on the reduction sequence. To investigate the kinetics of the reduction, galvanostatic electrolysis was performed on Slag C (with 9 wt.% TiO_2 compared to 33 wt.% for Slag A). In the experiment, a thinner Mo WE (1 mm D) was used, along with a smaller graphite crucible (20 mm OD x 14 mm ID x 20 mm H, Baofeng Graphite) to contain the 5 g of Slag C. The current was held at 5 A for 317 min at an internal temperature of 1823 K inside the vertical tube furnace. The resulting cell voltage stabilized over time around -2.4 V, and its reported in Figure 6.7.

For this experiment, the working electrode was not pulled out of the molten slag after electrolysis, but instead it was allowed to cool down in the melt. The rest of the post-mortem microscopy procedure was as previously described, and the composition surrounding the working electrode was mapped using EDS (Figure 6.8). The presence of carbon came from the coating required to improve the secondary electron signal from the slag (non-conductive oxides) in the electron microscope. The carbon layers deposited on the surface of the sample are transparent to the electron beam but conductive. At -2.4 V, similar value to the potentiostatic electrolysis experiment, the EDS maps show that Ti and Si ions were also reduced from the melt.

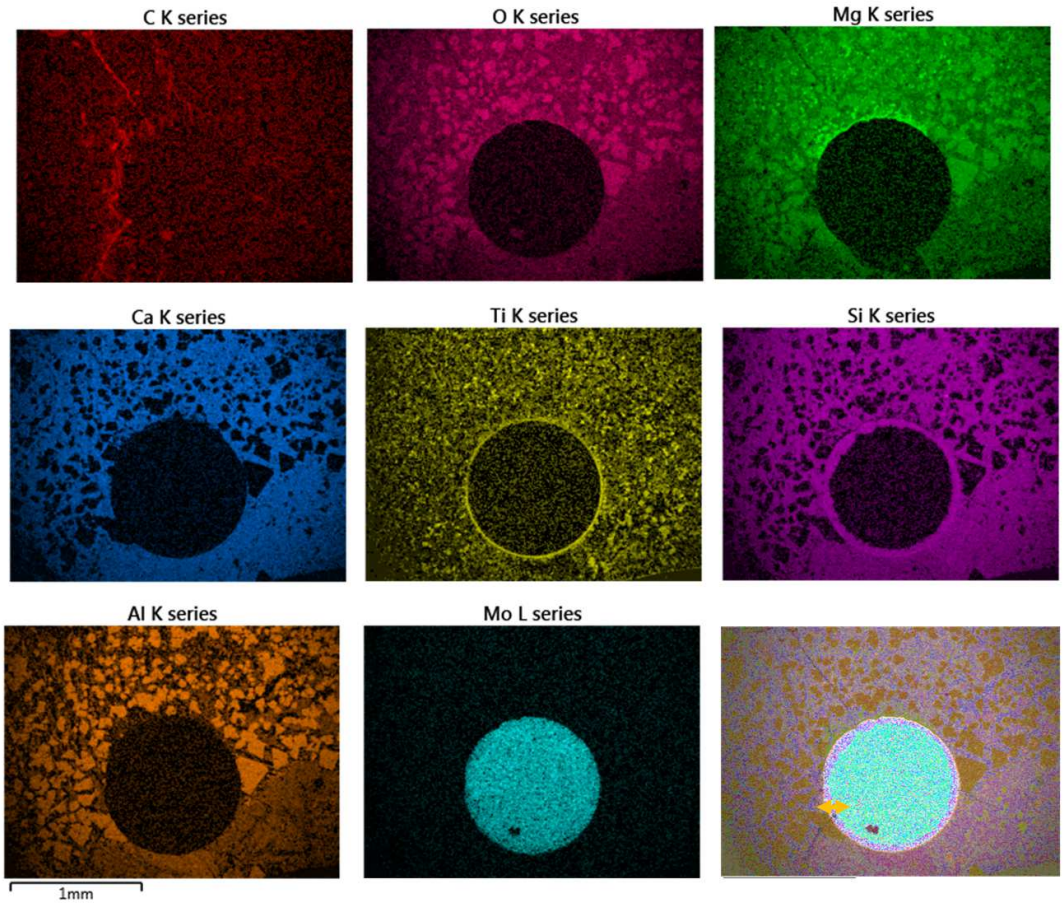

FIGURE 6.8: EDS composition maps of the molybdenum working electrode and the electrolytic deposit surrounding it after the galvanostatic experiment performed on Slag C, showing the same product morphology as Figure 6.5.

In accordance with a longer electrolysis time, there is a significantly bigger reduced layer of metal in the surface of the molybdenum working electrode compared to the potentiostatic electrolysis of Slag A. The composition of the various product regions formed in the reduced layer was measured by EDS to experimentally verify the predicted negligible effect of TiO_2 concentration on altering the slag's electrodeposition sequence (see Figure 6.9).

Similar as for Slag A, a gradient of alloy composition was formed at the surface of the molybdenum electrode with the reduced Ti and Si metals (Region II), which can be correlated to the different Z-contrast in the back-scatter electron image. Si diffused further into the Mo working electrode, lowering its activity towards the thermodynamically stable Mo_5Si_3 alloy. Closer to the interface with the bulk electrolyte (i.e. Region V, also depleted of TiO_2), the concentration of Ti increases in the alloy, forming a gradient of alloy compositions that resembles Region IV in Figure 6.5. The lack of an intermediate Region III in Figure 6.9 confirmed that a compact reduced metallic layer likely formed during the potentiostatic electrolysis on Slag A and broke on cooling due to the effect of pulling the electrode out of the

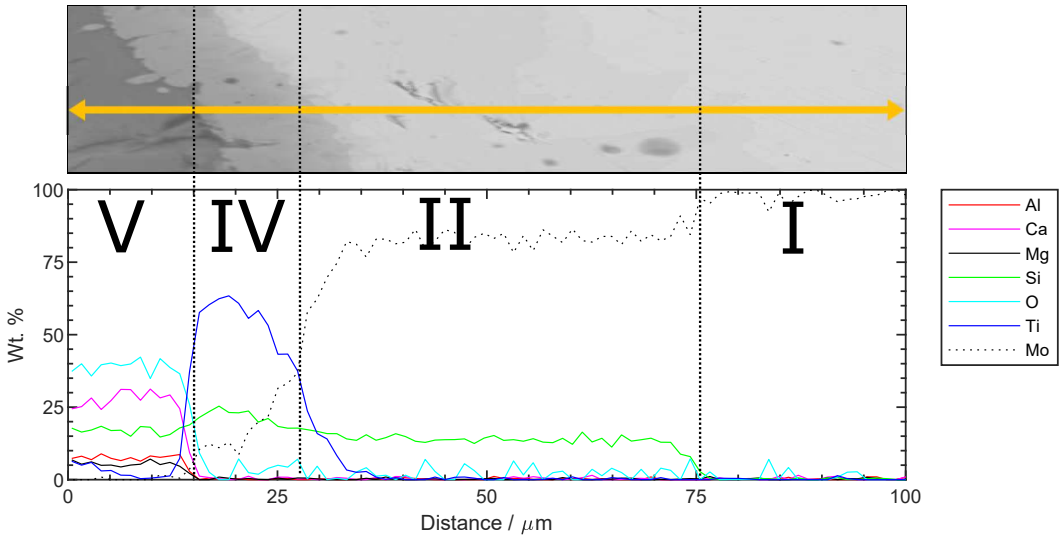

FIGURE 6.9: EDS linescan of the various product regions formed in the reduced layer around the molybdenum working electrode shown in Figure 6.8.

melt.

Alloys of silicon and titanium were also found dispersed in the area of the bulk electrolyte adjacent to the working electrode in Slag C. Hence, in this work, Ti was never selectively extracted as the electrolysis product for any of the TiO_2-bearing silicate slags. The results indicate that the extraction of pure metallic Ti from TiO_2 – SiO_2 – Al_2O_3 – MgO – CaO slag is unlikely without the prior removal of SiO_2. Even though it was out of the scope of the current study, the small potential window between the reduction of silicon and titanium ions from the melt motivates the study that further chemical modifications to the oxide system, such as changes in the concentration of the electronegative species [183], could have in the deposition series of the electrolyte.

While producing titanium metal would be the highest added-value product, the proven electrolytic extraction of Ti-Si alloys will still be a profitable endeavour if implemented as these alloys are gaining traction in the market for their use as high-temperature structural materials [204]. Ti-Si alloys have a wide range of potential applications [215], from microelectronics to the aerospace industry, due to their low density (4.32 g cm^{-3} [203]), high melting point (up to 2403 K for Ti_5Si_3 [212]), and high temperature stiffness (from room temperature to 1273 K, the Young's modulus only decreases from about 160 to 143 GPa for Ti_5Si_3, and 250 to 215 GPa for $TiSi_2$ [216]). Traditionally, these alloys have been produced from pure Si and Ti metals which are reacted to form intermetallics and solid solutions of the two components [203]. Considering the price of metallic Ti and the extra processing required to form Ti-Si alloys, electrolysis from a molten slag has the potential to reduce the costs of production. A further in-depth techno-economical study would need to be performed to assess the viability of this production method.

6.4 Conclusions

This work demonstrates the production of high purity alloys as an avenue to reuse TiO_2-rich ironmaking slag, an industrial by-product. The experiments performed in this study indicate that titanium-silicon alloys are the main products of the electrochemical reduction of TiO_2 – SiO_2 – Al_2O_3 – MgO – CaO slags. It was concluded that changing the amount of TiO_2 and SiO_2 in the system will not yield either titanium or silicon as a pure metallic product. Thermodynamic simulation validated experimental results. To alter the electrochemical sequence, future work could explore modifying the chemistry of the system, e.g. using a supporting electrolyte.

Chapter 7

Determination of the Partial Contributions to the Electrical Conductivity of TiO_2 – SiO_2 – Al_2O_3 – MgO – CaO Slags: Role of the Experimental Processing Conditions

Abstract

The pendant droplet technique was used inside a modified floating zone furnace to avoid containment contamination when evaluating the effect of the experimental processing conditions on the electrical conduction of molten $TiO_2 - SiO_2 - Al_2O_3 - MgO - CaO$ slags. Electrochemical impedance spectroscopy was used to measured the electrolyte resistance of the slag. Electronic and ionic transference numbers were obtained from stepped-potential chronoamperometry experiments in order to quantify the contribution of the electronic/ionic conductivity to the total electric conductivity. The results show that these slags are mixed conductors, where current is carried by ionic and electronic carriers. The oxygen partial pressure dependence of the electronic transference numbers, t_e, indicated a semiconducting mechanism in the molten slag. The ratio of the different valences of the transition metal ions had a predominant effect on the t_e. The TiO_2 content also favoured electronic conduction, while the effect of temperature and structure was less noticeable within the temperature and composition range studied.

7.1 Introduction

The use of molten oxide electrolysis (MOE) to produce metals has been proven more sustainable and environmentally friendly than the common, carbon-intensive, traditional metallurgical processes [85]. The potential to reduce emissions to the environment increases if large-scale waste materials are used as feedstock for this process. Along these lines, previous work [156] has shown that the electrochemical recovery of metals from molten $TiO_2 - SiO_2 - Al_2O_3 - MgO - CaO$ slag, a by-product of some ironmaking processes, is feasible. Moreover, Ti-bearing slag has been proposed as a substitute for rutile as the feedstock for the titanium industry [175]. However, a more extensive understanding of the electrical properties of this complex oxide system in its molten state is paramount in the design of industrial electrolytic cells.

Knowledge about the electrical resistivity of the melt is essential to establish the thermal balance of the electrochemical cell [65], as the ohmic drop affects the cell voltage of the electrochemical reaction of interest [159] and it is one of the major sources of heat generation in a high temperature electrolysis reactor [160]. To simulate a process where titanium is continuously extracted from the slag, the determination of the variability of specific electrical conductance or total electrical conductivity (σ, S cm^{-1}) with TiO_2 concentration is necessary. For $TiO_2 - SiO_2 - Al_2O_3 - MgO - CaO$ slags, it has been found to vary from 0.2 S cm^{-1} to 2 S cm^{-1} with concentrations up to 30 wt.% of TiO_2 [174, 217]. This value keeps increasing as the concentration of TiO_2 increases, with Hu *et al.* [175] reporting values up to 141 S cm^{-1} for molten high titania $TiO_2 - Ti_2O_3 - FeO - SiO_2 - Al_2O_3 - MgO - CaO$ slags.

The electrical properties of molten transition metal oxide bearing slags depend on the valence of the transition metal, as might be expected from a mechanism of semiconduction [218]. However, few studies proceed then to quantify the contributions to such behaviour. This is of particular importance in the electrolysis of molten oxide electrolytes, where the current is known to be transported through the oxide melt by both ionic and electronic charge carriers [157, 158, 175, 219], and, consequently, the charge transport mechanism across the electrolyte defines how much of the applied current is used in the reaction of interest. Transference numbers quantify the contribution of each charge carrier, which helps to determine the current efficiency [158]. Fried *et al.* [157] developed the framework to perform transference number measurements in titanate melts, but their study was limited to a narrow range of compositions and to temperatures below those required for the electrolysis of molten slag.

The purpose of the present study is to quantify the contribution of the ionic and

TABLE 7.1: Electrolyte compositions (wt.%) measured by XRF in ascending order of their predicted liquidus temperature, T_{liq}. Predicted solidus temperature, T_{sol}, and optical basicity, Λ_{corr}, calculated according to [220] are given.

	TiO_2 wt.%	CaO wt.%	SiO_2 wt.%	Al_2O_3 wt.%	MgO wt.%	Λ_{corr} -	T_{sol} K	T_{liq} K
Slag A	33	18	15	19	15	0.629	1486	1803
Slag B	15	24	25	18	18	0.635	1494	1823
Slag C	9	25	26	20	19	0.633	1494	1883

electronic charge carriers in the electrolysis of $TiO_2 - SiO_2 - Al_2O_3 - MgO - CaO$ slags. Transference number measurements were performed to determine to what extent the conductive mechanism is affected by changing the experimental processing conditions, such as temperature, atmosphere and electrolyte composition. Transference numbers were obtained using stepped-potential chronoamperometry (SPC), and their contribution to the mixed conduction mechanism in the molten slag was discussed.

7.2 Experimental

7.2.1 Sample preparation

Reagent grade TiO_2 (99.9%, CERAC Inc.), SiO_2 (99.4%, CARLO ERBA Reagents), Al_2O_3 (98%, CARLO ERBA Reagents), $(MgCO_3)_4 \cdot Mg(OH)_2 \cdot 5\,H_2O$ (99%, SIGMA-ALDRICH), and $CaCO_3$ (99.95%, CERAC Inc.) powders were used as starting materials to prepare three compositions of a synthetic $TiO_2 - SiO_2 - Al_2O_3 - MgO - CaO$ slag. The compositions studied in this paper are representative of Ti-bearing slag formed in the ironmaking process in New Zealand. The TiO_2 concentration has been lowered, while keeping the relative amounts of the other oxides approximately constant, to simulate a process where only titanium is continuously extracted from the slag. X-ray fluorescence spectroscopy (XRF, Siemens/Bruker SRS3000) was used to measure the compositions of the samples (see Table 7.1). The steps to prepare the final, rod-shape samples used in the furnace have been described before [156].

7.2.2 Electrochemical measurements and operation

In this work, all the electrochemical measurements were carried out by contacting a pendant droplet of molten slag with electrodes inside a modified thermal imaging furnace (TX-12000-I-MIT-VPO-PC, Crystal Systems Corp.). This containerless technique, and details regarding the assembly of the electrodes and electrical connections to the potentiostat, have been described before [13, 156]. Briefly, the sintered sample was suspended from the upper furnace shaft inside a quartz tube

(Technical Glass Products Inc.), while the electrode probe was inserted through the bottom port. Their position was adjusted using two individual stepper motors with submillimeter precision. Real time visualization during experimentation was achieved through a flat window in the quartz tube using a camera (EOS Rebel T5i DSLR, Canon Inc.) with telescopic lens.

At the beginning of each experiment, the electrochemical cell was purged three times before turning on the furnace. Argon gas (UHP 99.999%, 50 ppm O_2 or 100 ppm O_2; Airgas Inc.) at a flow rate of 200 mL min^{-1} was used to refill the chamber and during operation. The molten droplet was contacted with a type C thermocouple (W−Re (5 wt.%) | W−Re (26 wt.%)) to determine the operating temperature with $\pm$ 1% maximum error. Once the operating temperature (i.e. furnace lamp power) was chosen, the pendant droplet was formed by lowering the sample until its bottom end was in the hot zone. At the hot zone, the sample was rotated until the pendant droplet was stable. Then, the electrodes were raised up into the molten droplet to an immersion depth of approximately 2 mm. A sudden change in the open circuit potential (OCP), alongside the *in situ* visualization, confirmed that the electrodes had contacted the molten droplet.

For all measurements, a three-electrode configuration held inside an Al_2O_3 four-bore tube was used. The working (WE), counter (CE) and pseudo-reference electrode (REF) consisted of individual metallic wires immersed into the molten slag droplet. This type of reference electrode can provide a stable potential [192], and it is commonly used in MOE. Iridium (Ir > 99.9 %, diameter = 0.5 mm, Furuya Metals Co., Ltd.) was chosen as the electrode material due to its high melting point and mechanical stiffness. Both properties are required to repeatedly insert thin electrode wires into the molten slag. Moreover, Ir does not react with the slag or oxidise under the experimental conditions [156]. Its application on the electrolysis of molten oxides has been validated before [13, 156, 191].

All the electrochemical measurements were conducted using a potentiostat (Gamry Reference 3000). Each measurement began by recording the OCP. The ohmic resistance of the electrolyte between the working and pseudo-reference electrode (R_{slag}, Ω) was calculated from EIS measurements at OCP. The amplitude of the AC signal was 10 mV over a frequency range of 100 kHz to 1 Hz (10 points/decade). The analysis of the impedance data is detailed in the next section. Transference number measurements were obtained using SPC in order to quantify the fraction of the charge carried by ionic (anions and cations) or electronic (electrons and holes) carriers. Temperatures in the vicinity of T_{liq} were chosen, ranging from 1773 to 1933 K. For each measurement, the working electrode was maintained at OCP for 15 seconds before being stepped to 0.01 V vs Ir for 30 seconds (see Figure 7.1). Cyclic voltammetry confirmed that the SPC measurements were within a potential window where

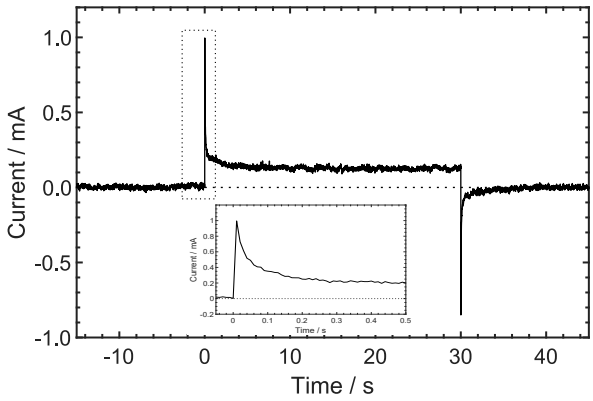

FIGURE 7.1: Current vs time response for Slag B at 1933 K following a potential step from OCP to 0.01 V vs Ir (at t = 0 s) then back to OCP (at t = 30 s). Inset: magnified view of the short time current decay.

no faradaic reactions occurred. 100 samples per second were recorded to accurately capture the current response to the potential step.

7.2.3 Considerations and measurement principles for the determination of

Phase relations

The phase relations were required in order to study the slags at temperatures in the vicinity of T_{liq}. Open and closed symbols in the experimental results represent measurements performed below and above a sample's T_{liq}, respectively. For each slag composition, at a total pressure of 1 atm, the phase relations were predicted as a function of temperature using the thermodynamic software FactSage 7.2 [19]. Model parameters are from FToxid and FactPS databases. The solidus temperature (T_{sol}), minimum temperature for any liquid phase to be stable, and the T_{liq}, maximum temperature for any solid phase to be stable, were determined. These values are reported in Table 7.1, and were calculated for P_{O_2}= 10^{-6} atm. In our previous work [156], differential scanning calorimetry (DSC) and *in situ*, high temperature X-ray powder diffraction (XRD) techniques were employed to validate the predictions.

Electrolyte resistance

EIS measurements were used to measure the total resistance between the working and pseudo-reference electrode. The impedance spectrum presented in Figure 7.2 was recorded at OCP for Slag C at 1903 K. A modified Randle's circuit was used to fit the impedance spectra. The equivalent circuit used to model the interfacial impedance between solid electrodes (REF | electrolyte | WE) is given in the inset of Figure 7.2. Randle's circuit was modified to account for the positive imaginary component present above 25 kHz. This inductive component, L1, is a characteristic of high temperature measurements at high frequencies, and associated with the long electrode leads required in the assembly of the electrical connections to the

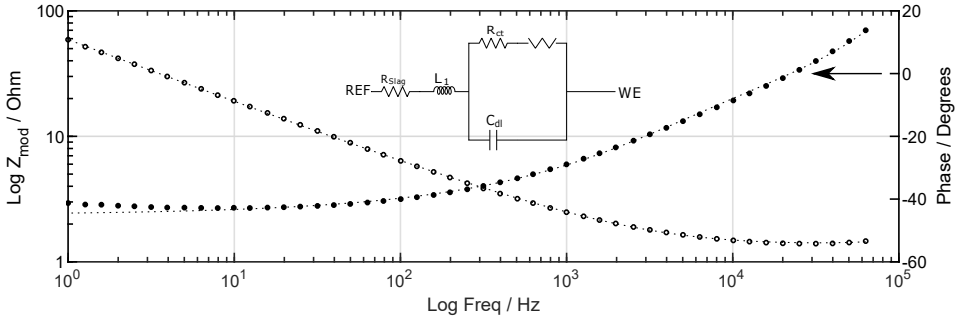

FIGURE 7.2: Bode plot recorded at OCP for Slag C at 1903 K (10 mV excitation, 100 kHz to 1 Hz). The experimental data is represented with points while a line is used for the fitted model. Inset: equivalent circuit diagram used to model impedance measurements in this study.

potentiostat [191]. Between 25 kHz to 5 kHz, the nearly constant real component of the impedance is associated with the electrolyte resistance. The presence of such a feature in this frequency range is consistent across silicate slags [221]. R_{slag} is obtained when the imaginary part of the impedance is zero to exclude the polarization effect, i.e. frequency-dependent impedance associated with double layer capacitance, which corresponds to the 45° shift in the phase angle below 5 kHz.

Typical R_{slag} values for the experiments ranged from 1 to 3 Ω. Overall, the magnitude of the electrolyte resistance varied with the slag composition, the atmosphere used, and electrode configuration (i.e. size of working electrode, and its distance to the pseudo-reference electrode [222]). In this work, the distance between both electrodes was approximately 2 mm and the area of the working electrode was 0.035 cm^2. In order to obtain a more precise value of R_{slag}, the ohmic contributions from the lead wire and electrode were subtracted. The resistance from the electrode's electrical connections was measured at room temperature to be approximately 0.3 Ω. The resistance corresponding to the electrode wire exposed to the operating temperatures was calculated from electrical resistivity data [223] to be on the order of 10^{-5} Ω.

The effect of the electrolyte resistance in fast transient electrochemical measurements must be taken into account [222]. In SPC measurements, the applied square pulse of voltage is susceptible to perturbation due to the R_{slag} producing a lag between the potential applied by the potentiostat and the potential of the working electrode. The cell time constant controls the time domain over which the distortion to the potential applied to the cell is significant. For systems where no faradaic reactions occur at the potential applied to the cell, the time constant is defined by

the charging time of the double-layer, $R_{slag}C_{dl}$, where C_{dl} is the double layer capacitance. The associated current will drop to virtually zero after a time equivalent to a few time constants [222]. For the electrode geometries used in this work, the time associated with double-layer charging is in the range of $10^{-5} - 10^{-6}$ seconds, which is consistent with reports for molten oxides [157, 191]. The experiments were designed to minimize its effect by choosing a time scale on the order of seconds for the experiments, and a resolution time of 10 milliseconds to accurately capture the current response to the potential step. Furthermore, a least squares regression was used to model the initial second of the current peak decay in order to exclude the current associated with the double layer charging from the current response in the calculation of transference numbers, detailed in the next section.

Ionic and electronic charge carrier contribution

While the use of EIS to measure electrolyte's ohmic resistance has been robustly used across aqueous and non-aqueous media, there is no standardised technique to measure transference numbers in corrosive, ultra-high melting temperature electrolytes such as the $TiO_2 - SiO_2 - Al_2O_3 - MgO - CaO$ slag. Olsen *et al.* [162] reviewed different experimental methods for measuring transference numbers, such as nuclear magnetic resonance and Radio Tracer, Hittorf, ac-impedance, dc-polarization (i.e. SPC) and the concentration cell. They concluded that the predominant Hittorf method is as effective as the SPC for the determination of transference numbers if the ion pairs, i.e. electron donor/acceptor couples, are present and mobile. In MOE, where these conditions are met, SPC is normally chosen since the Hittorf method is technically difficult in non-aqueous solutions. This method has been used previously for measuring transport properties of oxide melts [157–160], sulfide melts [224], salts [161], and even solid oxide electrolytes and polymers [162].

The transference numbers obtained using this technique are always positive[1], and express how charge is carried across the electrolyte. In a mixed conductor, the ionic transference number, t_i, is the fraction of the current that is carried by ionic charge carriers. The contribution of the electronic charge carriers is referred to as the electronic transference number, t_e. Both contributions sum to unity:

$$t_i + t_e = \frac{I_i}{I_t} + \frac{I_e}{I_t} = 1 \tag{7.1}$$

where I_i is the current carried by ionic charge carriers, I_e is the current carried by electronic charge carriers, and I_t is the total electric current. Provided the charge carries are distributed homogeneously in the melt, i.e. the same voltage is applied

[1]The sign of transference numbers calculated from SPC technique do not reflect the direction of transport. These transference numbers are called *internal* as they are referred to a fixed amount of a compound or ion [161].

to all of them, the partial contributions to the total electrical conductivity can be calculated from the corresponding transference numbers as:

$$\sigma_{i/e} = \sigma \cdot t_{i/e} \tag{7.2}$$

Fried *et al.* [157] proved this technique capable of differentiating between the ionic and electronic conductivity (σ_i and σ_e, S cm^{-1}) in titanate melts. Their model studies the charge transport dynamics in the bulk melt originated as response to an electric field (stepped-potential) for a system with mixed conduction. Based on the assumption of quasi-neutrality in an imposed field model, if there are no faradaic reactions occurring at the potential applied, the dynamics in the bulk melt result from the division of current between the diffusion of ions and ohmic conduction (ion drift and electron drift).

The model isolates the charge transport dynamics in the bulk by defining time limits that exclude dynamics arising from the electrode processes and external circuit elements, as well as any bounding double layers. On this time scale it is demonstrated that, if the cell time constant for the system under study is small compared to the time scale of the experiment, there is no net charge accumulation in the bulk, and the current in the bulk is merely ohmic. Hence, the material in the bulk will remain uncharged, sustaining the quasi-neutrality assumption. This approach was validated for this work by comparing the cell time constant (microseconds, discussed in the previous section) to the time scale of the charge transport dynamics in the bulk (seconds). A limitation of the technique is that it cannot distinguish which ion is the charge carrier if there are a plurality of mobile ionic species.

Transference numbers can be calculated by monitoring the total electric current response to a potential step as a function of time (see Figure 7.1). After the potential is applied, the current decay as a function of time can be correlated to the transition from mixed to pure electronic conduction. Consequently, the t_e can be calculated from the value of the two limiting cases, the initial current peak and the value at the long-time limit:

$$t_e = \frac{I_{t\to\infty}}{I_{t\to 0}} \tag{7.3}$$

To exclude the double-layer charging time, $3 \cdot R_{slag}C_{dl}$ was chosen as the short-time limit. This conservative approach supposes an underestimate of maximum 2%, if compared to starting the model at the peak of the current response, and assures that the current value associated with the double-layer charging time would have been completely accounted for at $t \to 0$ [222]. Therefore, when the model starts, there is a uniform concentration of ions outside the double layers, and $I_{t\to 0}$ is purely ohmic (ion + electron drift). At the long-time limit, $t \to \infty$, the ion concentration will no longer be uniform. However, since no faradaic reactions are occurring at the

electrodes, diffusion balances drift, and $I_{t\to\infty}$ is, again, solely ohmic (only electron drift).

7.3 Results and Discussion

7.3.1 Conductive mechanism

Molten metal oxide electrolytes are proven mixed conductors, where current is conducted by ionic and electronic carriers [158]. Experimentally, the mixed conduction nature of $TiO_2 - SiO_2 - Al_2O_3 - MgO - CaO$ slags can be identified from the shape of the current response to the applied potential step in the SPC measurements (see Figure 7.1). The ionic contribution is noticeable upon removal of the applied potential, when a current is measured as a result of the diffusion of ions during relaxation. This observation is in agreement with what has been reported previously in titanate melts [157]. The electronic contribution is illustrated by the non-zero value of $I_{t\to\infty}$. As discussed in the previous section, any current present at $t \to \infty$ is representative of electronic conduction.

In molten transition metal oxide bearing slags, pure electronic charge transfer, as reported for solid glasses [63], is an unlikely mechanism for the electronic conduction. Free electrons in the melt are instead attracted to the 3d-orbitals of the transition metals cations [63]. Mott [225] associated the electronic conduction to the semiconducting character of these melts, where the different oxidation states of the transition metal cations would act as ion pairs. For the $TiO_2 - SiO_2 - Al_2O_3 - MgO - CaO$ slags under study, EIS measurements were used to determine the temperature dependence of electrolyte resistance. The electrolyte resistance decreased with increasing temperature suggesting that the slag may act as a semiconductor. This is consistent with expectations for a melt containing TiO_2, a known semiconductor [157]. Furthermore, semiconducting behaviour has been seen in most of the Earth's mantle minerals [226], including ferrous and titanate melts [157, 175, 219].

The electronic conduction on many metal oxides has been proven polaronic in nature [226]. Recently, Barati and Coley [219] explained the electronic contribution to the mixed conduction of FeO_x – SiO_2 – CaO slags with a diffusion-assisted charge transfer model. Briefly, the distance between the ferrous and ferric ions has to be sufficiently short to activate the tunnelling of electrons through the ion pair. The short-range electron-lattice interaction derived by this hopping mechanism between low- to high-valence ions is commonly refereed to as small polaron. This model was also used by Hu *et al.* [175] to explain the electrical conductivity values for $TiO_2 - Ti_2O_3 - FeO - SiO_2 - Al_2O_3 - MgO - CaO$ high-titania slags. In order to

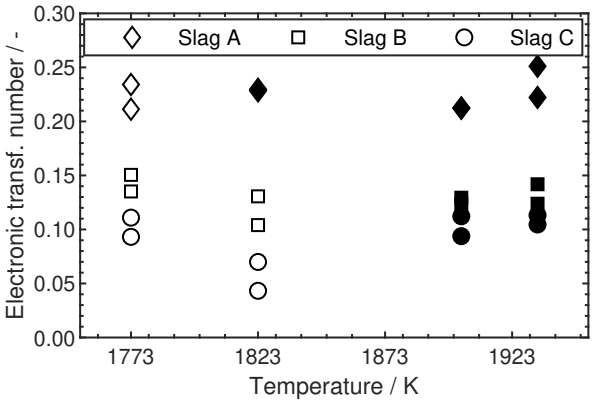

FIGURE 7.3: Electronic transference number variation with temperature for Slag A, Slag B and Slag C at a fix partial pressure of oxygen of 10^{-6} atm. Measurements below the predicted T_{liq} are presented with open symbols.

extend this theory to $TiO_2 - SiO_2 - Al_2O_3 - MgO - CaO$ slags, the dependence of the transference numbers on oxygen potential, temperature, TiO_2 content and melt structure will be discussed in the following sections.

7.3.2 Effect of TiO_2 content

It is known that the electrical conductivity of titanium containing slags is predominantly ionic [172, 227]. However, in slags containing high concentrations (>70 wt.%) electronic conduction has been reported to dominate [175]. Slag A (33 wt.% TiO_2), Slag B (15 wt.% TiO_2) and Slag C (9 wt.% TiO_2) were used to quantify the effect of TiO_2 concentration during electrolysis on the electronic conduction of the Ti-bearing slags.

The electronic transference number of the different slags as a function of temperature ranged from 0.04 to 0.25, and was found to vary with temperature and slag composition (see Figure 7.3). Across all the temperatures studied, the t_e increased as TiO_2 concentration increased. Ducret *et al.* [160] reported a similar behaviour in the electronic transference numbers with the concentration of FeO in $FeO - CaO - MgO - SiO_2$ melts. Fried *et al.* [157] identified titanium's multivalence as responsible for the increase in electronic conduction, facilitating charge hopping. As the concentration of titanium cations increases in the melt, the easier it becomes to find a neighbouring ion, and an increase in the electronic conduction is expected. Accordingly, the t_e was lowest for Slag C, the slag with the lowest TiO_2 concentration, and highest for Slag A with the highest TiO_2 concentration.

The effect of the titania content of the melt on the total electrical conductivity is more complex. An increase of the titania content does not necessarily correlate with an increase on the total electrical conductivity. Mori mapped the total electrical conductivity for $FeO_x - TiO_2$ melts at 1673 K [228], and $CaO - SiO_2 - TiO_2$ melts at 1693 K [227]. Mori observed an increase in the total electrical conductivity with

increasing TiO_2 for the latter, while a decrease was observed for the former with TiO_2 concentration up to 40 wt.%. Such contradicting behaviour is associated to the complex relation of TiO_2 with the structure of these slags. This effect will be further explored in Section 3.5.

7.3.3 Effect of temperature

The electronic transference number were measured as a function of composition and temperature between 1773 and 1933 K (see Figure 7.3). Temperatures around T_{liq} were chosen to investigate the effect of multi-phase conditions on the transference numbers. For Slag C and Slag B, t_e decreased initially. This is common for measurements made at $T_{sol} < T < T_{liq}$ where solid and liquid phases coexist. In that two phase region, the solid phase fraction decreases with increasing temperature, which facilitates ionic mobility. That increases the ionic transference number, and, consequently, decreases t_e.

From there, the t_e increased as temperature continued to increase since both slag compositions are above their T_{liq}. Such increase can be attributed to molten semiconduction, in particular, to small polaron hopping as it is a thermally activated process; however, the effect of temperature on electronic conduction has been reported to be negligible above the liquidus temperature [158]. This is consistent with measurements made for Slag A. The insensitivity of t_e to temperature is most pronounced for Slag A since most of the SPC measurements for this slag composition were done above its liquidus temperature (closed symbols in Figure 7.3). Sokhanvaran *et al.* [159] associated the increase of the electronic transference numbers to an increase in the disassociation of a cryolite-silica melt at temperatures above the T_{liq} that leads to an increase in the multivalent anions. The effect of the temperature seems to also correlated with the structure of these slags. This effect will be further explored in Section 3.5.

7.3.4 Effect of oxygen potential

P_{O_2} is known to influence the ratio of the different valences of the transition metal ions present in the slag. Three different gas atmospheres were used to study the effect of the partial pressure of oxygen on the electronic conduction of Slag A (see Figure 7.4). From 1823 to 1933 K, the t_e increased with a decrease in the oxygen potential. All measurements were done at temperatures above the T_{liq}. In this molten state, the electronic transference number dependency on the P_{O_2} is an indication of a semiconducting mechanism [218]. According to the model proposed by Barati and Coley [219], an increase in the ratio of the different valences is expected to increase the t_e. The larger the ratio between oxidation states of the transition metal, the higher the likelihood that two ions with different valence states will be close enough for the charge to jump from the lowest to the highest valence

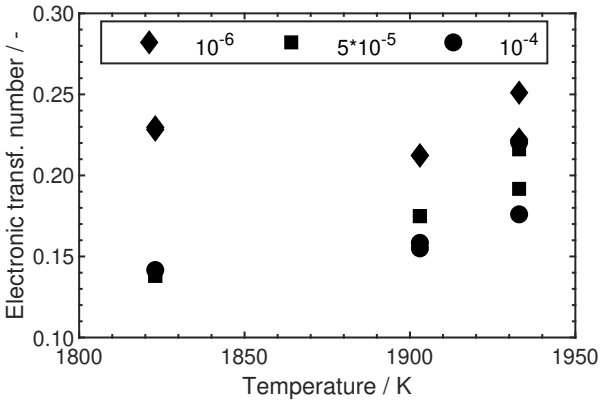

FIGURE 7.4: Electronic transference number variation with temperature for different partial pressures of oxygen (atm) for Slag A.

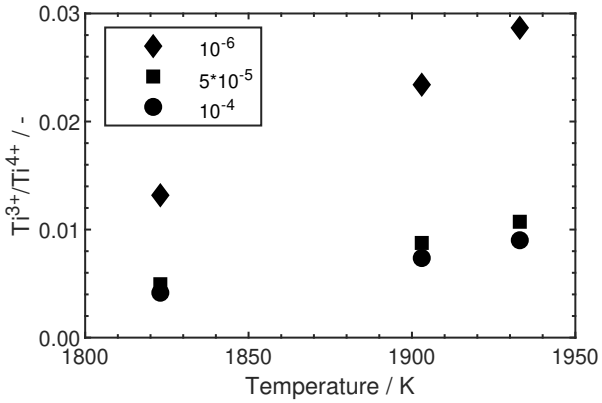

FIGURE 7.5: The predicted equilibrium speciation ratio, between Ti^{3+} and Ti^{4+}, variation with temperature for various partial pressures of oxygen (atm) for Slag A.

state. In titanium bearing slags, the distribution among Ti^{4+}, Ti^{3+}, and Ti^{2+} valence states depends on slag composition, temperatures and oxygen partial pressures. Tranell *et al.* [209] investigated the redox behaviour of titanium in $CaO-SiO_2-TiO_x$ slags with up to 52.3 wt.% TiO_2, and found that most reduced titanium was in Ti^{3+} valence in the melt at oxygen partial pressures between 10^{-12} and 10^{-7} atm. In the present study, similar experimental conditions were used, and hence all reduced titanium in the slag is reported as Ti^{3+}.

The effect of the temperature and P_{O_2} on the Ti^{3+} / Ti^{4+} ratio were predicted for Slag A using FactSage (see Figure 7.5). The ratio between Ti^{3+} and Ti^{4+} increases with increasing temperature. This is consistent with the endothermic character of the reduction of TiO_2 to Ti_2O_3 [229]. Ti^{4+} is the most predominant titanium oxidation state in the melt. This is consistent with thermodynamic predictions in the temperature range studied, where any Ti_2O_3 is spontaneously oxidized to TiO_2 [167]. The concentration of Ti^{3+} increases with decreasing the oxygen partial pressure, as lower oxygen potentials favours the reduction of Ti^{4+} [209].

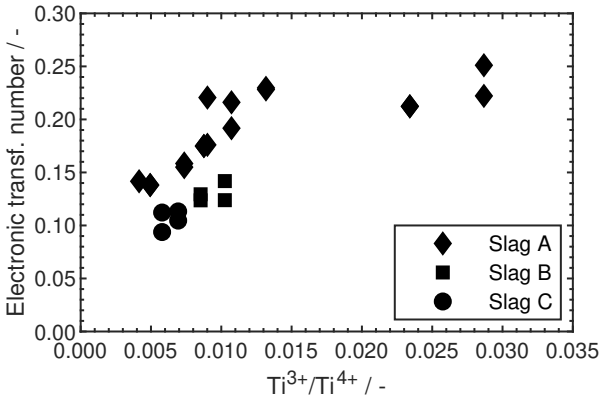

FIGURE 7.6: Electronic transference number variation with the predicted equilibrium speciation ratio, between Ti^{3+} and Ti^{4+}, measured for Slag A, Slag B and Slag C above their predicted T_{liq}.

The ability of electrons to act as charge carriers depends on the availability of unoccupied electronic states. Ti^{3+} has been found to increase electronic conductivity by creating holes in the valence band in crystalline titanium sesquioxide [230]. An increase in concentration of Ti^{3+} is proposed to be the main contribution to the reported increase in t_e (see Figure 7.6). Since electron mobility is usually much higher than ionic mobility, it is speculated that a bit of mixed valence is sufficient to generate electronic conductivity.

7.3.5 Effect of melt structure

Initial attempts to explain the conductive mechanism of molten oxides were derived from the theory of electric conduction in ionic liquids [231, 232]. This approach, even though successful to explain the behaviour in molten salts, fails in its application to complex molten silicates because it does not consider short-range ordering [63]. Mysen [64] and, more recently, Min and Tsukihashi [63] reviewed the XRD, nuclear magnetic resonance and raman spectroscopy literature and found that a 3-dimensional interconnected network of tetrahedral silicate anionic units was consistent within silicate slags. The effect of structural changes (eg. phase transitions) on the total electrical conductivity on solid silicate minerals has been studied before [226]. As free ions in the slag are the only ionic charge carriers [174], ionic conduction strongly depends upon structure [63]. The location of metal cations in the silica network at their substitutional Si sites or at interstitial sites in the free volume affects the degree of polymerisation and, hence, the transport properties of silicate melts [64, 220].

The effect of the melt structure is expected to prevail for the ionic conduction as it is achieved by the migration of ions [63]. The Nernst-Einstein equation defines the total electrical conductivity in an ionic conductor as proportional to the number and mobility of charge carriers [226]. It is then expected that the slag depolymerization

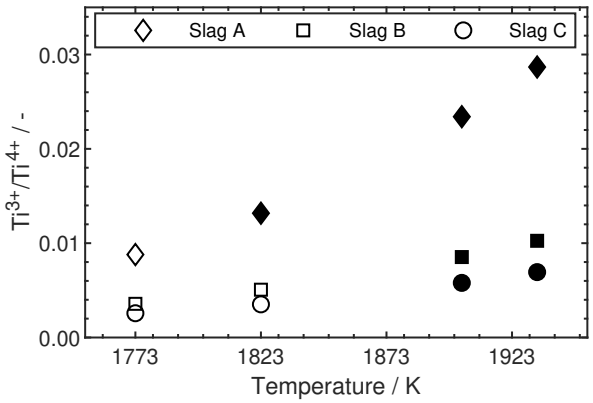

FIGURE 7.7: The predicted equilibrium speciation ratio, between Ti^{3+} and Ti^{4+}, variation with temperature and slag composition at a fix partial pressure of oxygen of 10^{-6} atm. Measurements below the predicted T_{liq} are presented with open symbols.

will positively influence the ionic conduction facilitating the movement of ions through the melt. The optical basicity, Λ, is a common metric used in process metallurgy to measure the degree of depolymerization of silicate systems [220]. In oxide networks, it indicates the proportion of basic oxides. In more acidic slags (eg. higher fraction of the network-forming $SiO_4{}^{4-}$ tetrahedral units) the degree of polymerization is higher. Λ is a concept derived from the bonding characteristics of the Lewis acid-base theory [233], and it has been experimentally correlated to the position of equilibrium for redox reaction within the melt [233] and to parameters such as viscosity in ironmaking slags [234].

The optical basicity calculated for the different slag compositions was corrected (see Λ_{corr} in Table 7.1) to account for the numbers of Ca^{+} cations needed to charge balance the Al^{3+} incorporated into the silicate network [220]. Slag A has the lowest Λ_{corr}, so it should present a bigger opposition to ionic diffusion than Slag B and Slag C. This is consistent with Slag A having the highest t_e (see Figure 7.3). However, the values of Λ_{corr} are very close for all slag compositions, indicating a similar degree of polymerization and of ionic mobility. Additionally, above 1773 K, TiO_2 does not have any significant effect on viscosity, with values less than 0.5 Pa.s [153, 178]. The low and almost constant viscosity along with the small deviation in Λ_{corr} indicates that the influence of structure in the ionic conduction for the temperatures and composition measured will be minor.

With regards to the slag chemistry, the effect is more prevalent on the electronic conduction due to the electronic conduction mechanism of these transition metal cation-bearing slags [63]. As explained before, hopping conduction requires neighbouring ions of different valence for the charge transfer to occur [158]. Previous research [201, 209] has shown that the amount of Ti^{3+} in the melt increased with the decreasing basicity when the temperature and oxygen partial pressure were

kept constant. A less basic system is more polymerized, it contains fewer free oxygen anions, and more Ti^{3+} [233]. This is consistent with the trend observed with reducing atmospheres in Section 3.4. The Ti^{3+} / Ti^{4+} ratio was predicted using FactSage for Slag A, Slag B and Slag C at a fixed partial pressure of oxygen of 10^{-6} atm (see Figure 7.7). The predicted ratio increased, specially above the T_{liq}, with increasing temperature as discussed in the previous section.

The amount of Ti^{3+} predicted changed slightly with increasing TiO_2 concentrations from 9 wt.% (Slag C) up to 33 wt.% (Slag A). The values agree with those reported by Tranell *et al.* [209] for the amount of TiO_2 in the melt. However, it is worth noting that Tranell *et al.* [209] observed a more complex relation between the amount of TiO_2 in the melt and the Ti^{3+} / Ti^{4+} ratio. For concentrations up to 14 wt.% in $CaO-SiO_2-TiO_x$, an increase of TiO_2 lead to a decreased in the ratio, while the trend was reversed if the concentration of TiO_2 was increased up to 50 wt.%. This behaviour can be related to a change of the oxygen coordination state of Ti^{4+} with TiO_2 content [64]. The contradictory effect of TiO_2 content on the total electrical conductivity of titania containing slags without silica [228] and titania containing slags with silica [227] may be also attributed to this complex relationship. Accordingly, incorporating the actual structural changes associated with TiO_2 addition is a hard task with on-going research efforts [235].

7.4 Conclusions

The mixed conduction mechanism of molten $TiO_2 - SiO_2 - Al_2O_3 - MgO - CaO$ slags was assessed using EIS and SPC measurements, where the contribution of the ionic and electronic charge carriers was quantified as temperature, oxygen partial pressure, and electrolyte composition were varied. The main conclusions are summarized as follows:

1. Across all the temperatures studied, the t_e increased as TiO_2 concentration increased from 9 to 33 wt.%. Further experiments must be done before extrapolating to other concentrations as the oxygen coordination state of Ti^{4+} has been reported to change with TiO_2 content [64].

2. The effect of temperature on the t_e was minor for the range of temperatures studied. However, the trend of the t_e changed around T_{liq}. It was found that t_e increased with temperature above the T_{liq}, as expected from thermally-activated polaron hoping. t_e increased again as temperature decreased below the T_{liq} as the solid phase fraction increased in the two-phase region.

3. Decreasing the oxygen potential, from 10^{-4} to 10^{-6} atm, increased the partition between Ti^{3+} and Ti^{4+}. The oxygen partial pressure dependence of t_e is an indication of a semiconducting mechanism in the molten slag.

4. The influence of structure in the ionic conduction was minor for the slags studied as the degree of depolymerization and the viscosity were nearly constant [153, 178] within the temperature and composition range investigated.

The electronic transference number of the different slags ranged from 0.04 to 0.25 and was found to vary mainly with oxygen potential and total titanium content. This is consistent with the diffusion-assisted charge transfer model recently used to explain electronic conduction on molten FeO_x bearing slags [219]. The understanding gained about the conductive mechanism of the slag in relation with its physical-chemical properties and the extent to which it is affected by changing the experimental processing conditions provides valuable information that is required to optimize the recycling of the slag.

Chapter 8

Main Findings and Outlook

This chapter aims to conclude this work by summarizing its main findings and providing suggestions for future research on the electrochemical reduction of titanium from ironmaking slag.

Main Findings

This doctoral thesis focuses on evaluating the feasibility of using ironmaking slag, produced from titanomagnetite concentrates, as an electrolyte to electrolytically extract titanium metal. It was hypothesized that due to the mixed oxide nature of the slag, no additional supporting electrolyte would be needed for the implementation of an electrochemical route and that sufficient ionic conductivity would be present in the molten slag such that titanium could be extracted. Research efforts were centred on closing the scientific gap around the characterization of slag in its molten state. In particular, determining the physicochemical properties, the electrochemical behaviour and the electrical properties of the melt.

To do so, a laboratory scale, electrolytic cell was designed inside a vertical tube furnace and used to perform electrochemical measurements at the extreme temperatures required to melt the slags. The reliability of our experimental method was verified by computational thermodynamic calculations. A thermodynamic model was developed using the software package FactSage 7.2 [19] to predict the thermodynamic cell voltages required for the electrolytic extraction of metals from the slag. The model was validated by comparing experimental DSC and in situ high-temperature XRD measurements with the predicted phase relations for the slags. From 1486 K to 1960 K, the synthetic slag compositions studied melt over a broad range of temperatures. Ironmaking slag is a high melting oxide mixture, with temperatures higher than 1450 K required for melting. According to the thermodynamic predictions, the minimum temperature for a liquid phase to be stable (T_{sol}) shows little variation with the titania content in the slag, while the liquidus temperature is expected to increase.

An important experimental aspect of the electrochemical reduction of titanium

from ironmaking slag that is quite often overlooked is the the effect of entrained iron species on its performance as a molten oxide electrolyte. The presence of iron in the melt, even in small quantities, increased considerably the electronic conduction in the melt, hindering the faradaic efficiency of the electrolysis. Furthermore, if pure titanium metal is the desired product, the melt should be free of any iron as it is easier to reduce than the target metal and it would contaminate the final metallic product.

Even though the processing conditions were optimized to reliably operate in the vicinity of the slag's liquidus temperature, severe technical challenges were present. The challenges were mainly related to materials compatibility, which limited operation to reducing conditions and the use of graphite to contain the slag. To overcome these constraints, the pendant droplet technique was employed inside a modified thermal imaging furnace [13, 156], enabling precise measurement while avoiding any potential contamination. This containerless approach was used to investigate the electrochemical behaviour of TiO_2 – SiO_2 – Al_2O_3 – MgO – CaO slags in their molten state, where iridium was used in a three-electrode configuration to perform cyclic voltammetry and potentiostatic electrolysis measurements. Post-mortem microscopy analysis showed the formation of Ir – Ti – Si alloys, while oxygen evolution was observed thanks to real-time visualisation during experimentation, proving that the electrochemical recovery of metals from molten ironmaking slags is feasible.

The initial electrolysis experiments showed that Ti and Si were deposited together. The Ti content in the different alloy phases was always larger than that of Si, which suggested that Ti might be kinetically favoured. This is interesting since, thermodynamically, Si reduction from the melt was predicted to be the most favourable, which suggests that Si would be preferentially deposited. The effect of varying the amount of TiO_2 and SiO_2 in the slag composition on the electrochemical reduction sequence as a function of temperature were predicted using FactSage. According to the thermodynamic predictions, independent of temperature, titanium reduction is preferred only when there is no silica in the system. However, the model used is purely thermodynamic and has no consideration for the kinetics of the process. Hence, due to the small potential window between Ti and Si reduction, further electrolysis experiments changing the amount of TiO_2 in the slag were performed to elucidate if the overpotentials at the electrodes could be able to alter the reduction sequence and selectively reduce titanium. The experiments confirmed that titanium-silicon alloys are the main products of the electrochemical reduction of TiO_2 – SiO_2 – Al_2O_3 – MgO – CaO slags and validated that changing the amount of TiO_2 and SiO_2 alone will not be able to yield titanium or silicon as a pure metallic product.

Finally, in order to complete the assessment of the use of ironmaking slag

as electrolyte for the electrolytic extraction of titanium metal, electrochemical impedance spectroscopy and stepped-potential chronoamperometry experiments were performed to investigate the electrical behaviour of such a process. The results confirmed that these slags are mixed conductors, where current is carried by both ionic and electronic carriers. The influence of structure in the ionic conduction was minor for the slags studied as the degree of depolymerization and the viscosity were nearly constant [153, 178] within the temperature and composition range investigated. Since electron hopping between oxidation states had a predominant effect on enhancing electronic conduction, in order to sustain a current efficiency that enables high production rates while minimizing energy consumption, the operating conditions of the cell should be chosen so the ratio of the different valences of the titanium ions present in the slag is minimized.

Outlook

It is the author's belief that the current push for sustainability and environmental awareness will continue to motivate work into developing electrolytic metal production routes to replace the existing capital-intensive and environmentally harmful beneficiation operations. There, the electrochemical extraction of high-purity metals from their oxides provides an unrivaled, unique pathway towards clean metal production. Hence, in light of the results of this work on the electrochemical reduction of titanium from ironmaking slag, the following recommendations for future work are suggested:

- The results of this work encourage the use of the pendant droplet technique in a modified thermal imaging furnace as a methodology to accelerate the pace of characterization of titanium-bearing slags. The containerless features of this method combined with the real-time visualization capabilities of the modified furnace could be further used to calculate physical properties (such as density, viscosity, surface tension, interfacial tension, or contact angle) of the ironmaking slag at the extreme operating temperatures. The use of the pendant droplet method [236] has already been established for measuring thermophysical properties of high temperature, reactive liquids [189]. A further characterization of these properties at the operating temperatures will be required for the development and industrial operation of a MOE electrochemical cell.

- The fact that Si is deposited to a much lesser extent than expected thermodynamically in comparison with Ti, might indicate that Si is probably not released from SiO_2 but rather from some more stable and more complex ions based on $CaSiO_3$ or Ca_2SiO_4. Further research needs to address the non-ideal behaviour of the liquid oxide melt. The cell potential of the reactions should be calculated with the chemical potential of the reduced metals in the intermetallic

or solid solutions rather than in the pure metallic phase. Nakanishi and Allanore [188] reported that a non-ideal mixing behaviour in the molten state for the $La_2O_3 - Y_2O_3$ mixture led to selective extraction of La, contradicting simple thermodynamic predictions. However, there is a lack of reliable thermodynamic description for the electrochemically reduced phases at the high operating temperatures, e.g. no experimental ternary Ir – Si – Ti phases have been reported and no predicted phase relations are available. The lack of thermodynamic data makes detailed analysis of metal deposition challenging. Utilizing Nakanishi and Allanore [188] approach for Gibbs energy measurement might offers a potential avenue to thermodynamic property measurements at ultra-high temperatures.

- The effect of the interactions of the different slags' constituents on its thermochemical and electrical properties remains largely uncertain. Experimentation on simpler synthetic slag systems could help getting a deeper insight into the complex mixed oxide nature of the ironmaking slag. This may lead to finding operating conditions that improve the performance of ironmaking slag as a sole electrolyte (e.g. reducing the high temperature required or the electronic conductivity). Ultimately, the determination of the redox-structure dependence on molten oxides [237] is the key to unlocking the full potential of MOE.

- The small potential window between the cell voltage for the reduction of silicon and titanium ions from the melt motivates the study of the effect of further chemical modifications to the ironmaking slag system could have in the deposition series of the electrolyte. In this work, as the goal was to operate directly from the ironmaking process, the composition of the slag was bounded to the pseudo-quinary TiO_2 – SiO_2 – Al_2O_3 – MgO – CaO system. However, further changes in the concentration of the electronegative species [183], and the addition of additives [202] have been proven successful at shifting the electrodeposition potential of rare earth metals in molten salts, enabling their otherwise difficult separation.

- A further in-depth techno-economic study would need to be performed to assess the viability of this production method. While the highest added-value product from the electrolysis of ironmaking slag would be titanium metal, the proven electrolytic extraction of Ti – Si alloys could still be a profitable endeavour if implemented as these alloys are gaining traction in the market for their use as high-temperature structural materials [203, 215, 216].

Appendix A

Co-Authorship Forms

UNIVERSITY OF CANTERBURY
Te Whare Wānanga o Waitaha
CHRISTCHURCH NEW ZEALAND

Deputy Vice-Chancellor's Office
Postgraduate Office

Co-Authorship Form

This form is to accompany the submission of any thesis that contains research reported in co-authored work that has been published, accepted for publication, or submitted for publication. A copy of this form should be included for each co-authored work that is included in the thesis. Completed forms should be included at the front (after the thesis abstract) of each copy of the thesis submitted for examination and library deposit.

Please indicate the chapter/section/pages of this thesis that are extracted from co-authored work and provide details of the publication or submission from the extract comes:

A condensed version of Chapter 3 has been published as a conference proceedings:

S. Martin-Treceno, C. Bishop, A. Marshall, M. Watson, Value extraction from waste in the steelmaking industry, in: Chemeca 2018, Institution of Chemical Engineers, Queenstown, NZ, 2018, pp. 28.1–28.9

Please detail the nature and extent (%) of contribution by the candidate:

The candidate performed 90% of drafting and writing the paper.

Certification by Co-authors:

If there is more than one co-author then a single co-author can sign on behalf of all.

The undersigned certifys that:

- The above statement correctly reflects the nature and extent of the PhD candidate's contribution to this co-authored work
- In cases where the candidate was the lead author of the co-authored work he or she wrote the text

Name: *Aaron Marshall* Signature:  Date: *3/11/2020*

UNIVERSITY OF CANTERBURY
Te Whare Wānanga o Waitaha
CHRISTCHURCH NEW ZEALAND

Deputy Vice-Chancellor's Office
Postgraduate Office

Co-Authorship Form

This form is to accompany the submission of any thesis that contains research reported in co-authored work that has been published, accepted for publication, or submitted for publication. A copy of this form should be included for each co-authored work that is included in the thesis. Completed forms should be included at the front (after the thesis abstract) of each copy of the thesis submitted for examination and library deposit.

Please indicate the chapter/section/pages of this thesis that are extracted from co-authored work and provide details of the publication or submission from the extract comes:

Chapter 5 is a reproduction of the publication:

S. Martin-Treceno, N. Weaver, A. Allanore, C. M. Bishop, A. T. Marshall, M. J. Watson, Electrochemical behaviour of titanium-bearing slag relevant for molten oxide electrolysis, Electrochimica Acta 354 (2020) 136619.

Please detail the nature and extent (%) of contribution by the candidate:

The candidate performed all the experimental work and the data analysis, along with 80% of drafting and writing the paper.

Certification by Co-authors:

If there is more than one co-author then a single co-author can sign on behalf of all.

The undersigned certifys that:

- The above statement correctly reflects the nature and extent of the PhD candidate's contribution to this co-authored work
- In cases where the candidate was the lead author of the co-authored work he or she wrote the text

Name: *Aaron Marshall* Signature: A Marshall Date: *3/11/2020*

Bibliography

(1) United Nations, *The sustainable development goals report*, 2019, p 61.

(2) United Nations, *Transforming our world: The 2030 agenda for sustainable development*, 2015.

(3) Nakanishi, B. R. On the electrolytic nature of molten aluminum and rare earth oxides, Ph.D. Thesis, Massachusetts Institute of Technology, 2018.

(4) The history of ironsand, `https://www.nzsteel.co.nz/new-zealand-steel/the-story-of-steel/the-history-of-ironsand/`, Accessed: 2017-10-07.

(5) Fang, Z. Z.; Middlemas, S.; Guo, J.; Fan, P. A new, energy-efficient chemical pathway for extracting Ti metal from Ti minerals. *Journal of the American Chemical Society* **2013**, *135*, 18248–18251.

(6) Le Cornec, D.; Galoisy, L.; Izoret, L.; Cormier, L.; Trcera, N.; Calas, G. Structural role of titanium on slag properties. *Journal of the American Ceramic Society* **2020**, 1–9.

(7) Opus International Consultants Ltd. *Use of melter slag as aggregate in open-graded emulsion mixes*; tech. rep. 112; Transfund New Zealand Research Report, 1998.

(8) Waseda, Y.; Toguri, J. M., *The structure and properties of oxide melts: application of basic science to metallurgical processing*; River Edge: World Scientific: 1998.

(9) Chen, G. Z.; Fray, D. J.; Farthing, T. W. Direct electrochemical reduction of titanium dioxide to titanium in molten calcium chloride. *Nature* **2000**, *407*, 361–364.

(10) Allanore, A.; Yin, L.; Sadoway, D. R. A new anode material for oxygen evolution in molten oxide electrolysis. *Nature* **2013**, *497*, 353–356.

(11) Beck, T. R. ECS Classics: Hall and Héroult and the discovery of aluminum electrolysis. *Electrochemical Society Interface* **2014**, *23*, 36.

(12) Yan, X. Y.; Fray, D. J., Chapter 6 - Molten salt alectrolysis for sustainable metals extraction and materials processing – A review In *Electrolysis: theory, types and applications*, Kuai, S., Meng, J., Eds.; Nova Science: New York, 2010, pp 255–302.

(13) Nakanishi, B. R.; Allanore, A. Electrochemical study of a pendant molten alumina droplet and its application for thermodynamic property measurements of Al – Ir. *Journal of The Electrochemical Society* **2017**, *164*, E460–E471.

(14) Ilyushechkin, A. Y.; Duchesne, M. A.; Hla, S. S.; Macchi, A.; Anthony, E. J. Interactions of vanadium-rich slags with crucible materials during viscosity measurements. *Journal of Materials Science* **2013**, *48*, 1053–1066.

(15) Jiao, H.; Tian, D.; Wang, S.; Zhu, J.; Jiao, S. Direct preparation of titanium alloys from Ti-bearing blast furnace slag. *Journal of The Electrochemical Society* **2017**, *164*, D511–D516.

(16) Martin-Treceno, S.; Bishop, C.; Marshall, A.; Watson, M., Value extraction from waste in the steelmaking industry In *Chemeca 2018*; Institution of Chemical Engineers: Queenstown, NZ, 2018, pp 28.1–28.9.

(17) Hughes, T. The development of ultra-high temperature experimental capabilities for the electrolytic extraction of titanium from New Zealand Steel's iron slag, MA thesis, University of Canterbury, 2018.

(18) Weaver, N. Thermodynamic characterisation and simulation for the electrolytic extraction of titanium from oxide melts, MA thesis, University of Canterbury, 2020.

(19) Bale, C. et al. FactSage thermochemical software and databases, 2010 - 2016. *Calphad* **2016**, *54*, 35 –53.

(20) Emsley, J., *Nature's building blocks: An A-Z guide to the elements*; Oxford University Press: 2011.

(21) Green, J.; Batchelor, J.; Yuen, D. The manufacture of steel, `https://nzic.org.nz/ChemProcesses/metals/8A.pdf`, Accessed: 2017-10-30.

(22) World steel production, `https://www.worldsteel.org/media-centre/press-releases/2017/world-steel-in-figures-2017.html`, Accessed: 2017-10-30.

(23) U.S. Geological survey, Mineral commodity summaries 2018, Unit state geologic, Washington, 2018, `https://minerals.usgs.gov/minerals/pubs/mcs/2018/mcs2018.pdf`, Accessed: 2018-05-24.

(24) Allanore, A. Electrochemical engineering for commodity metals extraction. *The Electrochemical Society Interface* **2017**, *26*, 63–68.

(25) De Réaumur, R.-A. F., *Memoirs on steel and iron. A translation from the original printed in 1772*; University of Chicago Press: 1956.

(26) Rackley, S. A., Chapter 5 - Carbon capture from industrial processes In *Carbon capture and storage*, Rackley, S. A., Ed.; Butterworth-Heinemann: Boston, 2010, pp 95 –102.

(27) Babich, A.; Senk, D., 17 - Recent developments in blast furnace iron-making technology In *Iron ore*, Lu, L., Ed.; Woodhead Publishing: 2015, pp 505 –547.

(28) The ironmaking process, `https://www.nzsteel.co.nz/new-zealand-steel/the-story-of-steel/the-science-of-steel/the-ironmaking-process/`, Accessed: 2020-10-07.

(29) NZS aggregates, https://www.nzsteel.co.nz/products/aggregates/, Accessed: 2018-06-05.

(30) Royal Society of Chemistry: titanium, http://www.rsc.org/periodic-table/element/22/titanium, Accessed: 2017-09-30.

(31) Katrak, F. E., Potential growth in non-aerospace usage of titanium and implications for titanium process and product R&D In *Titanium industry workshop*, Welches, OR, USA, 1997, pp 71–90.

(32) U.S. Geological survey, Mineral commodity summaries: titanium, https://minerals.usgs.gov/minerals/pubs/commodity/titanium/index.html, Accessed: 2017-10-11.

(33) Froes, F. H. S.; Gungor, M. N.; Ashraf Imam, M. Cost-affordable titanium: the component fabrication perspective. *JOM* **2007**, *59*, 28–31.

(34) U.S. Geological survey, Mineral commodity summaries: aluminium, https://minerals.usgs.gov/minerals/pubs/commodity/aluminium/index.html, Accessed: 2017-10-11.

(35) U.S. Geological survey, Mineral commodity summaries: iron and steel crap, https://minerals.usgs.gov/minerals/pubs/commodity/iron_&_steel_scrap/index.html, Accessed: 2017-10-11.

(36) Van Vuuren, D. S. A critical evaluation of processes to produce primary titanium. *J. South. Afr. Inst. Min. Metall.* **2009**, *109*, 455–461.

(37) Song, Y.; Dou, Z.; an Zhang, T.; Liu, Y. Research progress on the extractive metallurgy of titanium and its alloys. *Mineral Processing and Extractive Metallurgy Review* **2020**, *0*, 1–17.

(38) Fray, D. J. Novel methods for the production of titanium. *International Materials Reviews* **2008**, *53*, 317–325.

(39) Fang, Z. Z.; Paramore, J. D.; Sun, P.; Chandran, K. S. R.; Zhang, Y.; Xia, Y.; Cao, F.; Koopman, M.; Free, M. Powder metallurgy of titanium – past, present, and future. *International Materials Reviews* **2017**, 1–53.

(40) Hunter, M. A. Metallic titanium. *Journal of the American Chemical Society* **1910**, *32*, 330–336.

(41) Lam, R. K. F. High purity titanium refining by iodide purification. *Titanium extraction and processing* **1997**, 3–22.

(42) Kroll, W. J. Method for manufacturing titanium and alloys thereof, Patent Application No. US 2,205,854, Jul. 1938.

(43) Turner, P. C.; Hartman, A. D.; Hansen, J. S.; Gerdemann, S. J., Low cost titanium - myth or reality In *TMS Annual Meeting*, New Orleans, LA, USA, 2001.

(44) *Summary of emerging titanium cost reduction technologies*; tech. rep.; EHK Technologies, 2004.

(45) Van Vuuren, D. S., Direct titanium powder production by metallothermic processes In *Titanium powder metallurgy*, Froes, F. H., Ed.; Butterworth-Heinemann: Boston, 2015, pp 69–93.

(46) The Essential Chemical Industry: titanium, `http://www.essentialchemicalindustry.org/metals/titanium.html`, Accessed: 2017-11-02.

(47) Zhang, Y.; Fang, Z. Z.; Sun, P.; Zheng, S.; Xia, Y.; Free, M. A perspective on thermochemical and electrochemical processes for titanium metal production. *JOM* **2017**, *69*, 1861–1868.

(48) Gerdemann, S. J.; Oden, L. L.; White, J. C., Continuous production of titanium powder In *TMS Annual Meeting*, Indianapolis, IN, USA, 1997.

(49) Okabe, T. H.; Waseda, Y. Producing titanium through an electronically mediated reaction. *JOM* **1997**, *49*, 28–32.

(50) Kraft, E. H., Overview of emerging titanium technologies In *International Titanium Association Conference*, Scottsdale, AZ, USA, 2005.

(51) Okabe, T. H.; Sadoway, D. R. Metallothermic reduction as an electronically mediated reaction. *Journal of Materials Research* **1998**, *13*, 3372–3377.

(52) Takeda, O.; Uda, T.; Okabe, T. H., Chapter 2.9 - Rare earth, titanium group metals, and reactive metals production In *Treatise on process metallurgy*, Seetharaman, S., Ed.; Elsevier: Boston, 2014, pp 995 –1069.

(53) Allanore, A. Contribution of electricity to materials processing: historical and current perspectives. *JOM* **2013**, *65*, 130–135.

(54) Sadoway, D. R. Metallurgical electrochemistry. The interface between materials science and molten salt chemistry. *Materials Science Forum* **1991**, *73-75*, 555–555.

(55) Sirk, A. H. C.; Sadoway, D. R.; Sibille, L. Direct electrolysis of molten lunar regolith for the production of oxygen and metals on the moon. *ECS Transactions* **2010**, *28*, 367–373.

(56) Sadoway, D. R. Electrochemical processing of refractory metals. *JOM* **1991**, *43*, 15–19.

(57) Sadoway, D. R., Electrometallurgy In *Encyclopedia of materials science and engineering*, Bever, M., Ed.; Oxford: Pergamon Press, 1986, pp 1444–1447.

(58) Nohira, T. Novel electrochemical reactions in molten salts and ionic liquids and their applications. *Electrochemistry* **2020**, *88*, 477–488.

(59) Nohira, T.; Yasuda, K.; Ito, Y. Pinpoint and bulk electrochemical reduction of insulating silicon dioxide to silicon. *Nature Materials* **2003**, *2*, 397–401.

(60) Allanore, A. Features and challenges of molten oxide electrolytes for metal extraction. *Journal of the Electrochemical Society* **2015**, *162*, E13–E22.

(61) Sokhanvaran, S.; Lee, S.-K.; Lambotte, G.; Allanore, A. Electrochemistry of molten sulfides: copper extraction from $BaS-Cu_2S$. *Journal of The Electrochemical Society* **2015**, *163*, D115–D120.

(62) Jung, I.-H.; Van Ende, M.-A. Computational thermodynamic calculations: FactSage from CALPHAD thermodynamic database to virtual process simulation. *Metallurgical and Materials Transactions B* **2020**, *51*, 1851–1874.

(63) Min, D. J.; Tsukihashi, F. Recent advances in understanding physical properties of metallurgical slags. *Metals and Materials International* **2017**, *23*, 1–19.

(64) Mysen, B. O. Relationships between silicate melt structure and petrologic processes. *Earth-Science Reviews* **1990**, *27*, 281 –365.

(65) Poizeau, S.; Sadoway, D. R., Towards a design tool for self-heated cells producing liquid metal by electrolysis In *Light Metals 2011 - TMS 2011 Annual Meeting and Exhibition, February 27, 2011 - March 3, 2011*; TMS Light Metals; Minerals, Metals and Materials Society: 2011, pp 387–392.

(66) Elgrishi, N.; Rountree, K. J.; McCarthy, B. D.; Rountree, E. S.; Eisenhart, T. T.; Dempsey, J. L. A practical beginner's guide to cyclic voltammetry. *Journal of Chemical Education* **2018**, *95*, 197–206.

(67) Brownson, D. A.; Banks, C. E., Interpreting electrochemistry In *The handbook of graphene electrochemistry*; Springer: 2014, pp 23–77.

(68) Chapter 3 - Methods for assessing surface cleanliness In *Developments in surface contamination and cleaning*, Kohli, R., Mittal, K., Eds.; Elsevier: 2019; Vol. 12, pp 23 –105.

(69) Belyansky, M., Chapter 8 - Thin film deposition for front end of line: the effect of the semiconductor scaling, strain engineering and pattern effects In *Handbook of thin film deposition*, Seshan, K., Schepis, D., Eds., Fourth Edition; William Andrew Publishing: 2018, pp 231 –268.

(70) Ardebili, H.; Zhang, J.; Pecht, M. G., 8 - Defect and failure analysis techniques for encapsulated microelectronics In *Encapsulation technologies for electronic applications*, Ardebili, H., Zhang, J., Pecht, M. G., Eds., Second Edition; Materials and Processes for Electronic Applications; William Andrew Publishing: 2019, pp 317 –373.

(71) Simon, A. H., Chapter 7 - Sputter processing In *Handbook of thin film deposition*, Seshan, K., Schepis, D., Eds., Fourth Edition; William Andrew Publishing: 2018, pp 195 –230.

(72) Bounakhla, M.; Tahri, M. *X-ray fluorescence analytical techniques*; Report; Rabat, Morocco: National Center for Energy Sciences and Nuclear Techniques (CNESTEN), 2014.

(73) Chapter 7 - Characterization and simulation technologies of nanomaterial In *Fundamentals and applications of nano silicon in plasmonics and fullerines*, Nayfeh, M., Ed.; Micro and Nano Technologies; Elsevier: 2008, pp 153 –167.

(74) Goldstein, J.; Newbury, D.; Joy, D.; Lyman, C.; Echlin, P.; Lifshin, E.; Sawyer, L.; Michael, J., *Scanning electron microscopy and x-ray microanalysis*; Kluwer Academic Publishers: 2003.

(75) Mojumdar, S. C.; Sain, M.; Prasad, R. C.; Sun, L.; Venart, J. E. S. Selected thermoanalytical methods and their applications from medicine to construction. *Journal of Thermal Analysis and Calorimetry* **2007**, *90*, 653–662.

(76) Boettinger, W. J.; Kattner, U. R.; Moon, K.-W.; Perepezko, J. *NIST recommended practice guide: DTA and heat-flux DSC measurements of alloy melting and freezing*; tech. rep.; 2006.

(77) Gan, L.; Zhang, C.; Shangguan, F.; Li, X. A differential scanning calorimetry method for construction of continuous cooling transformation diagram of blast furnace slag. *Metallurgical and Materials Transactions B* **2012**, *43*, 460–467.

(78) Ferreira, E. B.; Lima, M. L.; Zanotto, E. D. DSC method for determining the liquidus temperature of glass-forming systems. *Journal of the American Ceramic Society* **2010**, *93*, 3757–3763.

(79) Kaufman, L; Bernstein, H, *Computer calculation of phase diagrams*; Academic Press New York: 1970.

(80) Saunders, N.; Miodownik, A. P., *CALPHAD (calculation of phase diagrams): a comprehensive guide*; Pergamon Press, New York: 1998.

(81) Hillert, M. The compound energy formalism. *Journal of Alloys and Compounds* **2001**, *320*, 161 –176.

(82) Pelton, A. D.; Blander, M. Thermodynamic analysis of ordered liquid solutions by a modified quasichemical approach — Application to silicate slags. *Metallurgical Transactions B* **1986**, *17*, 805–815.

(83) Current world population, `http://www.worldometers.info/world-population/`, Accessed: 2018-05-24.

(84) Global footprint network, `https://www.footprintnetwork.org/our-work/ecological-footprint/`, Accessed: 2018-05-24.

(85) Bataille, C.; Åhman, M.; Neuhoff, K.; Nilsson, L. J.; Fischedick, M.; Lechtenböhmer, S.; Solano-Rodriquez, B.; Denis-Ryan, A.; Steiber, S.; Waisman, H.; Sartor, O.; Rahbar, S. A review of technology and policy deep decarbonization pathway options for making energy-intensive industry production consistent with the Paris Agreement. *Journal of Cleaner Production* **2018**, *187*, 960–973.

(86) Li, Z.; Sun, Y.; Liu, L.; Wang, X.; Zhang, Z. Enhancement of rutile formation by ZrO_2 Addition in Ti-bearing blast furnace slags. *ISIJ International* **2015**, *55*, 1384–1389.

(87) U.S. Geological survey, Mineral commodity summaries, Unit state geologic, Washington, January 2020, `https://pubs.usgs.gov/periodicals/mcs2020/mcs2020-iron-steel-slag.pdf`, Accessed: 2020-09-30.

(88) Back, G. S.; Park, H. S.; Seo, S. M.; Jung, W. G. Exploring high-strength glass-ceramic materials for upcycling of industrial wastes. *Metals and Materials International* **2015**, *21*, 1061–1067.

(89) Piatak, N. M.; Parsons, M. B.; Seal II, R. R. Characteristics and environmental aspects of slag: a review. *Applied Geochemistry* **2015**, *57*, 236–266.

(90) Dai, W.; Li, Y.; Cang, D.; Zhou, Y.; Fan, Y. Effects of sintering atmosphere on the physical and mechanical properties of modified BOF slag glass. *International Journal of Minerals, Metallurgy, and Materials* **2014**, *21*, 494–502.

(91) Lin, B.; Wang, H.; Zhu, X.; Liao, Q.; Ding, B. Crystallization properties of molten blast furnace slag at different cooling rates. *Applied Thermal Engineering* **2016**, *96*, 432–440.

(92) Sun, Y.; Zhang, Z.; Liu, L.; Wang, X. Heat recovery from high temperature slags: a review of chemical methods. *Energies* **2015**, *8*, 1917–1935.

(93) Reuter, M.; Xiao, Y.; Boin, U., Recycling and environmental issues of metallurgical slags and salt fluxes In *VII International conference on molten slags, fluxes and salts*; The South African Institute of Mining and Metallurgy: 2004, pp 349–356.

(94) Sarkar, S.; Mazumder, D. Solid waste management in steel industry - Challenges and opportunities. *Eng. Technol. Int. J. Soc. Behav. Educ. Econ. Bus. Ind. Eng.* **2015**, *9*, 978–981.

(95) Sun, Y.; Zhang, Z. Utilization of high-temperature slags from metallurgy based on crystallization behaviors. *JOM* **2018**, 1–8.

(96) Fu, X.; Hou, W.; Yang, C.; Li, D.; Wu, X. Studies on Portland cement with large amount of slag. *Cement and Concrete Research* **2000**, *30*, 645–649.

(97) Motz, H.; Geiseler, J. Products of steel slags an opportunity to save natural resources. *Waste Management* **2001**, *21*, 285–293.

(98) Dippenaar, R. Industrial uses of slag (the use and re-use of iron and steelmaking slags). *Ironmaking and Steelmaking* **2013**, *32*, 35–46.

(99) Zhang, H.; Wang, H.; Zhu, X.; Qiu, Y.; Li, K.; Chen, R.; Liao, Q. A review of waste heat recovery technologies towards molten slag in steel industry. *Applied energy* **2013**, *112*, 956–966.

(100) Smith, M. P., Blast furnace ironmaking – A view on future developments In, 13th Global Congress on Manufacturing and Management, 2017; Vol. 174, pp 19 –28.

(101) Grossman, D., Glass ceramics In *Concise encyclopedia of advanced ceramic materials*, Brook, R., Ed.; Pergamon: Oxford, 1991, pp 170 –176.

(102) Pinckney, L. R., Glass-Ceramics In *Encyclopedia of physical science and technology*, Meyers, R. A., Ed., Third Edition; Academic Press: New York, 2003, pp 807 –816.

(103) Rahaman, M., 3 - Bioactive ceramics and glasses for tissue engineering In *Tissue engineering using ceramics and polymers*, Boccaccini, A. R., Ma, P. X., Eds., Second Edition; Woodhead Publishing: 2014, pp 67 –114.

(104) Karmakar, B., 7 - Glasses and glass-ceramics for biomedical applications In *Functional glasses and glass-ceramics*, Karmakar, B., Ed.; Butterworth-Heinemann: 2017, pp 253 –280.

(105) Tayeb, M. A.; Spooner, S.; Sridhar, S. Phosphorus: the noose of sustainability and renewability in steelmaking. *JOM* **2014**, *66*, 1565–1571.

(106) Wang, Z.; Sun, Y.; Sridrar, S.; Zhang, M.; Zhang, Z. Investigation on viscosity and non-isothermal crystallization behavior of P-bearing steelmaking slags with varying TiO_2 content. *Metallurgical and Materials Transactions B* **2017**, *48*, 527–537.

(107) Li, L. S.; Sui, Z. T. Physical–chemical behavior of selective enrichment of TiO_2. *Acta Physical Chemistry Sinica* **2001**, *17*, 845–849.

(108) She, X. F.; Sun, H. Y.; Dong, X. J.; Xue, Q. G.; Wang, J. S. Reduction mechanism of titanomagnetite concentrate by carbon monoxide. *Journal of Mining and Metallurgy, Section B: Metallurgy* **2013**, *49*, 263–270.

(109) Fried, N. A.; Sadoway, D. R., Titanium extraction by molten oxide electrolysis In *TMS Annual Meeting*, Charlotte, NC, USA, 2004.

(110) Sadoway, D. R. New opportunities for metals extraction and waste treatment by electrochemical processing in molten salts. *Journal of Materials Research* **1995**, *10*, 487–492.

(111) Norgate, T. E.; Wellwood, G. The potential applications for titanium metal powder and their life cycle impacts. *JOM* **2006**, *58*, 58–63.

(112) Jin, W.; Zhang, Y. Sustainable electrochemical extraction of metal resources from waste streams: from removal to recovery. *ACS Sustainable Chemistry & Engineering* **2020**, *8*, 4693–4707.

(113) Kraft, E. H., Summary of emerging titanium cost reduction technologies In *Low cost titanium workshop*, Baltimore, MD, USA, 2003.

(114) *The economics of titanium metal*; 4th ed. Roskill Information Services Ltd.: 2007.

(115) Pretorius, G. A method of producing titanium, Patent Application No. WO 2006/079887 A3, Dec. 2005.

(116) Cardarelli, F. Method for electrowinning of titanium metal or alloy from titanium oxide containing compound in the liquid state, Patent Application No. US 7,504,017 B2, Nov. 2002.

(117) Motsie, R. *An overview of South Africa's titanium mineral concentrate industry*; tech. rep.; Department of Mineral and Energy, Republic of South Africa, 2008.

(118) Doblin, C.; Chryss, A.; Monch, A., Titanium powder from the TiRO process In *Powder metallurgy of titanium*; Key Engineering Materials, Vol. 520; Trans Tech Publications: 2012, pp 95–100.

(119) Armstrong, D.; Anderson, R.; Jacobsen, L. Preparation of alloys by the Armstrong method, Patent Application No. US 2006/0150769 A1, Sep. 2003.

(120) Cordes, R. A.; Donaldson, A. *Titanium metal powder production by The plasma quench process*; tech. rep.; Idaho Titanium Technologies, ID, USA, 2000.

(121) Sanjurjo, A.; Thiers, E.; Lau, K.; Hildenbrand, D.; Krishnan, G.; Alvarez, E. Methods and apparatuses for producing metallic compositions via reduction of metal halides, Patent Application No. US 7,559,969 B2, Aug. 2004.

(122) Ginatta, M. V. Extractive metallurgy of primary titanium. *Light Metal Age* **2004**, *62*, 48–51.

(123) Rigby, G. D.; Ratchev, I. P.; Olivares, R. I.; Mukunthan, K.; Bliznyukov, S. A.; Shook, A. A., Polar titanium: development of the BHP billiton titanium metal production process In *21st Annual ITA Conference*, Scottsdale, AZ, USA, 2005.

(124) Van Vuuren, D. S.; Engelbrecht, A. D.; Hadley, T. D. Opportunities in the electrowinning of molten titanium from titanium dioxide. *JOM* **2005**, *57*, 53–55.

(125) Okabe, T. H.; Oda, T.; Y., M., Titanium powder production by preform reduction process In *10th World Conference on Titanium*, Hamburg, Germany, 2003.

(126) Ottensmeyer, R.; Plath, P. J., A new process for production of titanium In *10th World Conference on Titanium*, Hamburg, Germany, 2003.

(127) Abiko, T.; Park, I.; Okabe, T. H., Reduction of titanium oxide in molten salt medium In *10th World Conference on Titanium*, Hamburg, Germany, 2003.

(128) Withers, J. C.; Loutfy, R. O.; Laughlin, J. P. Electrolytic process to produce titanium from TiO_2 feed. *Materials Technology* **2007**, *22*, 66–70.

(129) Ono, K.; Suzuki, R. O. A new concept for producing Ti sponge: calciothermic reduction. *JOM* **2002**, *54*, 59–61.

(130) Tao, L. C. Producing brittle titanium metal, Patent Application No. US 3,005,698 A, Apr. 1959.

(131) Barbis, D. P.; Gasior, R. M.; Walker, G. P.; Capone, J. A.; Schaeffer, T. S., Titanium powders from the hydride–dehydride process In *Titanium powder metallurgy*, Froes, F. H., Ed.; Butterworth-Heinemann: Boston, 2015, pp 101–116.

(132) Sun, Y.; Li, J.; Wang, X.; Zhang, Z. The effect of P_2O_5 on the crystallization behaviors of Ti-bearing blast furnace slags using single hot thermocouple technique. *Metallurgical and Materials Transactions B* **2014**, *45*, 1446–1455.

(133) Van Tonder, W. South African titanium: Techno-economic evaluation of the alternatives to the Kroll Process, MA thesis, Stellenbosch University, 2010.

(134) Metalysis, `http://www.metalysis.com/`, Accessed: 2017-11-11.

(135) Paiste, D. Reinventing copper extraction with electricity, `http://energy.mit.edu/news/reinventing-copper-extraction-with-electricity/`, Accessed: 2020-11-11, 2014.

(136) Robertson, P. M., Electrochemical processing In *Encyclopedia of chemical technology*, Grayson, M., Eckroth, M., Eds.; Wiley: New York, 1978, pp 66–95.

(137) The Essential Chemical Industry: magnesium, `http://www.essentialchemicalindustry.org/metals/magnesium.html`, Accessed: 2017-11-16.

(138) Sadoway, D. R. Inert anodes for the Hall-Heroult cell: The ultimate materials challenge. *JOM* **2001**, *53*, 34–35.

(139) Gao, Y.; Yang, C.; Zhang, C.; Qin, Q.; Chen, G. Z. Magnesia-stabilised zirconia solid electrolyte assisted electrochemical investigation of iron ions in a $SiO_2-CaO-MgO-Al_2O_3$ molten slag at 1723 K. *Phys. Chem. Chem. Phys.* **2017**, *19*, 15876–15890.

(140) Allanore, A.; Sadoway, D. R. Extraction of liquid element by electrolysis of oxides, Patent Application No. US 8764962 B2, Aug. 2011.

(141) Lambotte, G.; Lee, S.; Sadoway, D. R.; Allanore, A.; Gadois, C.; Rinzler, C. C.; Zhao, Y.; Nose, K. Sulfides electrolyte for metal processing and extraction, Patent Application No. US 2020/0247670 A1, Dec. 2019.

(142) Fray, D. J.; Farthing, T. W.; Chen, Z. Removal of substances from metal and semi-metal compounds, Patent Application No. US 6,712,952 B1, Jun. 1999.

(143) Hyers, R.; Lambotte, G.; Humbert, M.; Bradshaw, R. Systems and methods for molten oxide electrolysis, Patent Application No. US 2020/0263313 A1, Sep. 2018.

(144) *Energy use patterns in metallurgical and non-metallic mineral processing*; Battelle-Columbus Laboratories; U. S. Bureau of Mines OFR 80-75: 1975.

(145) UN Department of Economic and Social Affairs, Population Division *World population prospects: the 2017 revision. Key findings and advance tables. Working paper no. ESA/P/WP/248*; 2017.

(146) Wiencke, J.; Lavelaine, H.; Panteix, P.-J.; Petitjean, C.; Rapin, C. Electrolysis of iron in a molten oxide electrolyte. *Journal of Applied Electrochemistry* **2018**, *48*, 115–126.

(147) Daehn, K.; Allanore, A. Electrolytic production of copper from chalcopyrite. *Current Opinion in Electrochemistry* **2020**, *22*, 110 –119.

(148) Dippenaar, R. Industrial uses of slag (the use and re-use of iron and steelmaking slags). *Ironmaking & Steelmaking* **2005**, *32*, 35–46.

(149) U.S. Geological survey, Mineral commodity summaries 2019, Unit state geologic.

(150) Van Oss, H. G. *Slag-iron and steel [Advance Release]*; 2016 Minerals Yearbook; U.S. Geological Survey, 2018.

(151) Standish, E.; Stefanescu, D.; Curreri, P., Ceramics for molten materials containment, transfer and handling on the lunar surface In *47th AIAA Aerospace Sciences Meeting including the New Horizons Forum and Aerospace Exposition*, 2009.

(152) Schiefelbein, S.; Sadoway, D. High-accuracy, calibration-free technique for measuring the electrical conductivity of molten oxides. *Metallurgical and Materials Transactions B* **1997**, *28*, 1141–1149.

(153) *Slag Atlas*, 2^{nd}; Verlag Stahleisen GmbH: Düsseldorf, 1995.

(154) Mills, K.; Yuan, L; Jones, R. Estimating the physical properties of slags. *Journal of the Southern African Institute of Mining and Metallurgy* **2011**, *111*, 649–658.

(155) Murariu, V.; Svoboda, J. The applicability of Davis tube tests to ore separation by drum magnetic separators. *Physical Separation in Science and Engineering* **2003**, *12*, 1–11.

(156) Martin-Treceno, S.; Weaver, N.; Allanore, A.; Bishop, C. M.; Marshall, A. T.; Watson, M. J. Electrochemical behaviour of titanium-bearing slag relevant for molten oxide electrolysis. *Electrochimica Acta* **2020**, *354*, 136619.

(157) Fried, N. A.; Rhoads, K. G.; Sadoway, D. R. Transference number measurements of TiO_2-BaO melts by stepped-potential chronoamperometry. *Electrochimica Acta* **2001**, *46*, 3351–3358.

(158) Barati, M.; Coley, K. S. Electrical and electronic conductivity of $CaO-SiO_2-FeO_x$ slags at various oxygen potentials: Part I. Experimental results. *Metallurgical and Materials Transactions B* **2006**, *37*, 41–49.

(159) Sokhanvaran, S.; Thomas, S.; Barati, M. Charge transport properties of cryolite - silica melts. *Electrochimica Acta* **2012**, *66*, 239 –244.

(160) Ducret, A.; Khetpal, D.; Sadoway, D. R., Electrical conductivity and transference number measurements of $FeO-CaO-MgO-SiO_2$ melts In *Molten salts XIII*, Trulove, P. C., DeLong, H. C., Mantz, R. A., Stafford, G. R., Matsunaga, M., Eds.; Electrochemical Society Inc: Pennington, 2002, pp 347–353.

(161) Ratkje, S. K.; Rajabu, H.; Førland, T. Transference coefficients and transference numbers in salt mixtures relevant for the aluminium electrolysis. *Electrochimica Acta* **1993**, *38*, 415 –423.

(162) Olsen, I.; Koksbang, R.; Skou, E. Transference number measurements on a hybrid polymer electrolyte. *Electrochimica Acta* **1995**, *40*, 1701 –1706.

(163) Zhang, L.; Zhang, W.; Zhang, J.; Li, G. Oxidation kinetics and oxygen capacity of Ti-bearing blast furnace slag under dynamic oxidation conditions. *Metals* **2016**, *6*, 105.

(164) Sundman, B An assessment of the Fe−O system. *Journal of phase equilibria* **1991**, *12*, 127–140.

(165) Okamoto, H. The C−Fe (carbon-iron) system. *Journal of Phase Equilibria* **1992**, *13*, 543–565.

(166) Du, H. Theory of smelting V and Ti-magnetite by blast furnace, 1996.

(167) Zhang, L.; Zhang, L.; Wang, M.; Li, G.; Sui, Z. Dynamic oxidation of the Ti-bearing blast furnace slag. *ISIJ international* **2006**, *46*, 458–465.

(168) Chung, Y.; Cramb, A. W. Dynamic and equilibrium interfacial phenomena in liquid steel-slag systems. *Metallurgical and Materials Transactions B* **2000**, *31*, 957–971.

(169) Goso, X.; Nell, J.; Petersen, J., Review of liquidus surface and phase equilibria in the $TiO_2-SiO_2-Al_2O_3-MgO-CaO$ slag system at P_{O_2} applicable in fluxed titaniferous magnetite smelting In *Advances in molten slags, fluxes, and salts: Proceedings of the 10th International Conference on molten slags, fluxes and salts 2016*, Reddy, R. G., Chaubal, P., Pistorius, P. C., Pal, U., Eds.; Springer International Publishing: Cham, 2016, pp 105–114.

(170) Ratchev, I. P.; Belton, G. R., A study of the liquidus temperatures of titanomagnetite smelting type slags In *5th International Conference on molten slags, fluxes and salts*, 1997, pp 387–393.

(171) Creager, S., 3 - Solvents and supporting electrolytes In *Handbook of electrochemistry*, Zoski, C. G., Ed.; Elsevier: Amsterdam, 2007, pp 57 –72.

(172) Mills, K. C.; Keene, B. J. Physical properties of BOS slags. *International Materials Reviews* **1987**, *32*, 1–120.

(173) Híveš, J.; Thonstad, J.; Sterten, A; Fellner, P. Electrical conductivity of molten cryolite-based mixtures obtained with a tube-type cell made of pyrolytic boron nitride. *Metallurgical and Materials Transactions B* **1996**, *27*, 255–261.

(174) Wang, S.; Li, G.; Lou, T.; Sui, Z. The conductivity and the crystallization of perovskite ($CaTiO_3$) from Ti-bearing blast furnace slag studied by A.C. Impedance method. *ISIJ International* **1999**, *39*, 1116–1119.

(175) Hu, K.; Lv, X.; Yu, W.; Yan, Z.; Lv, W.; Li, S. Electric conductivity of TiO_2 – Ti_2O_3 – FeO – CaO – SiO_2 – MgO – Al_2O_3 for high-titania slag smelting process. *Metallurgical and Materials Transactions B* **2019**, *50*, 2982–2992.

(176) Wiencke, J.; Lavelaine, H.; Panteix, P.-J.; Petitjean, C.; Rapin, C. The influence of iron concentration on the anodic charge transfer in molten oxide electrolysis. *Journal of the Electrochemical Society* **2019**, *166*, E489–E495.

(177) Rouaut, G.; Gheribi, A. E.; Chartrand, P. Modelling the electronic conduction in metals-molten salts mixtures. Application to cryolitic melts in Hall-Heroult cells. *Journal of Fluorine Chemistry* **2020**, 109597.

(178) Liao, J. L.; Li, J.; Wang, X. D.; Zhang, Z. T. Influence of TiO_2 and basicity on viscosity of Ti-bearing slag. *Ironmaking and Steelmaking* **2012**, *39*, 133–139.

(179) Híveš, J.; Fellner, P.; Thonstad, J., Transference numbers in Na(K) cryolite-based systems In *Molten salts chemistry and technology*; John Wiley & Sons, Ltd: 2014; Chapter 1.10, pp 95–101.

(180) Haarberg, G.; Sterten, A; Gudbrandsen, H; Olufsen, F; Rolseth, S A laboratory probe for bath acidity of cryolite-alumina melts. *Light Metals-Warrendale* **1998**, 367–370.

(181) Mohandas, K.; Fray, D. FFC Cambridge process and removal of oxygen from metal-oxygen systems by molten salt electrolysis: an overview. *Trans. Indian Inst. Met* **2004**, *57*, 579–592.

(182) Gibilaro, M.; Pivato, J.; Cassayre, L.; Massot, L.; Chamelot, P.; Taxil, P. Direct electroreduction of oxides in molten fluoride salts. *Electrochimica Acta* **2011**, *56*, 5410 –5415.

(183) Abbasalizadeh, A.; Malfliet, A.; Seetharaman, S.; Sietsma, J.; Yang, Y. Electrochemical extraction of rare earth metals in molten fluorides: conversion of rare earth oxides into rare earth fluorides using fluoride additives. *Journal of Sustainable Metallurgy* **2017**, *3*, 627–637.

(184) Chen, Z.; You, Y.; Morita, K. Synthesis and kinetics of titanium silicides from photovoltaic industry waste and steelmaking slag for silicon and titanium recovery. *ACS Sustainable Chemistry & Engineering* **2018**, *6*, 7078–7085.

(185) Allanore, A. Electrochemical engineering of anodic oxygen evolution in molten oxides. *Electrochimica Acta* **2013**, *110*, 587–592.

(186) Wang, D.; Gmitter, A. J.; Sadoway, D. R. Production of oxygen gas and liquid metal by electrochemical decomposition of molten iron oxide. *Journal of the Electrochemical Society* **2011**, *158*, E51–E54.

(187) Sibille, L.; Dominguez, J., Joule-heated molten regolith electrolysis reactor concepts for oxygen and metals production on the Moon and Mars In *50th AIAA Aerospace Sciences Meeting including the New Horizons Forum and Aerospace Exposition*, 2012, p 639.

(188) Nakanishi, B. R.; Allanore, A. Electrochemical investigation of molten lanthanum-yttrium oxide for selective liquid rare-earth metal extraction. *Journal of The Electrochemical Society* **2019**, *166*, E420–E428.

(189) Wu, M.; Caldwell, A. H.; Allanore, A., Surface tension of high temperature liquids evaluation with a thermal imaging furnace In *Advanced real time imaging II*, Nakano, J., Pistorius, P. C., Tamerler, C., Yasuda, H., Zhang, Z., Dogan, N., Wang, W., Saito, N., Webler, B., Eds.; Springer International Publishing: Cham, 2019, pp 33–41.

(190) Bandyopadhyay, D. The Ti–Si–C system (titanium-silicon-carbon). *Journal of Phase Equilibria and Diffusion* **2004**, *25*, 415–420.

(191) Caldwell, A.; Lai, E.; Gmitter, A.; Allanore, A. Influence of mass transfer and electrolyte composition on anodic oxygen evolution in molten oxides. *Electrochimica Acta* **2016**, *219*, 178 –186.

(192) Kahlert, H., Reference electrodes In *Electroanalytical methods: guide to experiments and applications*, Scholz, F., Bond, A., Compton, R., Fiedler, D., Inzelt, G., Kahlert, H., Komorsky-Lovrić, Š., Lohse, H., Lovrić, M., Marken, F., Neudeck, A., Retter, U., Scholz, F., Stojek, Z., Eds.; Springer Berlin Heidelberg: Berlin, Heidelberg, 2010, pp 291–308.

(193) Hemberger, Y.; Berthold, C.; Nickel, K. G. Wetting and corrosion of yttria stabilized zirconia by molten slags. *Journal of the European Ceramic Society* **2012**, *32*, Special Issue: ECerS XII, 12th Conference of the European Ceramic Society, 2859 –2866.

(194) Baucke, F. G. K., Reference electrodes in oxidic glass melts In *Handbook of reference electrodes*, Inzelt, G., Lewenstam, A., Scholz, F., Eds.; Springer Berlin Heidelberg: Berlin, Heidelberg, 2013, pp 229–241.

(195) Luisi, M.; Wilthan, B.; Pottlacher, G. Influence of purge gas and spacers on uncertainty of high-temperature heat flux DSC measurements. *Journal of Thermal Analysis & Calorimetry* **2015**, *119*, 2329–2334.

(196) Kim, H.; Paramore, J.; Allanore, A.; Sadoway, D. R. Electrolysis of molten iron oxide with an iridium anode: The role of electrolyte basicity. *Journal of the Electrochemical Society* **2011**, *158*, E101–E105.

(197) Murray, J. L. The Ir–Ti (iridium-titanium) system. *Bulletin of Alloy Phase Diagrams* **1982**, *3*, 205–211.

(198) Kawamura, K.; Yokokawa, T. Linear sweep voltammetry of Pb^{2+}/Pb^{0} in oxide melts: model and simulation of electrode process. *Journal of The Electrochemical Society* **1988**, *135*, 1447–1451.

(199) Branca, T. A.; Colla, V.; Algermissen, D.; Granbom, H.; Martini, U.; Morillon, A.; Pietruck, R.; Rosendahl, S. Reuse and recycling of by-products in the steel sector: recent achievements paving the way to circular economy and industrial symbiosis in Europe. *Metals* **2020**, *10*, 345.

(200) Martin, A.; Derge, G. The electrical conductivity of molten blast-furnace slags. *Trans. Amer. Inst. Min. Met. Eng* **1943**, *154*, 104–115.

(201) Li, J.; Zhang, Z.; Zhang, M.; Guo, M.; Wang, X. The influence of SiO_2 on the extraction of Ti element from Ti-bearing blast furnace slag. *Steel Research International* **2011**, *82*, 607–614.

(202) Wang, Y.; Ge, J.; Zhuo, W.; Guo, S.; Zhang, J. Electrochemical extraction of lanthanum in molten fluoride salts assisted by KF or NaF. *Electrochemistry Communications* **2019**, *104*, 106468.

(203) Jiao, H.; Wang, Q.; Ge, J.; Sun, H.; Jiao, S. Electrochemical synthesis of Ti_5Si_3 in $CaCl_2$ melt. *Journal of Alloys and Compounds* **2014**, *582*, 146 –150.

(204) Frommeyer, G.; Rosenkranz, R., Structures and properties of the refractory silicides Ti_5Si_3 and $TiSi_2$ and $Ti-Si-(Al)$ eutectic alloys In *Metallic materials with high structural efficiency*, Senkov, O. N., Miracle, D. B., Firstov, S. A., Eds.; Springer Netherlands: Dordrecht, 2004, pp 287–308.

(205) Gulbransen, E. A.; Andrew, K. F.; Brassart, F. A. Oxidation of molybdenum 550 to 1700°C. *Journal of The Electrochemical Society* **1963**, *110*, 952–959.

(206) Campbell, J. E.; Goodwin, H. B.; Wagner, H. J.; Douglass, R. W.; Allen, B. C. *Introduction to metals for elevated-temperature use*; tech. rep.; Defense Metals Information Center, Battelle Memorial Institute, Ohio, 1961.

(207) Gulbransen, E. A.; Andrew, K. F.; Brassart, F. A. The oxidation of graphite at temperatures of 600 to 1500°C and at pressures of 2 to 76 torr of oxygen. *Journal of The Electrochemical Society* **1963**, *110*, 476–483.

(208) Van Der Colf, J.; Howat, D. D. Rates of oxygen removal from titaniferous oxide melts in graphite crucibles. *Journal of The South African Institute of Mining and Metallurgy* **1979**, *79*, 343–347.

(209) Tranell, G.; Ostrovski, O.; Jahanshahi, S. The equilibrium partitioning of titanium between Ti^{3+} and Ti^{4+} valency states in $CaO-SiO_2-TiO_x$ slags. *Metallurgical and Materials Transactions B* **2002**, *33*, 61–67.

(210) Zhu, L.; Zhang, Q.; Chen, Z.; Wei, C.; Cai, G.-M.; Jiang, L.; Jin, Z.; Zhao, J.-C. Measurement of interdiffusion and impurity diffusion coefficients in the bcc phase of the Ti-X (X= Cr, Hf, Mo, Nb, V, Zr) binary systems using diffusion multiples. *Journal of Materials Science* **2017**, *52*, 3255–3268.

(211) Sobha Jayakrishnan, D., 5 - Electrodeposition: the versatile technique for nanomaterials In *Corrosion protection and control using nanomaterials*, Saji, V. S., Cook, R., Eds.; Woodhead Publishing Series in Metals and Surface Engineering; Woodhead Publishing: 2012, pp 86 –125.

(212) Massalski, T.; Murray, J.; Bennett, L.; Baker, H., *Binary alloy phase diagrams*; American Society for Metals: 1990.

(213) Prasad, S.; Paul, A. Growth mechanism of phases by interdiffusion and atomic mechanism of diffusion in the molybdenum-silicon system. *Intermetallics* **2011**, *19*, 1191–1200.

(214) Lei, Y.; Wang, C.; Ma, W.; Wu, J.; Wei, K.; Li, S.; Lv, G.; Morita, K. A novel approach to prepare high-purity Si and Si/$TiSi_2$ materials simultaneously using Ti-bearing blast furnace slag. *Journal of Alloys and Compounds* **2019**, *798*, 333 –341.

(215) Zhang, L.; Wu, J. Ti_5Si_3 and Ti_5Si_3-based alloys: alloying behavior, microstructure and mechanical property evaluation. *Acta Materialia* **1998**, *46*, 3535–3546.

(216) Rosenkranz, R.; Frommeyer, G.; Smarsly, W., Microstructures and properties of high melting point intermetallic Ti_5Si_3 and $TiSi_2$ compounds In *High temperature aluminides and intermetallics*, WHANG, S., POPE, D., LIU, C., Eds.; Elsevier: Oxford, 1992, pp 288 –294.

(217) Van Der Colf, J.; Howat, D. D. Viscosities, electrical resistivities, and liquidus temperatures of slags in the system $CaO-MgO-Al_2O_3-TiO_2-SiO_2$ under neutral conditions. *Journal of The South African Institute of Mining and Metallurgy* **1979**, *79*, 255–263.

(218) Van Der Colf, J.; Howat, D. D. Viscosities, electrical resistivities, and liquidus temperatures of slags in the system $CaO-MgO-Al_2O_3-TiO_2-SiO_2$ under reducing conditions. *Journal of The South African Institute of Mining and Metallurgy* **1979**, *79*, 327–333.

(219) Barati, M.; Coley, K. S. Electrical and electronic conductivity of $CaO-SiO_2-FeO_x$ slags at various oxygen potentials: Part II. Mechanism and a model of electronic conduction. *Metallurgical and Materials Transactions B* **2006**, *37*, 51–60.

(220) Mills, K. C. The influence of structure on the physico-chemical properties of slags. *ISIJ International* **1993**, *33*, 148–155.

(221) Gilbert, P., Electrochemical behavior of metals in the biological milieu In *Comprehensive biomaterials*, Ducheyne, P., Healy, K., Grainger, D., Hutmacher, D., Kirkpatrick, C., Eds.; Elsevier: 2015, pp 21–49.

(222) Bard, A. J.; Faulkner, L. R., *Electrochemical methods: fundamentals and applications*, 2^{nd} Edition; New York: Wiley: 2001.

(223) Arblaster, J. W. Selected electrical resistivity values for the platinum group of metals Part II: rhodium and iridium. *Johnson Matthey Technology Review* **2016**, *60*, 4–11.

(224) Cann, J. L. Methodology for determining electronic transference numbers in molten sulfide melts, MA thesis, Massachusetts Institute of Technology, 2017.

(225) Mott, N. Introductory talk: conduction in non-crystalline materials. *Journal of Non-Crystalline Solids* **1972**, *8-10*, 1 –18.

(226) Yoshino, T. Laboratory electrical conductivity measurement of mantle minerals. *Surveys in Geophysics* **2010**, *31*, 163–206.

(227) Mori, K. The electrical conductivity of the $CaO-SiO_2-TiO_2$ system and the behaviour of titanium-oxide. *Tetsu-to-Hagane* **1960**, *46*, 134–140.

(228) Mori, K. The electrical conductivity of molten slags containing titanium-oxide II. *Tetsu-to-Hagane* **1956**, *42*, 1024–1029.

(229) Schreiber, H. D. Redox processes in glass-forming melts. *Journal of Non-Crystalline Solids* **1986**, *84*, 129 –141.

(230) Yahia, J.; Frederikse, H. P. R. Electrical conduction in *p*-type titanium sesquioxide. *Phys. Rev.* **1961**, *123*, 1257–1261.

(231) Ghosh, J. C. The abnormality of strong electrolytes. Part I. Electrical conductivity of aqueous salt solutions. *Journal of the Chemical Society, Transactions* **1918**, *113*, 449–458.

(232) Dyre, J. C. The random free-energy barrier model for A.C. conduction in disordered solids. *Journal of Applied Physics* **1988**, *64*, 2456–2468.

(233) Duffy, J. A. A review of optical basicity and its applications to oxidic systems. *Geochimica et Cosmochimica Acta* **1993**, *57*, 3961–3970.

(234) Mills, K. C.; Sridhar, S. Viscosities of ironmaking and steelmaking slags. *Ironmaking and Steelmaking* **1999**, *26*, 262–268.

(235) Zhang, G. H.; Chou, K. C.; Zhang, J. L. Influence of TiO_2 on viscosity of aluminosilicate melts. *Ironmaking and Steelmaking* **2014**, *41*, 47–50.

(236) Berry, J. D.; Neeson, M. J.; Dagastine, R. R.; Chan, D. Y.; Tabor, R. F. Measurement of surface and interfacial tension using pendant drop tensiometry. *Journal of Colloid and Interface Science* **2015**, *454*, 226 –237.

(237) Shi, C.; Alderman, O. L. G.; Tamalonis, A.; Weber, R.; You, J.; Benmore, C. J. Redox-structure dependence of molten iron oxides. *Communications Materials* **2020**, *1*, 80.